INVESTIGATION OF SURFACTANT, SALT, AND ROCK INTERACTIONS FOR PERFORMANCE IMPROVEMENTS OF COMPLETION FLUIDS IN THE UNCONVENTIONAL LIQUIDS-RICH RESERVOIR OF WEST TEXAS

A Thesis

by

KANG HAN PARK

Submitted to the Office of Graduate and Professional Studies of
Texas A&M University
in partial fulfillment of the requirements for the degree of

MASTER OF SCIENCE

Chair of Committee,	David S. Schechter
Committee Members,	Ding Zhu
	James D. Batteas
Head of Department,	Duane A. McVay

May 2018

Major Subject: Petroleum Engineering

ABSTRACT

Due to their ultra-low permeability and extremely heterogeneous formations, unconventional liquids-rich reservoirs (ULR) need a support of an effective hydraulic fracturing for economic and commercial oil production. In recent years, the addition of surfactants to the fracturing fluids has been proven to be one of the effective improved oil recovery (IOR) methods in ULR. Meanwhile, rising hydraulic fracturing activities has ignited industrial and environmental concerns for increasing water demand and large volumes of high salinity flowback and produced water. This investigation studies the potential of surfactant and salt mixed aqueous phase solutions for performance improvement of completion fluids, and their interactions with different rock types. This study also provides guidance for the most favorable salt concentration for surfactant-added completion fluids which can potentially lead to economic and environmental benefits.

This study focuses on an ULR in West Texas. Five surfactants were selected and mixed at a constant concentration with brines. Brines with nine salinity variations were tested to accurately represent the fluids used or produced in the field, and to determine the most favorable salinity level. All fluids were tested with two different rock types, quartz rich and carbonate rich. Zeta potential, interfacial tension, and contact angle experiments were performed to measure the stability of the liquid film of rock particles, to analyze the impact of surfactant and salt on reducing interfacial tension, and to identify the initial wettability and wettability alteration ability of each fluid, respectively. Then, spontaneous imbibition with timely computer tomography (CT) scans were conducted to visually

observe the imbibition performance of completion fluids and to validate correlations between oil recovery and other experimented parameters.

Overall, the magnitude of zeta potential, and interfacial tension reduced strongly with increasing salinity, regardless of the presence of surfactant. Also, surfactants mixed with lower salinity brines showed the most effective wettability alteration, and the highest oil recovery factor compared to no or high salinity brines. Similar behaviors and results occurred for all aqueous phase solutions and in both rock types. Among all, wettability of the rock surface was determined to be the most influential factor for oil recovery.

DEDICATION

I dedicate this thesis to my parents, Tae Young Park and Mee Kyung Lee, and my sister, Jee Eun Park, for their continuous prayers, unconditional love, and lifelong supports.

ACKNOWLEDGEMENTS

I thank God, my Lord Jesus Christ, for the unconditional love, patience, sacrifices, blessings and strengths throughout this research and my entire life.

I would like to thank Dr. David S. Schechter, who has been not only an advisor but also a mentor, a motivator, and the best boss in the world. This work would not have been possible without his guidance and expertise.

I would like to thank my committee members, Dr. Ding Zhu and Dr. James D. Batteas, for their supports and involvements throughout this research.

I also thank all the faculty members and staffs at the Department of Petroleum Engineering at Texas A&M University, for providing the world's greatest learning environment throughout my both undergraduate and graduate studies.

Finally, I would like to thank my group members for their great friendship, and professionalism.

NOMENCLATURE

CA	Contact Angle
CR	Carbonate Rich
g/cc	Grams per Cubic Centimeter
gpt	Gallon per Thousand Gallons
HU	Hounsfield Unit
IFT	Interfacial Tension
mg/L	Milligrams per liter
mN/m	MilliNewton / meter
mV	MilliVolts
ppm	Parts Per Million
QR	Quartz Rich
RF	Recovery Factor
TDS	Total Dissolved Solids
T_{res}	Reservoir Temperature, °F
ULR	Unconventional Liquids-Rich Reservoir
WT	West Texas Formation
ZP	Zeta Potential

CONTRIBUTORS AND FUNDING SOURCES

Contributors

Part 1, faculty committee recognition

This work was supervised by a thesis committee consisting of Dr. David S. Schechter [advisor] and Dr. Ding Zhu of the Department of Petroleum Engineering and Dr. James D. Batteas of the Department of Chemistry.

Part 2, student/collaborator contributions

All experimental works and analyses for this thesis were solely completed by the student under the advisement of Dr. David S. Schechter, with background information provided by a private E&P company.

Funding Sources

This graduate study was funded by a research project agreement between the Department of Petroleum Engineering at Texas A&M University, and a private E&P company in the U.S.

TABLE OF CONTENTS

Page

LIST OF FIGURES

Page

LIST OF TABLES

Page

1. INTRODUCTION

Producing from ultra-tight and heterogeneous formations, unconventional oil has been the main contributor for the U.S. energy independence, accounting for almost 60% of total domestic crude oil production. U.S. Energy Information Administration predicts that, despite the continuing low crude oil price environment, the tight oil production is expected to increase more than 6 million barrels per day by 2040, exceeding the production from the conventional reservoirs in the U.S. (E.I.A. 2017). The Southwest, Dakotas/Rocky Mountains, and Gulf Coast regions have shown the most growth in tight oil production, and Southwest region is forecasted to have the most production out of all major onshore shale plays by 2040, producing almost 3 million barrels of oil per day, followed by Bakken of Dakotas/Rocky Mountains, and the Eagle Ford and Austin Chalk of Gulf Coast (E.I.A. 2017; Moniz et al. 2011).

It is undoubtable that this significant increase in unconventional oil production during the recent years was made possible by the combination of horizontal drilling and hydraulic fracturing. Using large volumes of water injected at high pressure, hydraulic fracturing generates highly permeable fractures in the formation for easier access to hydrocarbons. Also, horizontal drilling creates larger contact area throughout the production zone, leading to more economical and commercial production rate (Mohamed et al. 2015; Moniz et al. 2011; Pankaj and Kumar 2010). With these benefits, hydraulic fracturing in horizontal wells has been a successfully-implemented completion technique in the ultra-tight formation. However, with the advancing drilling technologies which

efficiently create longer lateral wells, developing effective hydraulic fracturing techniques like well-designed completion fluids has been one of the most important, yet challenging, factors.

Adding surfactant to the aqueous phase completion fluids is believed to have the ability to achieve better oil recovery in ULR by increasing the initial peak production rate. Highly active researches and laboratory experiments have been conducted to determine the impact of surfactant, and all observed significant increases in oil production compared to the fluids without chemical additives (Alvarez et al. 2014; Alvarez, J. O.Saputra, I. W. R. et al. 2017; Alvarez, Johannes O. et al. 2017; Alvarez and Schechter 2016a; Alvarez and Schechter 2017; Alvarez, J. O.Tovar, F. D. et al. 2017; Chen et al. 2000; Chen and Mohanty 2014; Neog and Schechter 2016; WangSeright et al. 2012a; Zheng and Rao 2010). Primarily, spontaneous imbibition process, which involves capillary pressure change by interfacial change and wettability alteration, was applied and studied throughout these researches. However, despite the increasing research interests on surfactant assisted imbibition in ULR, most of the aforementioned studies primarily focus on shale plays in Dakotas/Rocky Mountains and Gulf Coast region, and conducted with distilled water or brines with very little or no salinity.

Additionally, increase in hydraulic fracturing activities has ignited industry's and environment's concerns for rising water demand and high volume of produced water. Unconventional oil extraction in the U.S. between 2012 and 2014 used 17.5 billion gallons of water per year throughout the major onshore shale plays like Eagle Ford, Bakken, with almost double amount of the flowback-produced water (Kondash and Vengosh 2015).

Flowback-produced water is an inevitable resultant liquid of injected water from waterflooding or hydraulic fracturing, and formation brine. It contains high salinity and other naturally occurring minerals which require costly treatment or disposal. It has become one of the most problematic factors especially in Permian and Bakken during the recent unconventional development (Whitfield 2017). Many researches have been successfully conducted to determine the applicability of treated produced water for waterflooding and hydraulic fracturing (Khanamiri et al. 2015; Valluri et al. 2016; Veil et al. 2004; Wilson 2016). However, these studies were mainly conducted on conventional or very few unconventional formations, and very limited understandings of the interaction between salinity and surfactant in aqueous phase solutions exist.

1.1 Research Objectives and Scope

The objective of this study is to investigate the potential of surfactant-salt mixed aqueous phase solutions for performance improvement of completion fluids in an ultra-tight and heterogeneous ULR of Southwest region, focusing on the following:

- Generate surfactant-salt mixed aqueous phase solutions which accurately reflect the properties of completion fluids and produced water in the field
- Identify two dominant types of lithology in the ULR of West Texas and analyze the different interactions with various aqueous phase solutions
- Evaluate the colloidal stability between the surfactant-salinity mixed solutions and two types of rock particles by conducting zeta potential measurements
- Determine the interfacial tension (IFT) between crude oil and the aqueous phase solutions through IFT experiments at reservoir temperature

- Identify the initial wettability of the unconventional rock chips, and compare the impact of surfactant and salinity on wettability alteration by contact angle (CA) measurements at reservoir temperature
- Conduct spontaneous imbibition experiments with ULR cores at reservoir temperature to evaluate the imbibition performance of solutions
- Utilize timely computerized tomography (CT) scans to visually inspect the fluid penetration during the spontaneous imbibition process.
- Identify relationship between experimented parameters and oil recovery, and determine the most influential factor for higher oil recovery factor.
- Provide recommendations for the most favorable salinity level for surfactant-added completion fluids which can unlock the potential of utilization of high salinity produced water, and, ultimately, bring economic and environmental benefits.

1.2 Overview of Thesis Sections

This thesis is composed of six sections including the current section of introduction. Section 2 introduces relevant and recent researches available in the literature and various database. Thorough literature reviews have been conducted and discussed, including important findings from the previous researches, associated problems, and challenges currently facing in the industry. Section 3 provides a background information of a target ULR and various materials used for this study including core samples, brines, and surfactants. Section 4 describes a detailed workflow and experimental procedures applied in this study, including zeta potential measurement, interfacial tension

experiments, wettability alteration analyses and spontaneous imbibition. Section 5 discusses the results from each experiment, and identifies the most favorable condition of the fluid and the most influential parameter for the maximum oil recovery from the ULR. Lastly, Section 6 summarizes the overall results and significances, and provides recommendation and future work for continuing development of completion fluids and researches regarding ULR.

2. LITERATURE REVIEW

The majority of literatures available regarding surfactant-assisted imbibition focuses on the conventional and naturally fractured reservoirs. However, there have been growing numbers of researches and experimented results in unconventional shale plays in the recent years, including Barnett, Bakken, Eagle Ford, and Wolfcamp. There also have been many novel attempts to analyze the effect of salinity on oil recovery, and environmental studies to address the importance of water sources for the oil and gas exploration. This section primarily highlights the important findings from conventional studies, recent findings of the surfactant-assisted imbibition in unconventional plays, and background knowledges of salinity effect on fluids, in addition to related fundamental sciences and experimental methods.

2.1 Spontaneous Imbibition

Imbibition, by definition, is the process of wetting phase displacing the non-wetting phase into the capillary pores of the rock matrix, which is water displacing oil in unconventional shale reservoirs (Babadagli 2003). Spontaneous imbibition is imbibition process by capillary effect and/or buoyancy force when a core sample is submerged in aqueous phase solutions. (Hirasaki and Zhang 2004). In a strongly water-wet surface, spontaneous imbibition by capillary force is an important mechanism of oil recovery, which involves both concurrent and countercurrent imbibition (Morrow and Mason 2001). Because there is no significant pressure difference, viscous force is negligible, and capillary pressure forces the wetting phase fluid to push out the retained wetting phase

fluid in any direction of the matrix. However, the effect of capillarity weakens when the surface becomes strongly oil-wet system or if the interfacial tension (IFT) between oil and aqueous phase solution reduces, causing surface trapping of oil in the matrix, giving oil to have a strong tendency to adsorb on the rock surface. Under this condition, the dominant oil recovery mechanism shifts from capillary force to buoyancy force. Buoyancy, also referred to gravity drainage or osmotic forces, mechanism is driven by the reduction of IFT, the difference in density, and the acceleration of gravity. It forces higher density aqueous phase solution to penetrate downward in the matrix, displacing and replacing lighter density oil out upward from the pore spaces (Li et al. 2016; Schechter et al. 1994).

2.1.1 Oil Recovery Mechanisms

Schechter et al. (1994) experimented and distinguished the dominant oil recovery mechanisms during the imbibition process numerically in fractured conventional reservoirs. They introduced and analyzed the concept of inverse bond number, which involves the ratio of capillary pressure to gravity force, shown in **Eq. 1**.

$$N_B^{-1} = C\frac{\sigma\sqrt{\phi/k}}{(\Delta\rho)gH} \quad \text{.....} \quad (1)$$

N_B^{-1} is the inverse bond number, C is a capillary tube model constant of 0.4, ϕ is porosity, k is permeability, $\Delta\rho$ is density difference between phases, g is gravitational acceleration, and H is the height of the capillary rise. Part of their experiments consisted spontaneous imbibition using 15-mD limestone and 100-mD Berea sandstone cores. For 15-mD limestone cores, the rate of imbibition was fast at high N_B^{-1}, but oil droplets only exited through lateral faces of the core, while at intermediate N_B^{-1}, overall oil production

increased and occurred in both top and lateral faces, but, at a slower imbibition rate. Furthermore, when IFT was altered and reduced to ultra-low value of 0.1 mN/m, the rate of imbibition was the slowest, but the total volume of produced oil was significantly higher than the previous two cases. The imbibition behavior in 100-mD Barea sandstone showed different results, that high N_B^{-1} resulted in a slower and lower oil recovery while low N_B^{-1} showed much higher volume of recovered oil while the rate was delayed by little. Similar experiments were conducted using various types of cores, and, as a result, authors determined that when N_B^{-1} is larger than 5, capillary force becomes the dominant driving mechanism, and as N_B^{-1} becomes much less than 1 and close to 0, gravity drainage dominates the oil recovery. Lastly, when N_B^{-1} value is between 0.2 and 5, both capillary and gravity forces function as the recovery mechanism (Schechter et al. 1994).

2.1.2 Capillary Pressure

As mentioned above, both wettability and IFT are important parameters to understand the mechanism of capillary pressure. Capillary pressure is determined by the Young-Laplace equation, shown in **Eq. 2** below.

$$P_c = P_{nw} - P_w = \rho * g * h = \frac{2 * \sigma * \cos(\theta)}{r} \quad \text{.....} \quad (2)$$

P_c is capillary pressure, P_{nw} is pressure in non-wetting phase, P_w is pressure in wetting phase, ρ is density difference between phases, g is gravitational acceleration, h is height of capillary rise, σ is interfacial tension, θ is contact angle, and r is inner radius of capillary. It shows that the capillary pressure is pressure difference between non-wetting phase and wetting phase in the matrix, and is proportional to the interfacial tension and

the cosine of the contact angle, and inversely proportional to the radius of the pore (Abdallah et al. 2007; Hirasaki and Zhang 2004).

Especially in the unconventional liquids-rich reservoirs (ULR) with strongly oil-wet, heterogeneous, and ultra-tight formations, IFT, contact angle, and pore radius have a significant impact on capillarity. With its nano-scale pore radius, capillary pressure should be higher than the conventional reservoirs by marginal difference. However, the wettability of the reservoir determines the sign convention of capillary pressure. When contact angle is less than 90 degrees, water-wet, capillary pressure becomes positive, favoring water imbibition as an oil recovery mechanism, but, when contact angel is greater than or equal to 90 degrees, oil-wet, capillary pressure becomes 0 to negative, not favoring imbibition process (Alvarez and Schechter 2016b). This negative capillary pressure causes reservoir oil to be trapped inside of the pore, making it impossible for water to start the displacement. Therefore, determination and control of wettability of ULRs is a key to successful implementation of spontaneous imbibition as an improved oil recovery (IOR) method. Also, this supports the importance and the necessity of IFT reduction in order to reduce the negative capillarity, and to cause the buoyancy to take over as the dominant oil recovery mechanism.

2.1.3 Buoyancy / Gravity Drainage

Buoyancy, also referred to gravity drainage, supports the displacement of oil by water in a system with low interfacial between two immiscible fluids. This low interfacial tension condition helps the aqueous phase fluid with higher density to enter the matrix more easily, and to replace the oil with lighter density (Hirasaki and Zhang 2004).

However, it is generally accepted that the capillary pressure is the driving mechanism of oil recovery from the conventional reservoirs, and many believed that low IFT of immiscible fluids will decrease capillary pressure based on the **Eq. 1** above. Cuiec et al. (1990) showed in their experiment that the imbibition rate decreased when IFT is reduced in a tight chalk formation with permeability range of 1 to 3 mD. However, Schechter et al (1991) observed in their experiment that the sandstone cores, which have higher permeability than chalk, resulted in higher imbibition rate and final recovery of oil through reduction of the equilibrium IFT. They argued that this is an indication that during the spontaneous imbibition process, there is a crossover from capillary pressure dominated to buoyance dominated oil recovery mechanism, and suggested three separate regimes of imbibition which are capillary dominated, gravity dominated, and a region where both are dominant mechanism affecting oil recovery (Schechter et al. 1991).

Therefore, based on the highlighted findings above, it can be concluded that the objective of developing an effective spontaneous imbibition system is to combine the two dominant oil recovery mechanisms; capillary and gravity force. In order to achieve that, aqueous phase solution must have the ability to alter wettability from oil-wet to weakly/strongly water-wet surface, and to reduce the IFT down to ultra-low values (Hirasaki and Zhang 2004).

2.2 Surfactants

Surfactants, or surface active agents, are organic compounds which contain amphiphilic property in a single molecule. Amphiphilic, by definition, is having both hydrophilic and hydrophobic groups in a single molecule as a head group and tail group,

respectively, as shown in **Fig. 1**. This amphiphilic property of surfactants generates their behaviors and tendency for adsorption on surfaces and aggregation in solutions (Karsa 2006; Pletnev 2001). The hydrophilic head group can carry either negative or positive charge, both, or neither. Based on the polarity of the head group, surfactants are grouped into four main categories: non-ionic, anionic, cationic, and zwitterionic or amphoteric. Basic properties and typical components of each category are in **Table 1**. Also, typical hydrophobic group includes alkylbenzene, various isomers of alkyl and Alkylphenyl (Gadberry and Otterson 2006; Hepworth 2006; Hibbs 2006; Karsa 2006).

Surfactants have been well-known for their ability to reduce the interfacial tension and surface wettability, and widely applied and studied on conventional reservoirs by numerous researchers (Adibhatla and Mohanty 2008; Austad and Milter 1997; Chen et al. 2000, 2001; Chen and Mohanty 2014; Mohammed and Babadagli 2015; Spinler et al. 2000; Standnes and Austad 2000a, 2000b; Standnes et al. 2002). Mohammed and Babadagli (2015) stated that surfactants reduce the interfacial tension between aqueous phase solution and crude oil from high or intermediate values to ultra-low values, and the adsorption of the amphiphilic molecules on the rock surfaces causes wettability alteration, from oil-wet to water-wet. Austad et al (1997) investigated the effect of surfactant additives on chalk and dolomite cores, and concluded that the addition of surfactant improves spontaneous imbibition performance through countercurrent movement, followed by gravity drainage at late time. Chen et al (2000) also observed 40% increase in oil recovery from Yates cores when non-ionic surfactant was added to the aqueous phase solution, and provided the evidence of faster radial penetration of surfactant-added

fluid compared to brine through CT image analyses. Additionally, Spinler et al (2000) provided conclusion that low concentrations of surfactants can improve oil recovery through both spontaneous and forced imbibition through their surfactant research on chalk formations.

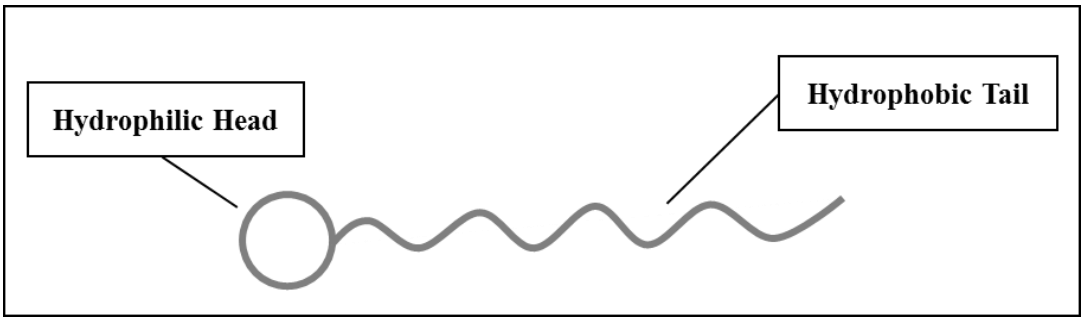

Fig. 1 – General Structure of Surfactant

Table 1 – Categories and Properties of Surfactants. Adapted from Gadberry and Otterson (2006)

Category	Charge	Typical Components
Non-ionic	No Charge	Polyoxyethylene Acetylenic Glycol Polyglucoside
Anionic	Negative	Sulphates Sulphonates Phosphate esters Carboxylate
Cationic	Positive	Ammonium Amines Pyridium
Zwitterionic (Amphoteric)	Both	Amine Oxide Betaine Aminocarboxylates

In addition to the conventional reservoirs, active researches started to take place recently to identify and determine the impact of surfactant in unconventional reservoirs. Initially, with the conventional hydraulic fracturing technique, recovery factors of ULRs and tight reservoirs are less 10% of the original oil in place (OOIP) (Alvarez and Schechter 2016a; Alvarez and Schechter 2017). Then, various researchers suggested and studied the application of surfactant-added completion fluids for hydraulic fracturing to improve initial production from major onshore shale plays of North America, including Bakken, Barnett, Eagle Ford, and Wolfcamp. As a result, surfactant-assisted spontaneous imbibition in ULRs also showed strong reduction of IFT, effective wettability alteration and significant increase in oil production, compared to regular slick water without surface active additives (Alvarez et al. 2014; Alvarez, J. O.Saputra, I. W. R. et al. 2017; Alvarez, Johannes O. et al. 2017; Alvarez and Schechter 2016a; Alvarez and Schechter 2017; Alvarez, J. O.Tovar, F. D. et al. 2017; Chen et al. 2000; Chen and Mohanty 2014; Neog and Schechter 2016; WangSeright et al. 2012a; Zheng and Rao 2010).

2.3 Water

The rapid development of unconventional oil and gas reservoirs led to a significant increase in hydraulic fracturing activities, which accelerated the water usage throughout the United States. This has caused growing risks for water depletion and competition in North America, and oil and gas industry as a whole are facing concerns about water resources and access for their exploration and production processes (Kondash and Vengosh 2015). In addition to the concern for water demands, operators have faced economic and environmental challenges associated with large volume of produced water.

Operators in Permian and Bakken, especially, have been eager to find alternative methods to store, or re-use the produced water due to increasing volume of water needed and their saltwater disposal wells (SWDs) reaching the maximum capacity (Whitfield 2017).

2.3.1 Water Usage

There have been very few researches that provided comprehensive and wide range of data about water usage associated with hydraulic fracturing. It was not until very recently that the oil and gas industry realized the importance of water resources, and actively began the data analyses and integrations for volume of used and produced water during the unconventional oil and gas production in the U.S. (Freyman 2014; Gallegos et al. 2015; Jackson et al. 2014; Kondash and Vengosh 2015; Nicot and Scanlon 2012; Scanlon et al. 2014; Veil et al. 2004; Vengosh et al. 2014; Wu et al. 2009).

2.3.1.1 Water Usage for Hydraulic Fracturing

Kondash and Vengosh (2015) evaluated the water footprint of hydraulic fracturing in the U.S. and presented that 66 billion liters of water per year has been used for unconventional oil extraction from 2005 to 2014. Among many major shale plays, Eagle Ford shale development used the most water of 4 million gallons per well, followed by Bakken, Woodford, and Permian shale plays, using more than 0.8 million gallons of water per well (Kondash and Vengosh 2015). Gallegos et al (2015) made a novel attempt to comprehensively compile up-to-date data on injected water volumes for hydraulic fracturing activities in unconventional oil and gas development. Through extensive data gathering and analyses from their commercial and proprietary IHS database of U.S. Oil and Gas Production and Well Data, authors generated a map of U.S. (**Fig. 2**) showing the

average volume of water injected per well during hydraulic fracturing process. It was observed that the regions with the highest average hydraulic fracturing water volumes per well, over 4 million gallons, were composed of more than 90% of horizontal wells, which has significantly larger contact area with the reservoir rock. Also, between 2000 and 2014, median volume of water for hydraulic fracturing had increased from 0.17 million gallons to more than 4 million gallons in horizontal wells of unconventional shale plays (Gallegos et al. 2015). One of the most active operators in unconventional shale development in the U.S., Chesapeake Energy, presented that their Eagle Ford and Niobrara liquid shales had used 6 million gallons per well and 3 million gallons of water per well, respectively, for their fracturing practices in 2011 (Mantell 2011).

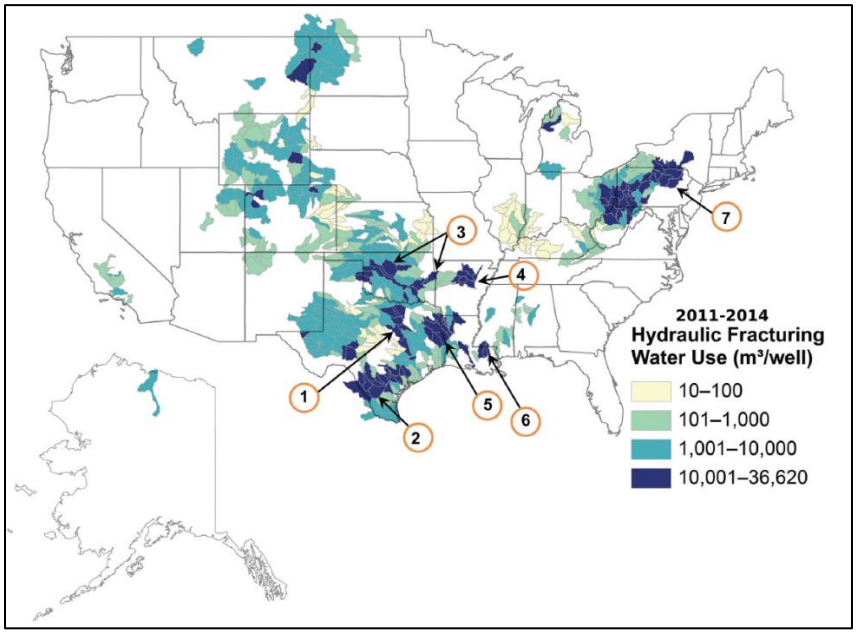

Fig. 2 – Average volume of injected water per well for hydraulic fracturing from Jan. 2011 to Aug. 2014. Reprinted with permission from Gallegos et al. (2015)

2.3.1.2 Challenges for Water Demands

As mentioned in the Introduction, Southwest region of the U.S. has the most potential for unconventional oil production with the help of growing Permian Basin development. As a results, Texas is expected to at least double its volume of used water for hydraulic fracturing in the future because of its intensified oil production (Freyman 2014). Eagle Ford and Permian Basin face some of the biggest challenges with water, such as pressures on water demand, and drought conditions for surface and ground water aquifers. This also has generated competition for water acquisition to shale developing counties and operating companies, forcing them to find methods to secure sufficient water resources for their unconventional development (Freyman 2014; Jackson et al. 2014; Kondash and Vengosh 2015).

2.3.2 Flowback and Produced Water

Waste water from unconventional shale development are commonly referred to two names: flowback and produced water (Sunshine 2017). Two names are sometimes used interchangeably, but each has its own characteristics. Flowback water is returned fluids of the injected water during hydraulic fracturing process, which contain various chemicals and proppants, and produced water is water produced during the production process along with oil and gas (Fakhru'l-Razi et al. 2009). However, they are generally grouped and referred as flowback and produced water (FPW) (Blewett et al. 2017).

2.3.2.1 Characteristics of Flowback and Produced Water

Produced water is believed to be originated from three primary sources: above or below formations, within the formation, and injected fluids with additives. Fakhru'l-Razi

et al. (2009) analyzed that the volume of produced water globally is estimated to be nearly 250 million barrels per day, which is almost 3 times more than the daily oil rate. Also, they distinguished the factors affecting volume of produced water, which are methods of drilling (horizontal or vertical), heterogeneity of wells, types of completion, water injection or waterflooding during enhanced oil recovery (EOR), and poor well integrity and well management.

Flowback and produced water is known to have various contaminants and byproducts from its initially-injected fluids with chemical additives, or minerals from underground. Main contaminants in FPW include high level of total dissolved solids (TDS), salinity, suspended solids, dissolved gas, heavy metals, and naturally occurring radioactive materials (SPE 2011). The properties of FPW varies by region, but generally, it shows TDS range of as low as 2,600 ppm to as high as 310,000 ppm, produces with dissolved gas like carbon dioxide, hydrogen sulfide and oxygen, and contains minerals such as calcium, sodium, potassium, magnesium, iron and aluminum (Fakhru'l-Razi et al. 2009). Because of its severe contaminations and large volumes, produced water has become a primary threat to water resources, through spills, disposal and leakage. FPW continues to draw major environmental concerns throughout the world and led to numerous researches in the U.S. to determine the characteristics and to discover effective methods to either dispose or utilize the FPW. Therefore, development of proper treatment methods and discovery of re-usability for wastewater has been considered as keys to protecting the environment and providing economic benefits, and numerous researches have been conducted to evaluate the most efficient water treatment method and the effect

of salinity and other organic materials on oil recovery (Blewett et al. 2017; Burnett 2011; Fakhru'l-Razi et al. 2009; Jackson et al. 2014; Johnston et al. 2016; Li et al. 2016; Mantell 2011; Rassenfoss 2017; Sharma et al. 2015; SPE 2011; Veil et al. 2004; Wells et al. 2017; Whitfield 2017; Wilson 2015, 2016).

2.3.2.2 Treatment of Flowback and Produced Water

There have been various attempts to develop proper treatment methods for FPW. To manage the waste water systematically, Veil (2007) proposed three pollution prevention steps which are using technologies to minimize the volume of produced water, reuse and recycle, or dispose if two previous steps are not applicable. Arthur et al. (2005) also proposed four options that oil and gas operators can use as part of the produce water management. They involve injecting produced water into the same formation, discharging produced water after treatment to meet the regulations, reusing in oil and gas development, or finding beneficial uses for irrigation, animal consumption and drinking water after treatment. Out of all options above, treatment of produced water is considered to be the most effective option, and general treatment processes are through four major categories: physical, chemical, biological and membrane treatment (Fakhru'l-Razi et al. 2009).

Cheasapeake Energy applied filtration as their preferred treatment methods for re-using produced water in their shale practices (Mantell 2011). After pumping produced water through 100-micron filter, followed by 20-micron filter, to remove suspended solids, filtered fluids were analyzed for their quality and re-used for fracturing jobs. As a result, approximately 230,000 gallons of produced water per well were used in Barnett shale development, and around 6% of the total water used for hydraulic fracturing in Fayetteville

shale was composed of produced water. Although this application led to the reduction in wastewater volume, less needs for fresh water resources, and mitigation of the traffic for water trucks, filtration process did not have the ability to filter small contaminants like salts or other scaling compounds, which can cause severe damages to wells and formation during the development (Mantell 2011).

2.3.2.3 Application of Flowback and Produced Water

Sharma et al. (2015) developed a water management plan called "Fit-For-Purpose treatment" of produced water, and performed a field-scale implementation of this method. Authors began by analyzing the characteristics of the produced water in Permian Basin of West Texas, both conventional and unconventional, and determined the feasibility for its re-application in hydraulic fracturing activities. Produced water from Permian Basin contained very high salinity, more than 220,000 mg/L in TDS, and had either high hydrogen sulfide concentration of 400-600 mg/L or iron concentration of 70 mg/L. Therefore, authors selected chlorine, chlorine dioxide, and hydrogen peroxide, which are oxidants used for hydrogen sulfide and iron removal, and performed chemical treatment of produced water while monitoring the water quality on the site. After six months of this pilot studies, treated water quality had significantly improved, with low hydrogen sulfide and iron concentration, qualifying for its use as a stimulation fluid. Also, friction reduction test and gel stability testing with cross-linkers all showed favorable results that this treated fluid was used for slick water stage of development wells in the area without any problem (Sharma et al. 2015).

Rassenfoss (2017) introduced a recent development in Marcellus play for re-using produced water. Antero Resources has built a water treatment plant called Clearwater, aiming to produce 1.7 million gallons of water and 2,000 tons of salt per day. Antero's Clearwater follows the following water treatment process: pretreatment to remove minerals, metals and radioactive materials from the raw FPW, thermal treatment to separate water and salt, and post-treatment to remove any remaining contaminants. After the separation of water and salt, Antero plans to use filtered water for their oil and gas development practices, and sell salts to generate more revenue. With the increasing demand for road salts, which takes up for 44 % of total salt consumption, along with chemical, agricultural and food industry, Antero's salt generation contributed to more than 3% of the road salt market in 2016 (Rassenfoss 2017).

2.3.2.4 Salinity

Mohanty and Chandrasekhar (2013) studied the impact of salinity and ionic composition on oil recovery for limestone cores. All of their measurements were conducted at 120^{o}C with the combination of contact angle, imbibition, core flooding, and ion analysis. Salinity of brines used for the experiment varied from approximately 800 ppm to as high as 180,000 ppm, and primary ions used were sodium, magnesium, calcium, chloride and sulfate. As a result, authors concluded that high salinity water with TDS level of around 43,000 ppm, which contains large number of magnesium and sulfate ions, changed the wettability of aged limestone samples from oil-wet to more water-wet. However, brine with calcium ions, but magnesium or sulfate, did not show successful wettability alteration in the calcite cores. Also, brine with 43,000 ppm of TDS showed

tendency to imbibe into the oil-wet matrix and resulted in doubled recovery factor compared to the formation brine waterflood case. Authors stated that the presence of mineral in brines and multi ion exchange led to more water-wet conditions of the rock due to desorption of organic acid minerals (Mohanty and Chandrasekhar 2013).

Valluri et al. (2016) conducted series of experiments to analyze the impact of sodium chloride and calcium chloride, specifically, on spontaneous imbibition in unconventional liquids reservoir. Using ULR cores from South Texas, authors varied the concentration of each salt from 1 to 15 wt. % to find the optimum salt concentration by contact angle, interfacial tension, and zeta potential experiments. This screening process confirmed that a brine with 2.5 wt. % sodium chloride and a brine with 5 wt. % calcium chloride showed the most effective wettability alteration, shifting the wettability of the rock from oil-wet to more water-wet surface. Then, these two selected brines, along with distilled water, were used for spontaneous imbibition experiment to examine their ability to enhance the oil recovery. As a result, both brines showed almost four times better oil recovery factor, from 2 % recovery to 7~8 % recovery, compared to distilled water which has negligible salinity. Also, both brines were observed to penetrate into matrix more effectively, based on image analyses of computerized tomography scans (Valluri et al. 2016).

2.4 Zeta Potential

Zeta potential (ζ) is defined as the electrical potential at the interface of a solid particle and liquid, in a system where any solid particle is suspended in liquid (Shehata and Nasr-El-Din 2015). Because of the attractive forces related to the Van der Waals'

forces and the electrostatic repulsion, an electric charge is developed at the boundary of hydrodynamic shear between solid particles and liquid (Johnson et al. 2010).

There are two primary liquid layers surrounding the particle, called the electrical double layer: Stern layer (an inner layer) with strongly associated ions, and diffuse region (an outer layer) with less associated ions (Instruments 2005). Ions with the opposite charge of the solid particles will make a physical contact with the particle, forming a strong Stern layer, and other ions, which are electrically attracted to the particle weakly, form a diffuse layer. When particles move within the system, ions within the layer move as well, while other ions in the bulk system will stay, and the potential measured at this boundary is zeta potential (Instruments 2005).

Zeta potential is a good indicator of the stability of the colloidal system. The higher the magnitude of the zeta potential, the more stable the system is. The boundary for stability is either ± 30 mV, where zeta potential value higher than 30 mV or lower than -30 mV is considered stable. When zeta potential falls between 30 mV and -30 mV, the repulsion between the solid particles are reduced, causing them to make flocculation, coagulation or aggregation (Johnson et al. 2010; Kakadjian et al. 2007).

Various factors affect the value of zeta potential and the sign convention, including pH, ionic strength, and surface charge, and change the behavior of liquid film layer and the adsorption of the ions. As a result, zeta potential is a function of surface charge, and composition of the aqueous phase solutions (Instruments 2005; Shehata and Nasr-El-Din 2015). The pH of the aqueous phase is one of the most critical factors for zeta potential because of the electric charges of acidic or alkali groups. Ionization of acidic groups gives

negatively charged surface to the solid particles, while basic groups give positively charged surface.

Jada et al. (2006) determined the surface charge of quartz sand by varying pH of the fluid using humic acid. At the pH level of 2.5, which is highly acidic, zeta potential of Fontainebleau quartz sand particles had the zeta potential of little higher than 10 mV. However, as pH level was increased to more basic range, zeta potential was reduced to 0 at the pH level of approximately 2.5, ultimately reaching a stable value of -40 mV at the pH level of 4 and higher. This experiment showed that, at low pH level, quartz sand particles showed positive surface with unstable colloidal system, but at neutral solution, surface charge of quartz sand becomes negative. Therefore, zeta potential measurement can be used for determining the surface charge of the solid particles (Jada et al. 2006).

Additionally, there have been numerous experimental studies to analyze the impact of salinity on zeta potential (Johnson et al. 2010; Kakadjian et al. 2007; Mahani et al. 2017; Shehata and Nasr-El-Din 2015; Valluri et al. 2016). Mahani et al. (2017) focused on the impact of brine salinity, rock type and pH on zeta potential using different types of carbonate rocks, and observed how the surface charge behaves at different salinity and pH level. Chalk, limestone, and dolomite rock samples were used for this experiment, and it was concluded that regardless of the rock type, the trends of zeta potentials were very similar. When carbonate rocks were exposed to high salinity water with TDS of 180,000 mg/L, the surface charge was positive and resulted in more oil wetting surface. Then, when salinity was lowered to 40,000 mg/L, zeta potential was reduced to negative values, and showed less oil-wet behavior. Dolomite particles showed the most positive zeta potential,

followed by limestone and chalk samples. Zeta potential was also affected by the level of pH when salinity was kept at constant, showing increase in zeta potential with increasing pH level. All types of carbonate rock showed sensitivity to pH and salinity, chalk particles showing the most reactivity, followed by limestone and dolomite. It is clear that zeta potential has a strong relationship with surface charge and surface wettability, and that wettability alteration is most effective at low salinity and higher magnitude of zeta potential. The potential mechanism behind this behavior includes low salinity flooding creating diffusion in the system to three-phase contact line (Oil/Brine/Rock), alteration of surface charges at each interfaces, increase of repulsive forces due to increased zeta potential, and expansion of electric double layer to change contact angle to less oil wet surface (Mahani et al. 2017).

Similarly, in the field of chemistry, Garg et al. (2016) performed a measurement of zeta potential and numerical simulation to find the behavior of zeta potential in various monovalent salts at different concentration. Using various monovalent salts like sodium chloride, potassium chloride, and calcium chloride, zeta potential was measured through experiments using sinusoidal electric responses, and also simulated using Monte Carlo simulations for the electrical double layer (EDL) of polystyrene latex (PSL) surfaces. As a result, authors observed a decrease in zeta potential magnitude with increasing salt concentration for all types of salt. At high concentration of salt, authors stated that zeta potential becomes negligible due to the extreme thinness of EDL (Garg et al. 2016).

2.5 Interfacial Tension

Interfacial tension (IFT) is one of the key parameters for understanding the mechanisms of oil recovery from the reservoir. Many researches in the past proved that interfacial tension and surface wettability strongly impacts the performance of spontaneous imbibition because of capillarity, buoyancy, or both (Chimienti et al. 1999; Hocott 1939; Schechter et al. 1991; Schechter et al. 1994). As stated in Section 2.1.2 above, capillary pressure is directly related to interfacial tension and contact angle. Therefore, lowering IFT was believed to decrease the capillary pressure in the reservoir, which makes the matrix to retain oil more strongly. However, it was observed that lowering IFT actually accelerated the imbibition rate, and improved the ultimate oil recovery factor, and many researchers concluded that lowering IFT shifts the oil recovery mechanism from capillarity to gravity drainage (Chimienti et al. 1999; Schechter et al. 1991; Schechter et al. 1994).

Interfacial tension, by definition, is the tension in the interface between two immiscible fluids (Hough 1966). IFT can occur in various forms of system: oil/water, water/air, or oil/air. This parameter can be measured through numerous techniques including pendent drop, sessile drop, Laser-Light-Scattering, and spinning drop method (Bagnall and Arundel 1978; Ghosh et al. 1988; Handy et al. 1983; Huh and Reed 1983; Rosen 1984). These methods involve a drop of oil phase displaced into an aqueous phase solution, and the shape of the drop and the volume of oil displaced are used to calculate IFT. Critical systematic errors occur when the three phase contact occurs during the experiment, which causes spinning drop method to be very difficult especially in a high

temperature and pressure environment, and Laser-Light-Scattering method to lack its practicality in a high pressure system. Due to their ability to avoid three phase contact and stability of measurements, the traditional pendant and sessile drop method have been widely applied in the oil and gas industry with the support of advanced digital video and image capturing technologies (Chimienti et al. 1999; Guo and Schechter 1997; Herd et al. 1992; Hough 1966).

2.6 Wettability

Wettability is another important parameter for understanding the mechanism of oil recovery, along with interfacial tension. It can be defined as the tendency of one fluid to adsorb on a solid surface in a system of other immiscible fluid (Hirasaki 1991). Wettability contributes to the flow and distribution of fluids in porous medium, and affects numerous petrophysical properties including reservoir capillary pressure, relative permeability, residual oil saturation, and irreducible water saturation (Anderson 1986a, 1986b). Reservoir wettability is strongly affected by the composition of hydrocarbon, surface characteristics, temperature, and the presence of polar materials like chemicals, but not so much affected by pressure (Alotaibi et al. 2011; Wang and Gupta 1995). Because of the significant influence of wettability, there have been large volumes of researches, literature reviews and experimental methods to more accurately and efficiently understand and analyze the original wettability of both conventional and unconventional reservoirs (Alvarez et al. 2014; Alvarez and Schechter 2016a, 2016b; Gupta and Mohanty 2008; Hirasaki and Zhang 2004; Mohamed et al. 2015; Neog and Schechter 2016; Treiber and Owens 1972; WangButler et al. 2012; WangSeright et al. 2012b; Wang and Gupta 1995).

2.6.1 Measurement of wettability

Wettability of the reservoir can be obtained through either qualitative or quantitative methods. In the wettability literature survey by Anderson (1986b), qualitative methods to measure wettability include relative permeability curves, capillary pressure curves, reservoir logs, and nuclear magnetic resonance, while quantitative methods include contact angles, Amott method, and the U.S. Bureau of Mines (USBM) methods. However, among all methods, three of the quantitative measurement methods, contact angle, Amott, and the USBM methods, are used the most frequently (Anderson 1986b).

2.6.1.1 Contact Angle Method

Contact angle method is used when measuring the wettability of a specific solid surface. It requires small rock chips and two immiscible fluids, usually oil and aqueous phase solution, to measure the contact angle, and surface of the rock needs to be polished and smoothed to avoid any issues associated with hysteresis (Alotaibi et al. 2011). Many methods of contact angle measurement like sessile or pendant drop method, tensiometeric method, capillary rise method, or tilting plate method have been used, but the sessile or pendant drop method is the most widely used in the oil and gas industry (Wang and Gupta 1995).

Sessile or pendant drop method was initially used for measuring interfacial tension, but later applied for the contact angle measurement. The procedure of this method is as follows: a small piece of rock is placed in an aqueous phase solution, a droplet of crude oil is displaced and formed at the tip of a small capillary tube or a needle, a droplet comes into contact with the rock surface, and the resulting angle between the oil droplet and the

rock surface is measured (Anderson 1986b; Wang and Gupta 1995). Generally, the wettability is believed to be oil-wet when contact angle is larger than 90°, and water-wet when smaller than 90°. However, to more clearly distinguish and identify the wettability of the reservoir rock surfaces, wettability classification in **Table 2** is used, grouping the wettability into oil-wet, intermediate (neutral) wet, and water-wet (Alotaibi et al. 2011; Anderson 1986a, 1986b). Additionally, contact angle method is widely applied to observe wettability alteration, to measure static and dynamic contact angle, and to examine various factors that can affect the contact angle, like temperature, pressure, and salinity (Anderson 1986b).

Table 2 – Wettability Classification for Contact Angle Method. Adapted from Anderson (1986a)

Contact Angle	Wettability
0° - 75°	Water Wet
75° - 115°	Intermediate Wet (Neutral Wet)
115° - 180°	Oil Wet

2.6.1.2 Amott Method

Unlike contact angle method, Amott method combines the process of drainage and imbibition to measure the average wettability of a whole core (Anderson 1986b). This method is based on the mechanism of wetting phase's tendency to imbibe into the core, displacing the non-wetting phase. Both spontaneous and forced imbibition processes are applied for this method using oil and brine, generally, and Anderson (1986b) explains the

procedure as following. First, the core is centrifuged under brine until it reaches the residual oil saturation. Then, the core is submerged in oil to initiate spontaneous imbibition, and the volume of displaced brine (V_{wsp}) is measured. After leaving it for more than 20 hours, the core goes through centrifuging stage until the further displacement of brine stops and reaches the irreducible water saturation. Total volume of displaced brine (V_w) is measured as well. Core at irreducible water saturation is then immersed in brine and the volume of oil displaced by imbibition of brine (V_{osp}) is measured. After 20 hours, the core is centrifuged in oil until it reaches the initial residual oil saturation. Total volume of displaced oil (V_{ot}) for this stage is measured. The test results are calculated to find displacement-by-oil ratio (δ_o) and displacement-by-water ratio (δ_w), as shown in **Eq. 3** and **Eq. 4**, respectively (Anderson 1986b).

$$\delta_o = \frac{V_{wsp}}{V_{wt}} \quad \text{.....} \quad (3)$$

$$\delta_w = \frac{V_{osp}}{V_{ot}} \quad \text{.....} \quad (4)$$

In addition to the Amott method above, some researchers implemented a modified test called the Amott-Harvey Index (Boneau and Clampitt 1977; Trantham and Clampitt 1977). Amott-Harvey method involves an additional procedure to prepare the core, which is centrifuging the core under brine and then under oil to reduce the core plug to irreducible water saturation. Then, same procedure as traditional Amott method is used to determine the wettability of the core plug. Amott-Harvey Index (I) is calculated as shown in **Eq. 5**, and the wettability categorization for each method is described in **Table 3** (Anderson 1986a, 1986b; Boneau and Clampitt 1977; Trantham and Clampitt 1977).

$$I = \delta_w - \delta_o = \frac{V_{osp}}{V_{ot}} - \frac{V_{wsp}}{V_{wt}} \quad \text{..... (5)}$$

2.6.1.3 USBM Method

The U.S. Bureau of Mines (USBM) method, similar to the Amott method, measures the average wettability of a whole core plug using centrifuge and capillary pressure curves. Developed by Donaldson et al. (1969) of U.S. Bereau of Mines, USBM method has a strength of resulting in a better sensitivity at intermediate wettability range compared to Amott method, but has a limitation of using only plug-size samples for measurements due to its centrifugation procedure. USBM method is conducted as following: core sample is centrifuged under oil to reach irreducible water saturation, core is centrifuged in brine until a capillary pressure reaches -10 psi (brine drive), then, core is again placed in oil and centrifuged (oil drive) until a capillary pressure reaches +10 psi. At each stage, average water saturations and capillary pressures are measured until the end points. These stages are, then, plotted in one graph into the brine drive curve and oil drive curve. Area under each curve is calculated and used in **Eq. 6** to determine the average wettability of the core sample. USBM wettability index is shown in **Table 3** (Anderson 1986a, 1986b; Boneau and Clampitt 1977; Donaldson et al. 1969; Trantham and Clampitt 1977).

$$W = \log\left(\frac{A_1}{A_2}\right) \quad \text{..... (6)}$$

Table 3 – Wettability Classification for Amott, Amott-Harvey, and USBM Method. Adapted from Anderson (1986b)

Method	Water Wet	Intermediate Wet	Oil Wet
Amott Wettability Index			
Displacement-By-Oil Ratio (δ_o)	Zero	Zero	Positive
Displacement-By-Water Ratio (δ_w)	Positive	Zero	Zero
Amott-Harvey Index (I)	$0.3 \leq I \leq 1.0$	$-0.3 < I < 0.3$	$-1.0 \leq I \leq -0.3$
USBM Wettability Index (W)	W near 1	W near 0	W near -1

2.6.2 Types of Wettability

Reservoir wettability can be affected by the geography of reservoirs, types of rock, types of hydrocarbon in place, and the formations' petrophysical properties. Treiber et al. (1972) conducted a laboratory examination to determine wettability of conventional reservoirs in the U.S., using contact angle method. Rock samples from 55 reservoirs in various states and foreign countries, including Alaska, New Mexico, Texas, Oklahoma, Wyoming, Canada and Argentina, were evaluated and grouped into two dominant lithology: 25 calcite (carbonate) reservoirs and 30 quartz (silicate) reservoirs. Out of 30 silicate reservoirs, 13 were determined to be water-wet, 2 intermediate-wet, and 15 oil-wet. On the other hand, among 25 carbonate reservoirs, only 2 were in the water-wet range, 1 in the intermediate, and 22 in the oil-wet range. Reservoirs with calcite dominant lithology showed more oil-wet system than quartz dominant lithology, and more than 70 percent of 55 conventional reservoirs showed either intermediate to oil-wet wettability. Authors also noted that the presence of calcium sulfate, a commonly found mineral in West Texas with a strong water-wet condition, in carbonate reservoirs can cause

microscopic variations in wettability, creating an inhomogeneous wettability, also known as Dalmatian wettability, condition throughout the reservoir. In conclusion, the purpose of this study was to show that a wide variation of reservoir wettability exists in the U.S. conventional reservoirs (Treiber and Owens 1972).

In contrast, there have been very limited researches on identifying the original wettability of unconventional shale plays. Alvarez and Schechter (2016b) gathered information from available literatures about the original wettability of major ULRs as part of their wettability, oil and rock characterization study. Provided information included studies on Eagle Ford, Bakken, Barnett, and Permian Basin shales, and almost all reservoirs were observed to be intermediate-wet to oil-wet, and measured through contact angle measurements. Authors also conducted their own contact angle experiments with Eagle Ford, Bakken, Barnett, and Wolfcamp core samples. As a result, all shale plays were determined to be intermediate to oil-wet. 8 samples from Bakken, Eagle Ford, and Barnett shale plays showed the average contact angle of 78.75°, 92.63°, and 93.5°, respectively, which falls in the intermediate wet range. 9 samples from Wolfcamp showed the most oil-wet behavior of 126.44, with the largest range of contact angle, representing strong heterogeneity. It can be concluded that not only a wide variety of original wettability also exists in ULRs like conventional reservoirs, but also unconventional shale plays show stronger heterogeneity, having a wide range of contact angle in a single shale play (Alvarez and Schechter 2016b).

3. BACKGROUND INFORMATION

The purpose of this section is to provide important background information about the ULR, and associated materials this investigation primarily focused on. A private E&P company, hereinafter COMPANY, funded this research under the non-disclosure agreement between the Harold Vance Department of Petroleum Engineering at Texas A&M University. Therefore, exact names, detailed descriptions, or proprietary information is not disclosed throughout this thesis.

3.1 ULR Description

As mentioned in the introduction, U.S. Energy Information Administration (2017) forecasted that the crude oil production from the lower 48 states of U.S. will continue to grow. Among many major shale plays in the U.S., Permian Basin has been the most active areas for exploration and production of both conventional and unconventional oil. It is also the only major U.S. shale play that showed increase in oil production, even after the industry's major downturn which began in late 2014. Southwest region of the U.S., with the help of Permian Basin, is expected to reach almost 3 million barrels of oil per day by 2040.

COMPANY owns one of the largest acreage in this region, and has been actively developing and operating with the support of horizontal drilling, long lateral lengths, and effective completion processes. Because of its tight matrix with ultra-low permeability, well-designed hydraulic fracturing process is required to deliver the maximum production from this region. Also, Permian Basin is known for its extreme heterogeneity, showing

different petrophysical properties, such as porosity, permeability, and lithology, throughout each pay zone. COMPANY has identified this heterogeneity and distinguished formations into two dominant lithology: carbonate rich and quartz rich. Although they are divided, horizontal wells drilled in this formation will be in contact with both rock types throughout their laterals.

This research focused on one of the most productive shale oil formations in Permian Basin of West Texas. This formation, hereinafter WT, is one of many pay zones deposited in Southwest region, which has significantly contributed to the boom of shale oil development in West Texas. WT is proven to have the biggest recoverable resource potential out of all other pay zones, and takes account for more than 50% of COMPANY's production wells in Permian Basin. In spite of enormous potential for oil recovery from this region, many operators in West Texas, including COMPANY, face problems associated with large volumes of produced water, as mentioned in section 2.3.2. COMPANY has dealt with this problem through either salt water disposal (SWD) or blending produced water and fresh water to apply for hydraulic fracturing activities.

Based on the key characteristics and issues associated with this ULR, this research is motivated by the mutual interests of investigating how to develop an effective fracturing fluid which can increase the initial production, determining the most favorable condition of blended water, and studying how aqueous phase solutions interact with each lithology.

3.2 Core Samples

ULR shale cores provided by COMPANY were used for this investigation. Sidewall cores with 1-inch in diameter and approximately 2.5-inches in length were

extracted from a well which runs through the formation WT. All cores initially were not preserved, but all samples contained a noticeable gaseous smell of hydrocarbon when opened in the room condition. As mentioned in the previous section, provided cores were classified into two types of rock: carbonate rich (WT CR) and quartz rich (WT QR), and distinct physical differences could be detected visually.

WT CR cores contained small white calcite blocks within each core, having more heterogeneity and light color, while WT QR cores showed comparably more homogeneous state with darker color. The initial condition of the cores can be found in **Fig. 3**, and due to their irregular shapes, provided cores went through a trimming process to form a cylindrical shape like **Fig. 4** for more precise volumetric calculations.

Fig. 3 – Initial Condition of the Cores: WT CR (Top) and WT QR (Bottom)

Fig. 4 – Trimmed Core Samples: WT CR (Left), WT QR (Right)

The ranges of depth for each rock type were similar, as both carbonate rich and quartz rich cores were collected from between 8860 ft. and 9000 ft. All of these cores were drilled and extracted from the same well, as shown in **Fig. 5**, and it indicates that an extreme heterogeneity is in place throughout the WT formation. To Identify and further understand the characteristics of minerology for each rock type, X-Ray Diffraction (XRD) technology was used. Even though there were some level of heterogeneity throughout the selected cores, detected minerals and the composition of each mineral from each set of cores were similar. As shown in **Fig. 6** and **Fig. 7**, both carbonate rich and quartz rich cores contained quartz, feldspar, pyrite, calcite, dolomite, and other clay minerals. Both showed a similar average wt. % of plagio, dolomite and other silicate minerals, but a clear distinction between two types of cores was observed in the composition of quartz and

calcite minerals: WT CR cores contain an average of 40% quartz and 16% calcite, while WT QR cores are composed of 53% quartz and only 2% of calcite mineral in average.

In addition to XRD analysis, few cores were selected for permeability and porosity measurements. COMPANY selected 4 WT CR cores and 7 WT QR cores, aside from the provided cores above, to be measured through Gas Research Institute (GRI) method. GRI total porosity, GRI gas porosity, and GRI permeability were measured, and the results showed a strong heterogeneity, as shown in **Table 4**. Average effective porosity and permeability of WT CR cores were slightly lower than WT QR cores, but strong variations in all parameters occurred for all rock types and at different depths. For this investigation, permeability is not used for any calculation, and porosity is assumed at 8% for volumetric calculations in the later sections.

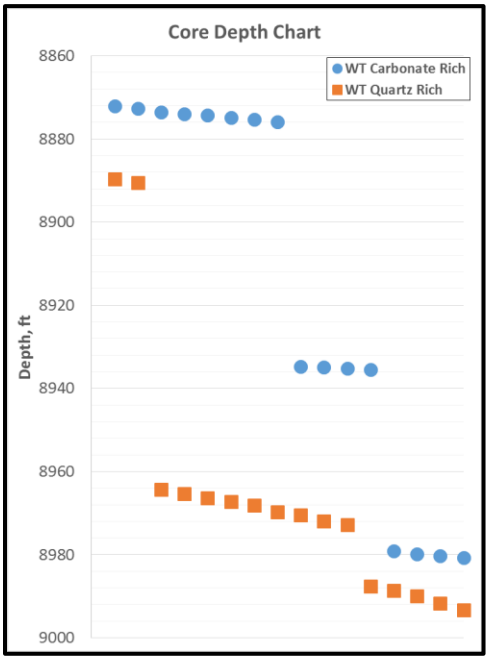

Fig. 5 – Depth Chart of Cores from WT Formation

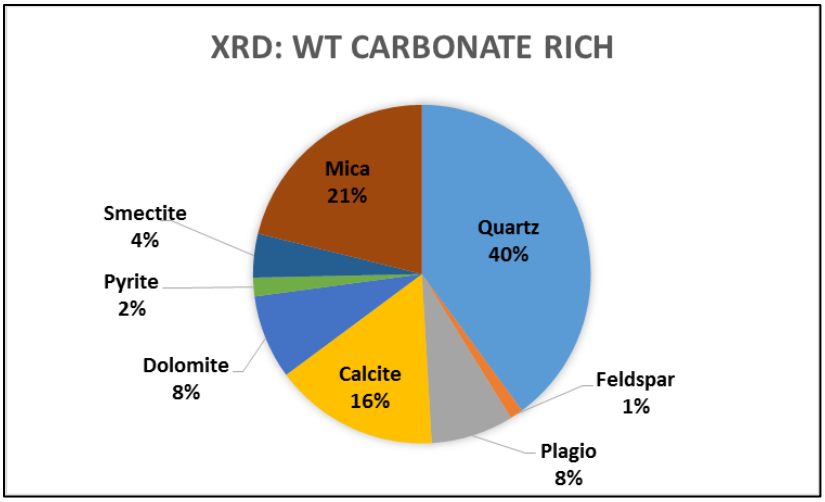

Fig. 6 – Average Mineral Composition of Carbonate Rich Cores of WT formation

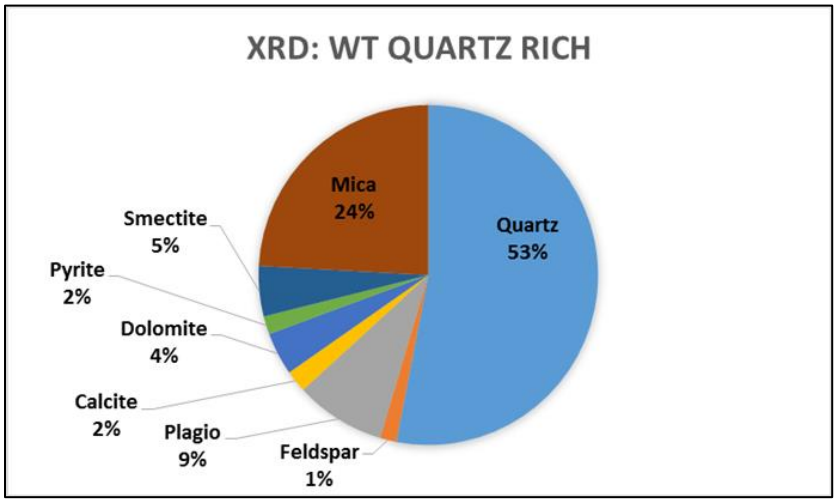

Fig. 7 – Average Mineral Composition of Quartz Rich Cores of WT formation

Table 4 – Petrophysical Properties of WT Formation

Core Type	Range of Depth	GRI Total Porosity	GRI Gas Porosity	GRI Perm, nD
WT Carbonate Rich	8870 ~ 8980	7.8	2.3	160.8
		4.6	2.3	27.4
		11.2	5.7	596.7
		9.9	1.8	585.0
	Average	8.4	3.0	342.5
WT Quartz Rich	8890 ~ 8990	13.5	8.0	853.7
		8.6	4.0	243.7
		11.2	5.6	591.8
		7.4	2.2	182.6
		8.4	3.0	217.3
		10.7	5.1	352.1
		10.0	4.0	329.5
	Average	10.0	4.6	395.8

Additionally, pore size distribution of each rock type was measured using Micromeritics' Accelerated Surface Area and Porosimetry System ASAP 2020. With approximately 0.5 grams of rock particles from each rock type, adsorption/desorption average pore diameter, BJH adsorption/desorption average pore width, median pore width, and the pore size distribution were measured and generated using its built-in correlation program. The results is shown in **Table 5**, and the pore size distribution for each rock type is shown in **Fig. 8** and **Fig. 9**. Both lithology showed similar distribution of pore size and similar median pore width of 1.5 nm, but WT CR showed slightly higher pore diameter and pore width from adsorption and desorption tests. However, the difference between two rock types are so small that it can be negligible, and it can be concluded that both rock types share a similar nano-scale pore width and pore size distribution throughout the formation.

Table 5 – Pore Size Measurements with ASAP 2020

	Adsorption Average Pore Diameter, nm	Desorption Average Pore Diameter, nm	BJH Adsorption Average Pore Width, nm	BJH Desorption Average Pore Width, nm	Median Pore Width, nm
WT Carbonate Rich	16.20	15.56	19.09	14.47	1.51
WT Quartz Rich	14.15	13.78	13.07	9.02	1.51

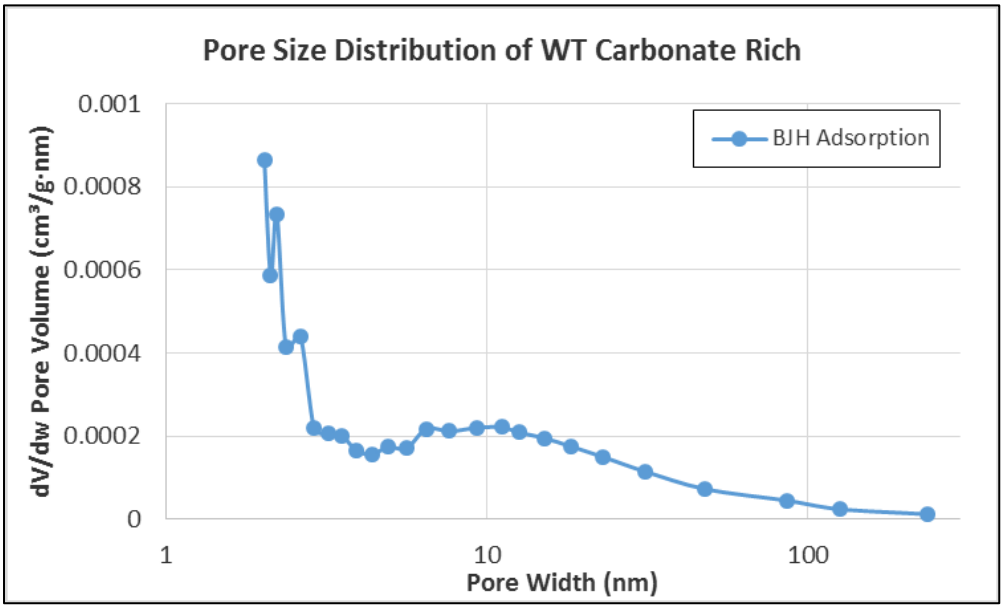

Fig. 8 – Pore Size Distribution of WT Carbonate Rich Cores

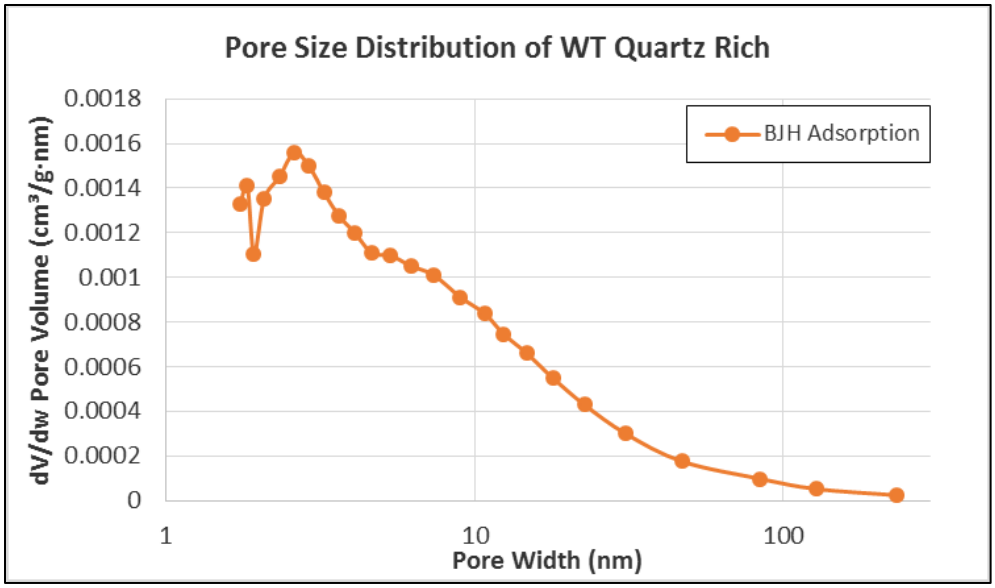

Fig. 9 – Pore Size Distribution of WT Quartz Rich Cores

3.3 Crude Oil

Crude oil used for this investigation was extracted from the same formation as the core samples were collected. 2 gallons of crude oil were provided by COMPANY from the field. The crude oil showed a mildly brown to dark brown color at room condition, as shown in **Fig. 10**. The reservoir temperature (T_{res}) is approximately 155° F (68.3°C), and the density of oil was measured at this temperature. Using Anton Paar's DMA 4100M densitymeter, shown in **Fig. 11,** measured density of the crude oil was 0.77 g/cc, and 41.34 °API at 60°F, and based on this density, it was classified as black oil. Also, this same oil was used with both carbonate rich and quartz rich cores throughout this investigation.

Fig. 10 – Crude Oil Sample of the WT formation at Room Condition

Fig. 11 – Anton Paar DMA 4100M Densitymeter

3.4 Brine / Salts

Water analysis reports for both injected water and produced water were provided by COMPANY. Based on the report, both types of water from the field were primarily composed of 3 cations, calcium (Ca), magnesium (Mg), and sodium (Na), and 3 anions, chloride (Cl), sulfate (SO_4), and bicarbonate (HCO_3). As shown in **Fig. 12**, Chloride occupies 60% of the total ionic components, followed by sodium, calcium, sulfate, bicarbonate and magnesium. To accurately create a laboratory synthetic brine which represents the actual water from the field, molecular weight of each ion was used for calculations. These calculations were used to determine the required salts for the brine, and to calculate the correct concentration of each salt.

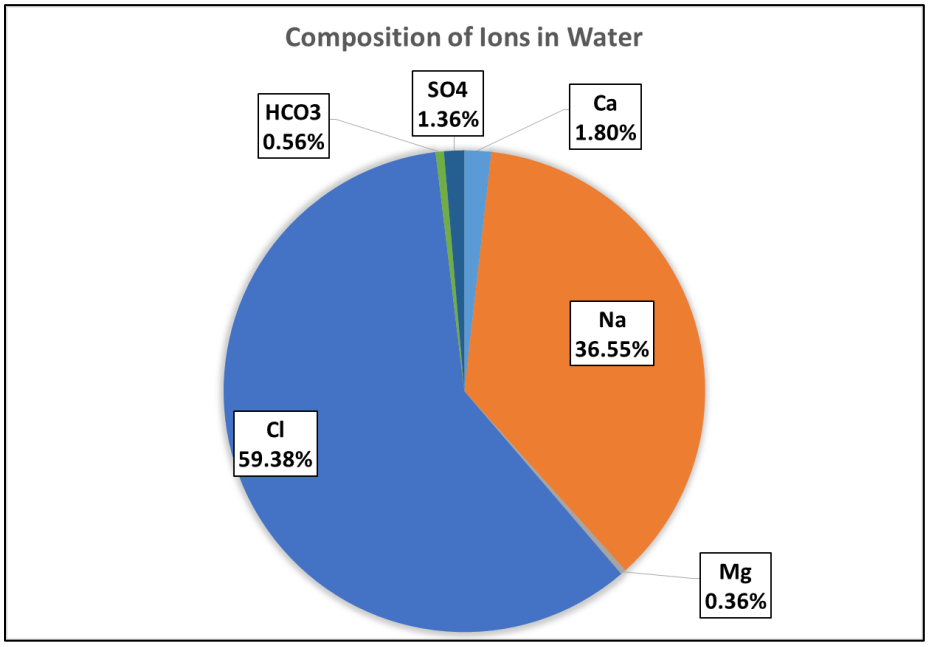

Fig. 12 – Composition of Ions in Water Collected from the Field

Types of salt required to create a synthetic brine were determined to be sodium chloride (NaCl), Calcium Chloride ($CaCl_2$), Magnesium Chloride ($MgCl_2$), Sodium Sulfate (Na_2SO_4), and Sodium Bicarbonate ($NaHCO_3$), and they were purchased from Cole-Parmer. Calculated concentration of each salt is shown in **Fig. 13** in percentage. Sodium Chloride forms a little more than 90% of a synthetic brine, while the other salts are contributing about 10 % combined. The exact amount of each salt is shown in **Table 6,** in a unit of ppm, which stands for parts per million. The unit "ppm" is equivalent of mg/L, and is widely used in the oil and gas industry. The total salinity of this brine is added to be 26,800 ppm, which is same as 26,800 mg/L, or 26.8 g/L, and approximately 2.7 wt.%. This salinity level, then, was multiplied and varied with 9 different multipliers, and 9 cases of salinity level were generated for this investigation. The multipliers for each case, and the corresponding salt concentration in ppm is shown in **Table 7**.

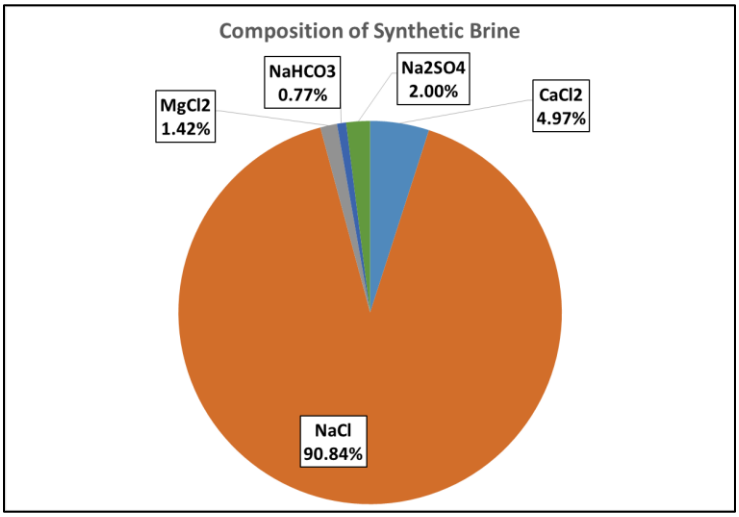

Fig. 13 – Composition of Salts in a Laboratory Synthetic Brine

Table 6 – Concentration of Each Salt for a Synthetic Brine

	Synthetic Brine	
	ppm	Percentage
NaCl	24,350	90.84%
$CaCl_2$	1,330	4.97%
$NaHCO_3$	530	2.00%
$MgCl_2$	380	1.42%
Na_2SO_4	210	0.77%
TDS	**26,800**	**100.00%**

Table 7 – Salinity Levels Tested in this Investigation

Case	Salinity, ppm	Multiplier
1	0	0
2	6,700	0.25
3	13,400	0.5
4	20,100	0.75
5	26,800	1
6	33,500	1.25
7	40,200	1.5
8	53,600	2
9	80,400	3

In addition to the salts listed above, Potassium Iodide (KI) was used for this investigation. KI is known to have the ability to increase the contrast of aqueous phase

solutions in X-Ray Computerized Tomography images, while not affecting important properties of the solution. After multiple trial and error with KI, the necessary concentration of KI which delivers the most effective enhancement to image contrast was determined to be 4 wt. %. This concentration was used for all spontaneous imbibition experiments, and more detailed information about this procedure is explained further in the later sections.

3.5 Surfactants

5 types of surfactant were used in this investigation. Chemical additives were provided by COMPANY and other manufacturers, and each has its own characteristics. Most chemicals showed both nonionic and anionic components such as sulfonate, alcohol, methanol, and glycol. **Table 8** shows more detailed information, nomenclature, components and other important properties.

All 5 chemicals were mixed with 9 types of brines in **Table 7**, above, to form aqueous phase completion solutions for experiments. The concentration of chemicals was kept constant at 1 gpt (gallon per thousand gallon), to analyze the salinity impact on surfactant-mixed completion fluids. The physical properties of chemicals vary as shown in **Fig. 14**, having its own viscosity, color, and scent, but these properties did not stand out when mixed with brines due to low concentration.

Table 8 – Characteristics of Each Surfactant Experimented

Surfactant Name	Code	Type	Primary Components	pH	Flash Point (°C)
Nano-Technology Fluid	NF	Nano Fluid	Isopropyl Alcohol, Citrus Terpenes	5 - 7	> 93
Surfactant 01	S01	Nonionic / Anionic	Alkyl sultaine, Ethylene Glycol, Alcohol, Sodium Chloride	6.8	> 93
Surfactant 02	S02	Nonionic / Anionic	Methanol, Sulfonate	7 - 8	43
Surfactant 03	S03	Nonionic / Anionic	Alkylbenzene sulfonate, Alcohols	5 - 7	> 93
Surfactant 04	S04	Nonionic / Anionic	Alcohols, Methanol	7 - 8	> 104

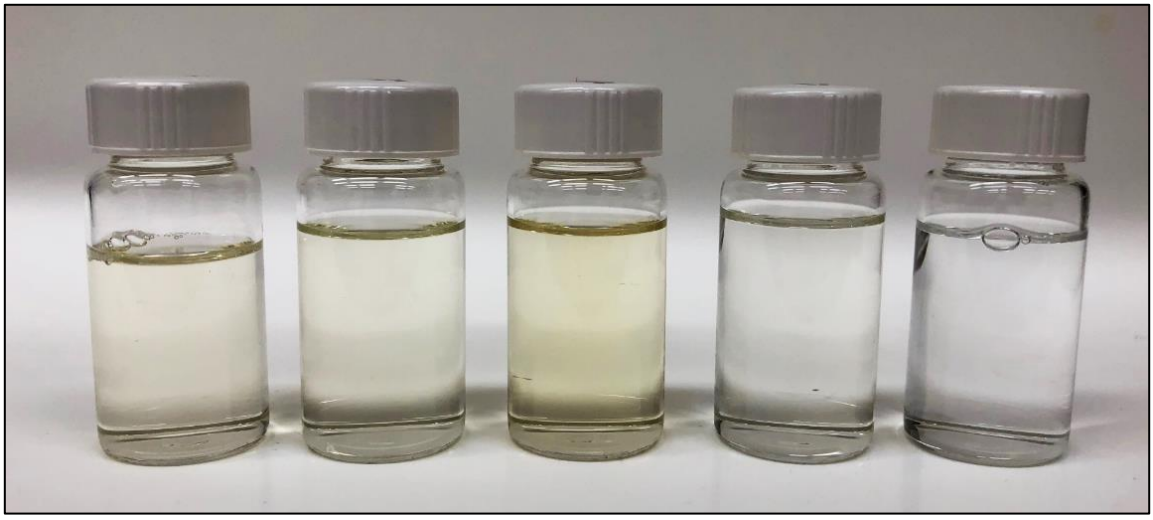

Fig. 14 – Initial Condition of Chemicals at Room Temperature: (From Left to Right) Nano-Technology Fluid, Surfactant 01, Surfactant 02, Surfactant 03, and Surfactant 04

4. EXPERIMENTAL PROCEDURES AND SETUP

4.1 Workflow

This investigation consists of 5 main experiments: zeta potential, interfacial tension, contact angle, spontaneous imbibition, and Computerized Tomography (CT) image scans. The overall workflow of this investigation, and the purpose of each experiment is shown in **Fig. 15**. A set of experiments begins with zeta potential measurement, followed by interfacial tension and contact angle measurements, and spontaneous imbibition with timely CT scans. Each experiment requires its own raw materials, device, method, setup, and technique which is explained in this section.

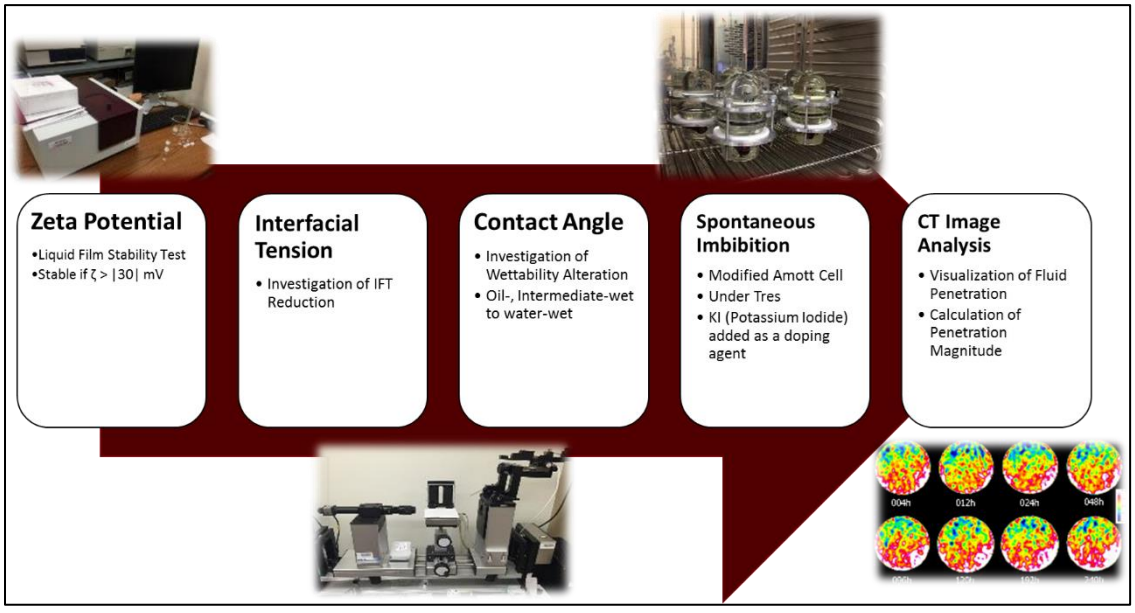

Fig. 15 – Overall Workflow of the Investigation

4.2 Zeta Potential Experiment

Zeta potential, which determines the stability of liquid film surrounding the rock particles, was measured with BrookHaven ZetaPALS device, **Fig. 16**. As described by Zhang (2005), materials needed for this measurement are rock particles and aqueous phase solutions. Rock chunks from core trimming were collected and crushed with mortar and pestle, and filtered through ASTM E-11 325 sieve with a diameter of 42 micron. Both carbonate rich and quartz rich rock particles were generated, and physical properties of each rock type can be found in **Fig. 17.**

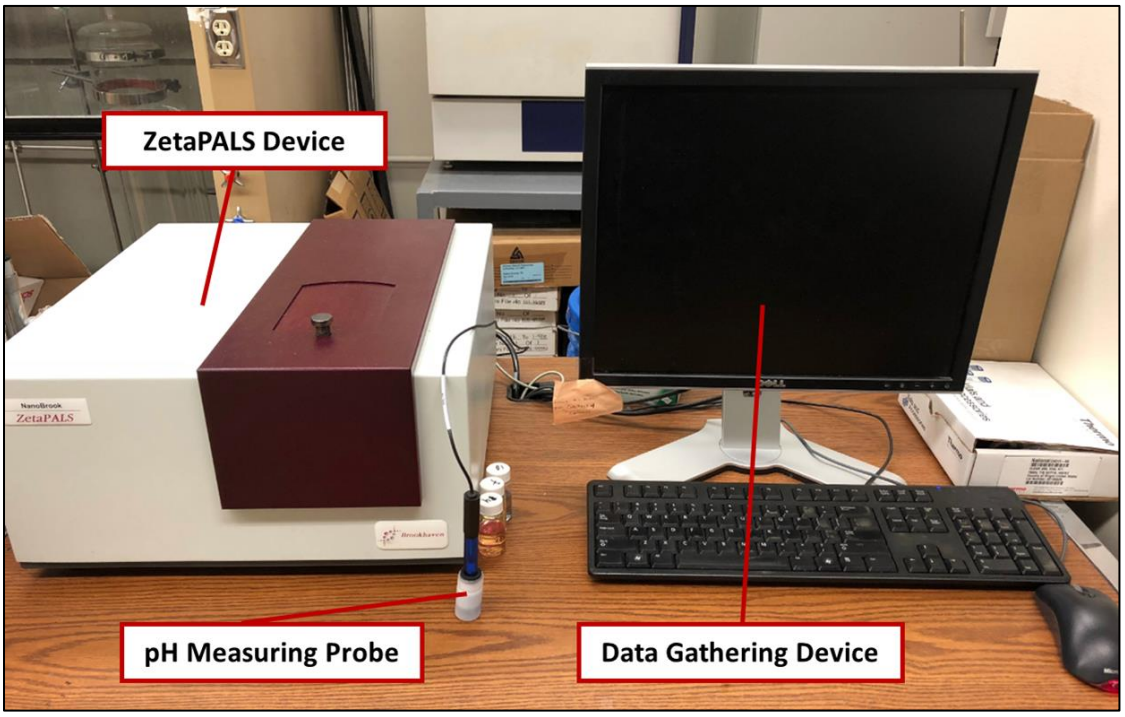

Fig. 16 – Zeta Potential Measurement Device

Fig. 17 – Crushed Rock Particles for Zeta Potential Measurement: WT CR (Left) and WT QR (Right)

Approximately 10~20 mL of aqueous phase solution was prepared for all cases of surfactant and salinity, and triple filtered with 0.2 μm PTFE syringe filter. Then, the rock particles were added to this filtered solution at the ratio of 1:10 or lower. Too much or too little rock particles causes the device to have an error, due to contamination or invisible rock particles, respectively. Therefore, the proper and consistent amount of rock particles must be added to the solution. Then, the solution with rock particles was sonicated at 40 Hz for 1 minute using a Q Sonica Sonicator device, as shown in **Fig. 18**, with its probe immersed into more than a half of fluid height. The sonicated solution, then, was kept in a room condition for another minute for stabilization.

A small amount of this mixed solution, about 1.5 mL, was placed in a small cuvette, and attached to an electrode which is connected to the device for the measurement. Using Phase Analytical Light Scattering (PALS) technique, the electrophoretic mobility

of solution and particles is correlated and calculated for zeta potential. Standard deviation of all measurements were kept under 3.00 mV, and were conducted at 77° F.

This device also has an ability to measure pH level of solutions. As shown in **Fig. 16**, pH probe is directly connected to the device. This probe is immersed into 10~20 mL of aqueous phase solutions to measure their pH level, with detailed pictures in **Fig. 19**. This probe, first, was calibrated using a conditioning fluids with various pH levels. For this experiment, 3-way calibration was performed using fluids with pH 4, 7, and 10. After this calibration process, pH measurements of all aqueous phase solution cases were conducted to observe the relationship between pH and the zeta potential.

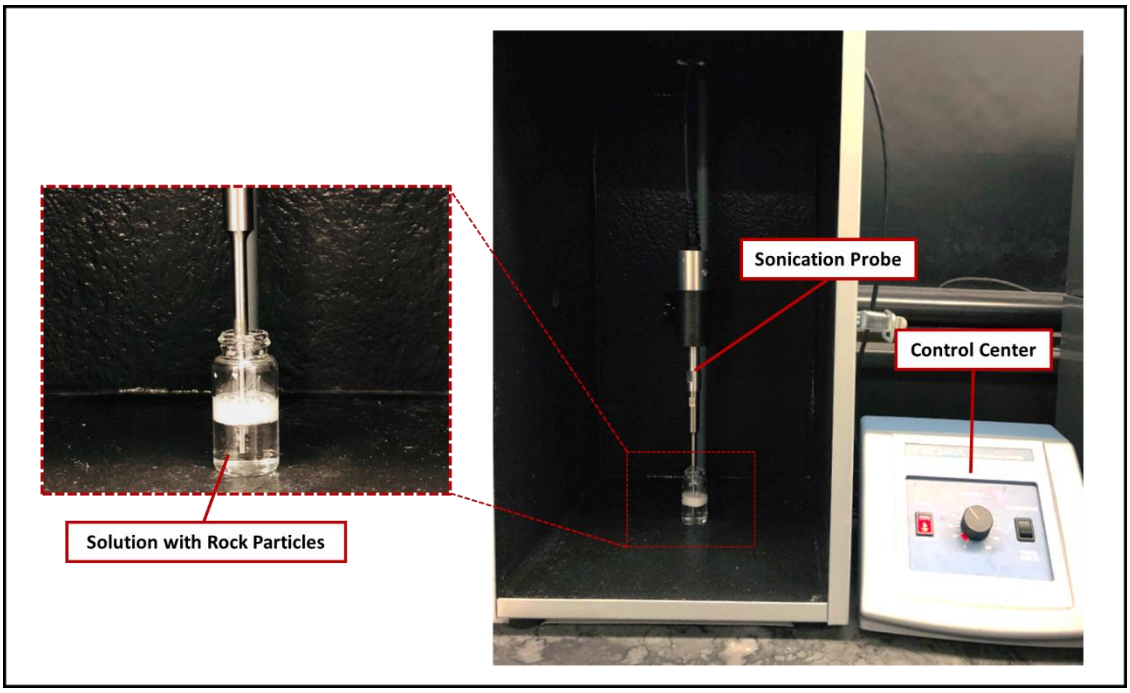

Fig. 18 – Sonication Process for Zeta Potential Measurement

Fig. 19 – pH probe for pH measurements

4.3 Interfacial Tension Experiment

Interfacial tension (IFT) experiment is to analyze the ability of surfactant and salt on IFT reduction. As one of the dominant oil recovery mechanism, buoyant force depends heavily on interfacial tension. This experiment, with the support of contact angle experiment explained later, provides one of the key parameters to investigate oil recovery mechanism more accurately, and potentially delivers a screening criteria for surfactant and salinity level.

IFT between the crude oil and each case of aqueous phase solution was measured with Dataphysics OCA 15 Pro device. **Fig. 20** shows the primary components involved for interfacial tension measurement device. The device setup includes Drop Shape Analyzer (DSA) software, heating plate, temperature control system, temperature sensor,

image capturing optical camera, dispensing unit and lighting source. DSA software allows users to control the necessary components of this device. Temperature control system controls the temperature of heating plate, which is used to heat the solutions to the reservoir temperature, and detects the temperature change of solutions using temperature sensor. Lighting source provides sufficient lights for the optical camera to capture video/image of the experiments.

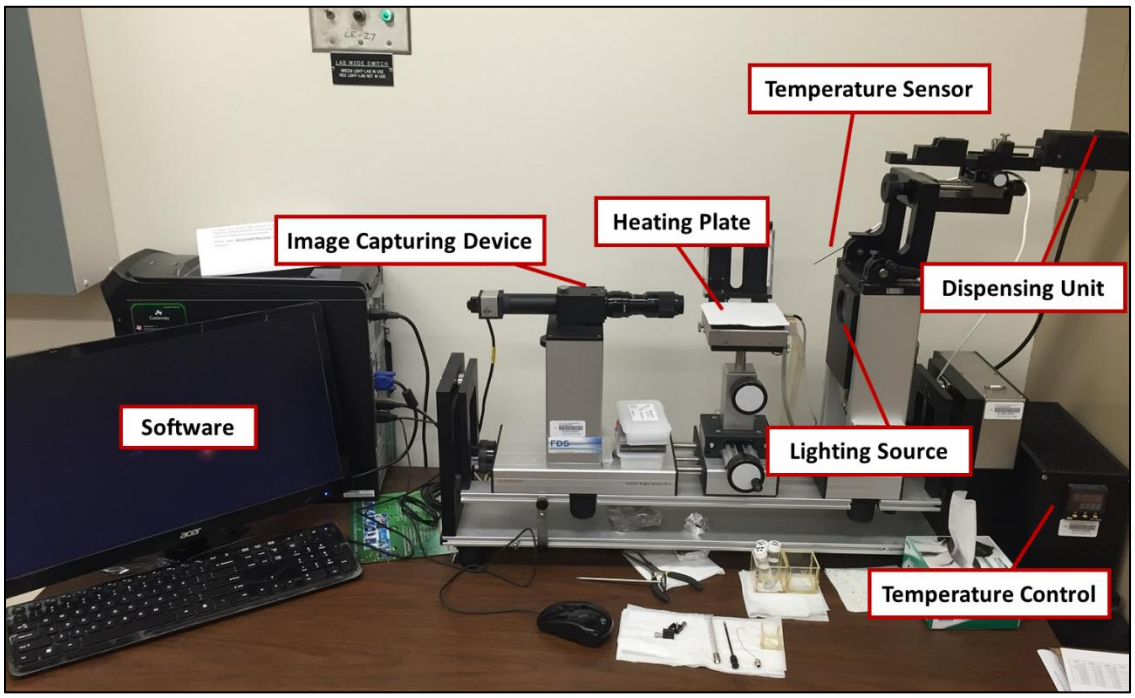

Fig. 20 – Interfacial Tension Measurement Device

Fig. 21 shows a schematic of the IFT measurement setup. As shown below, a cube-shaped container, a syringe and J-shaped capillary needle were used for this experiment. Because of the lighter density of oil compared to aqueous phase solutions, J-shaped capillary needle was required to dispense crude oil upwards, and to form a droplet within the ambient aqueous phase. First, 20~30 mL of aqueous phase solution was placed in a cube container, and heated to the reservoir temperature on the heating plate. A syringe with a capillary needle is lowered until the tip of the needle is submerged into the solution. Then, crude oil is dispensed using the software, and the optical camera records videos of oil droplet until it floats due to buoyancy. At the moment before when the oil droplet is detached from the needle, IFT was calculated based on the density of oil and water, the shape of pendant drop, and the volume injected, using pendant drop – bottom up method. The sample screenshot of the IFT measurement in DSA software is presented in **Fig. 22**, with each component labeled accordingly. All IFT measurements were conducted under the reservoir temperature of 155° F (68.3°C), and assumed that the temperature remains constant throughout the experiment.

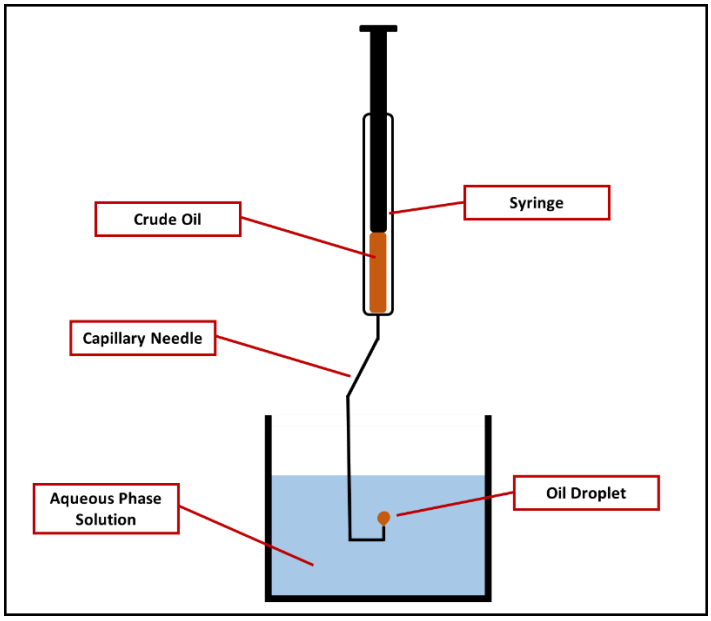

Fig. 21 – Schematic of Interfacial Tension Measurement Setup

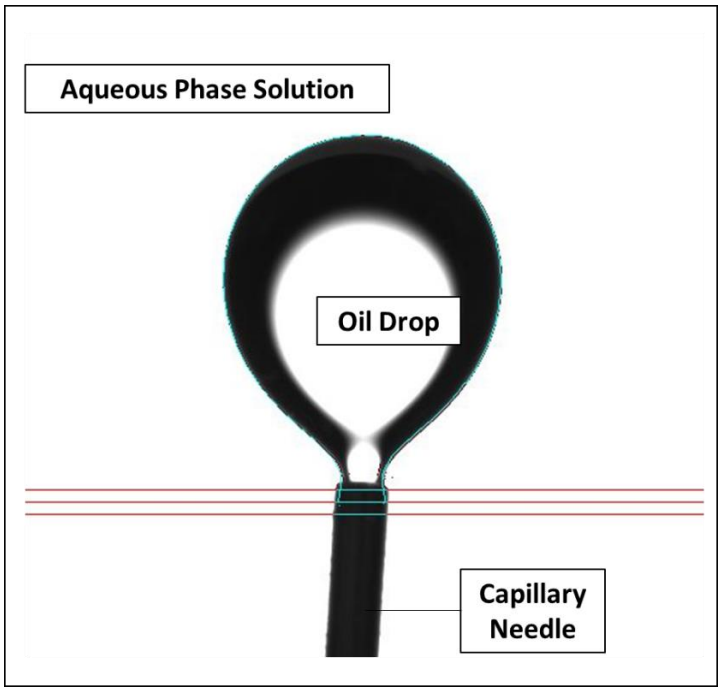

Fig. 22 – Sample Screen of DSA Software for IFT Measurement

4.4 Contact Angle Experiment

Contact angle experiment measures the original wettability of the samples and the wettability alteration ability of surfactant and salt. As mentioned before, wettability alteration of the surface has been the key factor that drives improved oil recovery from the unconventional liquids-rich reservoirs. In order to shift the negative capillary pressure (contact angle of larger than 90) to positive (contact angle less than 90), surface of rocks must be altered to water-wet surface.

Same device as the interfacial tension experiment, Dataphysics OCA 15 Pro, was used for contact angle experiment, with the additional component of rock chip stand. An important required material for this experiment was rock chips. Rock chips were generated from the rock debris collected from trimming process. Both carbonate rich and quartz rich rock debris were cut into small chips, as shown in **Fig. 23**, and polished well to have smooth surfaces. Smooth surface is required to accurately measure the static contact angle of crude oil droplet on the rock surface.

Carbonate rich rock chips initially showed lighter color with white calcite blocks in the matrix, and quartz rich rock chips showed more homogeneous and darker conditions. After generating 5 to 10 rock chips from each rock types, these rock chips were placed in a small container with crude oil, and stored in the oven for aging process. Aging, which is a process of restoring core samples to its original reservoir state, was conducted through temperature-drive mechanism at reservoir temperature of 155° F (68.3°C) for at least 3 weeks, as shown in **Fig. 24**.

Fig. 23 – Generated Rock Chip Samples and the Size Comparison (From Left to Right: Size 8.5 Aggie Ring, WT CR Rock Chips, and WT QR Rock Chips

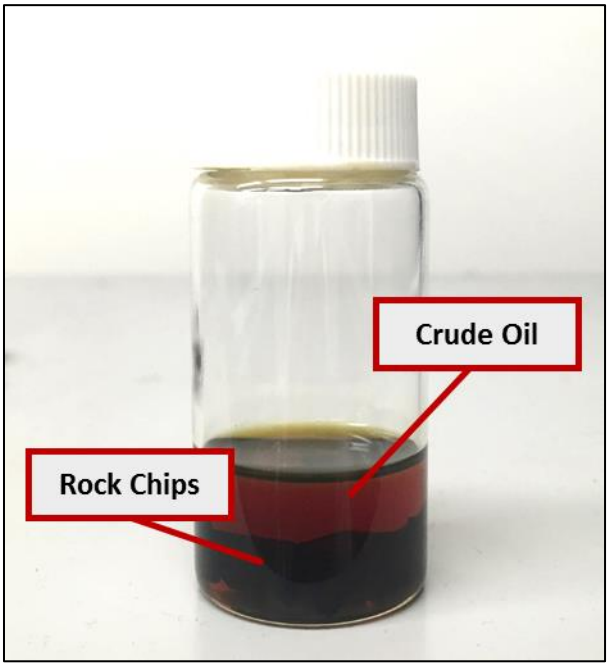

Fig. 24 – Aging of Rock Chip Samples for Contact Angle Measurements

As mentioned earlier, rock chip stand is an additional component needed for this experiment. One side of this tock chip stand has a void space for a J-shaped capillary needle to access to the surface of rock chips. Also, this stand allows rock chips to sit stably, and to be recorded accurately with image capturing device for observing behaviors of oil droplet on rock surface. **Fig. 25** shows a detailed schematic of contact angle measurement throughout this investigation, and a sample screenshot of DSA software when measuring contact angle is presented in **Fig. 26**, with corresponding labels for the material used. All experiments were conducted under the reservoir temperature, and measured at least 10 times with 5-10 different rock chips to accurately estimate and observe the wettability alteration ability of surfactant and salinity.

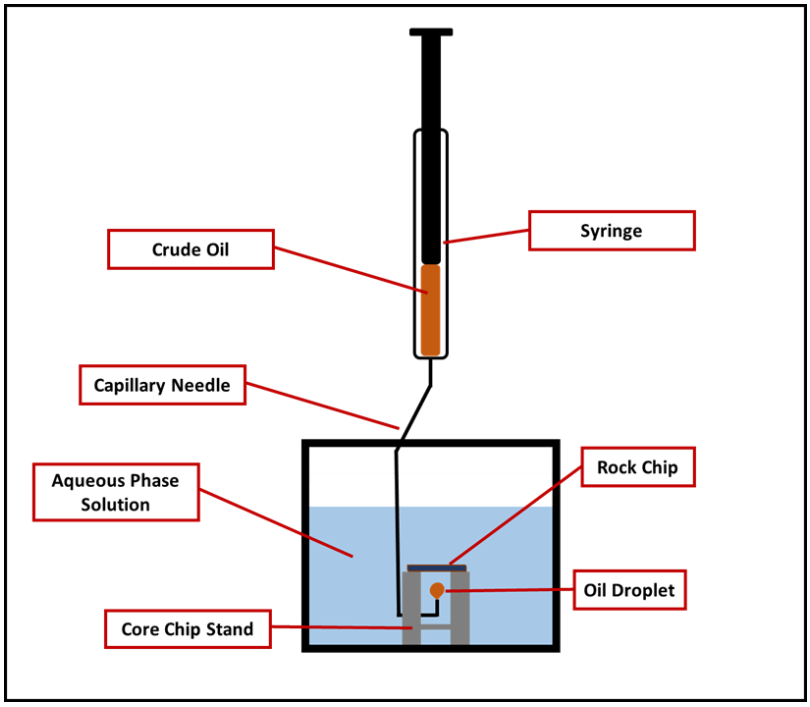

Fig. 25 – Schematic of Contact Angle Experiment

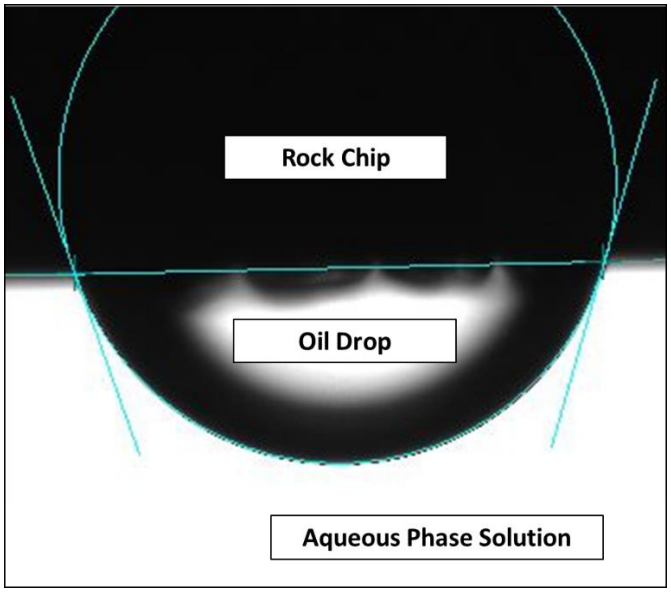

Fig. 26 – Sample Screen of DSA Software for Contact Angle Measurement

4.5 Spontaneous Imbibition Experiment

Spontaneous imbibition experiment is the final stage of the workflow for this investigation. After experimenting all cases of aqueous phase solution through zeta potential, interfacial tension, and contact angle measurement, surfactant types and salinity levels were selected to perform this imbibition. This experiment was used to observe and analyze the performance improvement of completion fluids, as well as interactions of surfactant, salt and rock during the imbibition process. Through this experiment, the impact of wettability alteration and interfacial tension reduction can be analyzed, and the relationship of each parameter to the ultimate oil recovery, and the dominant oil recovery mechanism can be concluded more in detail. Also, utilizing this experiment with Computerized tomography technology, which is explained in the next section, supports

visual inspections of the aqueous phase solution penetrating into the matrix during the imbibition process.

The most important material for this experiment is core sample. Like the rock chips used in contact angle experiments, trimmed core samples, like **Fig. 4**, are aged with the same crude oil. Size of cores was similar for all experiments, with 1 inch in diameter and about 2.5 inches in length. Aging process for core is similar to that of rock chip, but cores require much longer aging periods compared to small rock chips due to its size and the time required for oil, gas, or water inside the pores to be replaced by the crude oil. Core sample is stored in a container with crude oil, as in **Fig. 27**, and placed in an aging oven. For this investigation, all core samples were aged for at least a month, under the reservoir temperature of 155° F. Although the residual oil saturation could not be estimated, this investigation was based on the assumption of 100 % oil saturation with 8 % porosity for all core samples used.

A modified Amott Cell apparatus was used for spontaneous imbibition experiments. This cell is designed to hold a core stand and a core sample, immersed in the aqueous phase solution. On top of this cell, there is a graduated cylinder portion with tick marks to measure any produced oil from the imbibition process. **Fig. 28** shows the overall schematic of the modified Amott cell. Core stand is set on the bottom portion of the cell, and a core sample explained in the previous paragraph sits on top. Then, the top portion is mounted using the two steel O-ring, two smaller PTFE O-ring, and three screws to firmly seal the cell for the duration of the imbibition experiment under high temperature. Then, blended aqueous phase solution is added to the cell for the core to be completely immersed

in the fluid. After the cell is completely secured with no sing of leaking fluids, it is placed in the imbibition oven under the reservoir temperature for at least ten days.

Fig. 29 shows the setup of a typical spontaneous imbibition experiment under the reservoir temperature. Throughout the experiment, the graduated cylinder part on the top portion of the cell is used for measuring produced oil from the core sample. Each small tick marks represent 0.05 mL, with bigger tick marks representing 0.25 mL. The volume of produced oil is measured at a certain time interval, and the final volume of oil measured from this cell is used for recovery factor calculation presented in the later section.

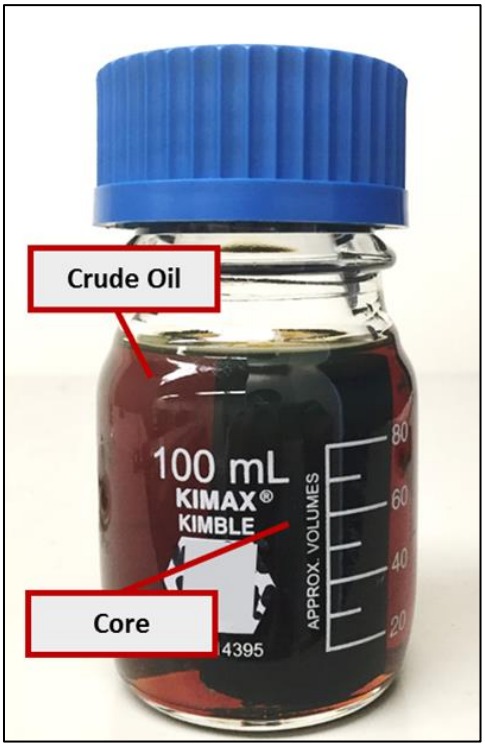

Fig. 27 – Aging of a Core Sample for Spontaneous Imbibition Experiments

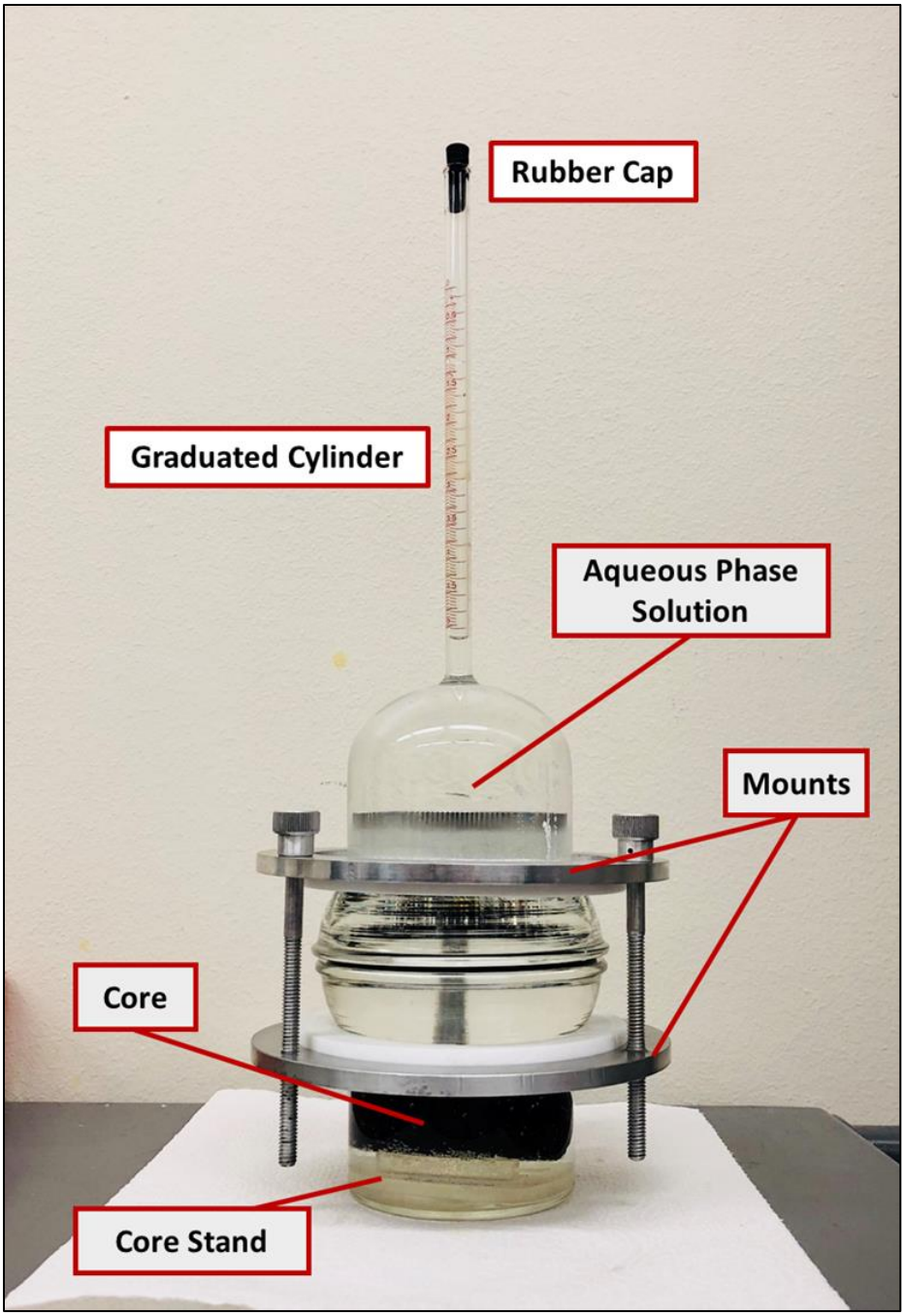

Fig. 28 – Setup of a Modified Amott Cell for Spontaneous Imbibition Experiments

Fig. 29 – A Setup of a Spontaneous Imbibition Experiment

4.6 Computerized Tomography Scans

Computerized Tomography (CT) technology provides the ability to visually inspect the fluid penetration to the core during the spontaneous imbibition experiments. This non-destructive imaging technology measures the attenuation of X-ray beams rotating around the object to generate cross sectional images of the object (Valluri et al. 2016). After setting up the spontaneous imbibition experiments, as explained in the previous section, each modified Amott cell is scanned with CT machine at a certain time interval. During the early time of the experiment, cells are scanned every four hours, and the time interval gradually increases until the termination of the each imbibition experiment.

Toshiba Aquilion TSX-101A Medical CT-Scan device, **Fig. 30**, was used for this part of the experiment. The key CT scan parameters are as following: helical scans, 135 kV, 280 mA, 1 second rotation time, 0.5 mm of slice thickness, and 0.3 mm of interval. Due to small size of the core samples used for imbibition, a small-small (SS) field of view was used to obtain clear CT images.

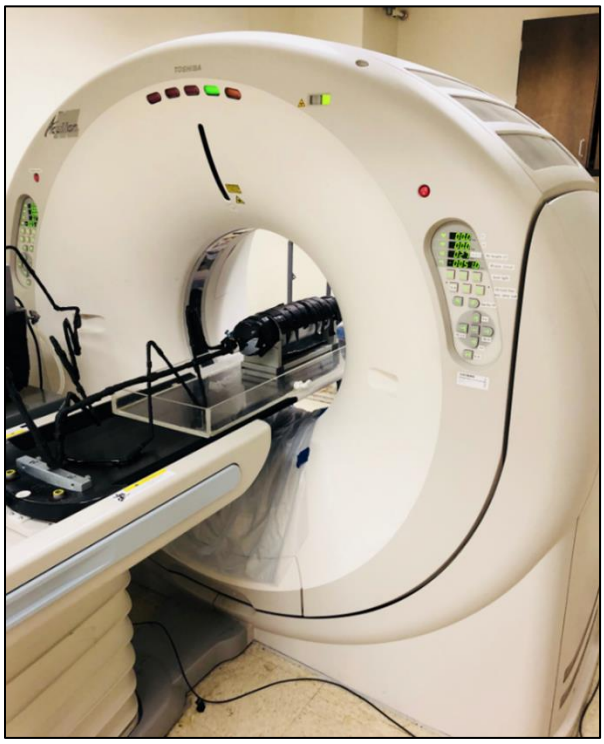

Fig. 30 – Computerized Tomography Machine

The image analysis was performed with ImageJ, an open source software, and examples of CT images are shown in **Fig. 31**. This software was used to measure the CT number, in Hounsfeld Units (HU). This CT number is represented based on the density of

any phase present within the object. Throughout this investigation, the CT number was primarily based on the density of rock, crude oil, and air. The average CT number of the materials used in this investigation are as following: air with -1000 HU, oil with around -200 to -300 HU, aqueous phase solutions from 700 ~ 1000 HU, and core samples from 2000 ~ 3000 HU. Aqueous phase solutions, specifically, contain 4 wt. % of potassium iodide (KI) as a doping agent, which makes the CT number to reach close 1000 HU and helps visually inspect the fluid penetration in the CT images. The average CT number of a whole core at each time is analyzed with ImageJ, and the penetration magnitude, suggested by Alvarez et al. (2014), was calculated based on the **Eq. 7** below to quantitatively analyze the indication of fluid imbibition.

$$Penetration\ Magnitude\ (PM) = CT_t - CT_{base} \quad \cdots\cdots\cdots\cdots\cdots\cdots\cdots\cdots\cdots\cdots\cdots\cdots\cdots\cdots \quad (7)$$

CT_t is the average CT number at a certain time, and CT_{base} is the initial average CT number of the core. As mentioned before, oil has low negative CT number while aqueous phase solutions have high positive CT number. Positive penetration magnitude indicates that the average CT number at the end of spontaneous imbibition experiment is higher than the initial average CT number. This can be concluded that as the aqueous phase solution is replacing the oil inside of the core, the average CT number of core increases due to penetration of high density solutions. Therefore, it has been proven that the higher penetration magnitude corresponds to higher oil recovered during the imbibition.

Generally, throughout this investigation, penetration magnitude was calculated based on the average CT number at 240 hour as CT_t, and at 4 hour as base. Because the density is temperature sensitive parameter, CT_{base} was measured after 4 hours from the

start of imbibition experiment, assuming that it takes approximately 4 hours for the entire system of a modified Amott cell to reach the reservoir temperature. Also, to mitigate the fluctuation of average CT number for each periodical scan, time it takes to transport a modified Amott cell from the imbibition oven to the CT scanner was minimized.

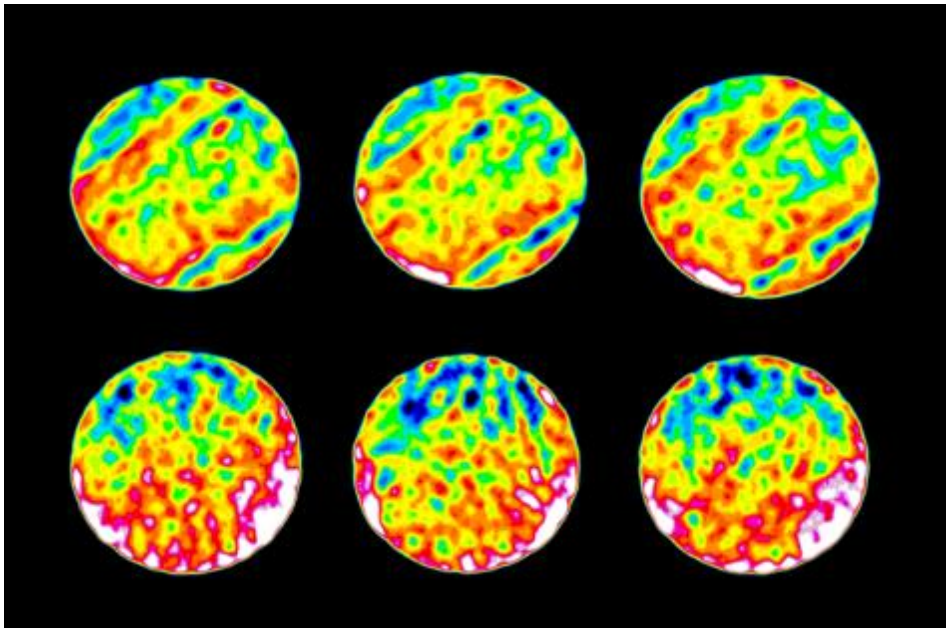

Fig. 31 – Scanned Cross-sectional CT Image Examples of WT Cores

5. RESULTS

5.1 Zeta Potential

As explained in the background information, total of fifty four cases of aqueous phase solution, composed of five chemical-added solutions and a brine at nine different salinity levels, were tested. Also, for zeta potential, all solutions were sonicated, stabilized, calibrated, and measured with two types of rock particles, carbonate rich and quartz rich, to determine the difference in liquid film stability and their electrophoretic behaviors. Along with zeta potential measurement, pH for each solution was measured to see any noticeable change and impact of pH level on zeta potential.

For all fluid cases with both rock types, the magnitude of zeta potential showed decreasing trend with increasing salinity. All solutions started at a stable negative zeta potential of lower than -30 mV, but all resulted in a value close to 0, some even to low positive zeta potential, in higher salinity. These results indicate that the repulsive energy between rock particles is reduced due to thinning of electrical double layer when the salinity is increased to above certain ionic strength. Also, this extreme thinness of electrical double layer on both rock types causes the surface to become even more hydrophobic, not creating an effective adsorption of either surfactant or salts due to low force to keep rock particles apart from each other. Therefore, this can be concluded that the oil-wet, or oleophilic surface of the rock is less likely to experience strong wettability alteration even when exposed to surfactant and salt ions throughout the contact angle or spontaneous imbibition experiments.

These results also supported to confirm the analysis on the surface charge of each rock type. In general, quartz sand particles show a negative surface charge in neutral solution, while carbonate particles are known to have a positively charged surface (Jada et al. 2006). In this investigation, zeta potential of quartz rich particles showed stronger negative values compared to carbonate rich particles, which indicates that the presence of calcite blocks within the carbonate rich rocks influence the surface charge of the formation. Additionally, pH level had almost negligible sensitive to the salinity, because most of salts used for this experiment were neutral salts. H^+ and OH^- ions, which are the pH determining ions that enter the inner part of the electrical double layer and interact with the surface, were not present enough to alter pH to either acidic or basic level.

Overall, all measurements for zeta potential were measured with the standard deviation of less than 3.00 mV. The results of zeta potential, pH, and standard deviation for each fluid are shown in **Table 9** through **Table 14**, and **Fig. 32** through **Fig. 37**. The overall comparison for all fluid cases at different salinity is also presented in **Fig. 38**, and the trend of zeta potential for each lithology can be found in **Fig. 39** for carbonate rich rock particles and **Fig. 40** for quartz rich. Note that, the quantitative comparison of the numerical values is not as significant as the weakening trend or behavior of zeta potential, because of many variables associated with heterogeneity of rock particles or the chemical reaction of surfactants in open room condition.

Table 9 – Zeta Potential Measurements of Brine at Different Salinity

Zeta Potential*, mV				
Fluid	**ppm**	**pH**	**Carbonate Rich**	**Quartz Rich**
Water	0	7.10	-35.89	-35.98
	6,700	7.38	-23.94	-24.18
	13,400	7.44	-11.99	-12.38
	20,100	7.93	-11.71	-10.03
	26,800	7.58	-11.42	-7.68
	33,500	7.69	-4.94	-6.82
	40,200	7.81	1.54	-5.96
	53,600	7.61	5.79	-2.79
	80,400	7.23	5.63	1.33
* Standard Deviation: < 3.00 mV				

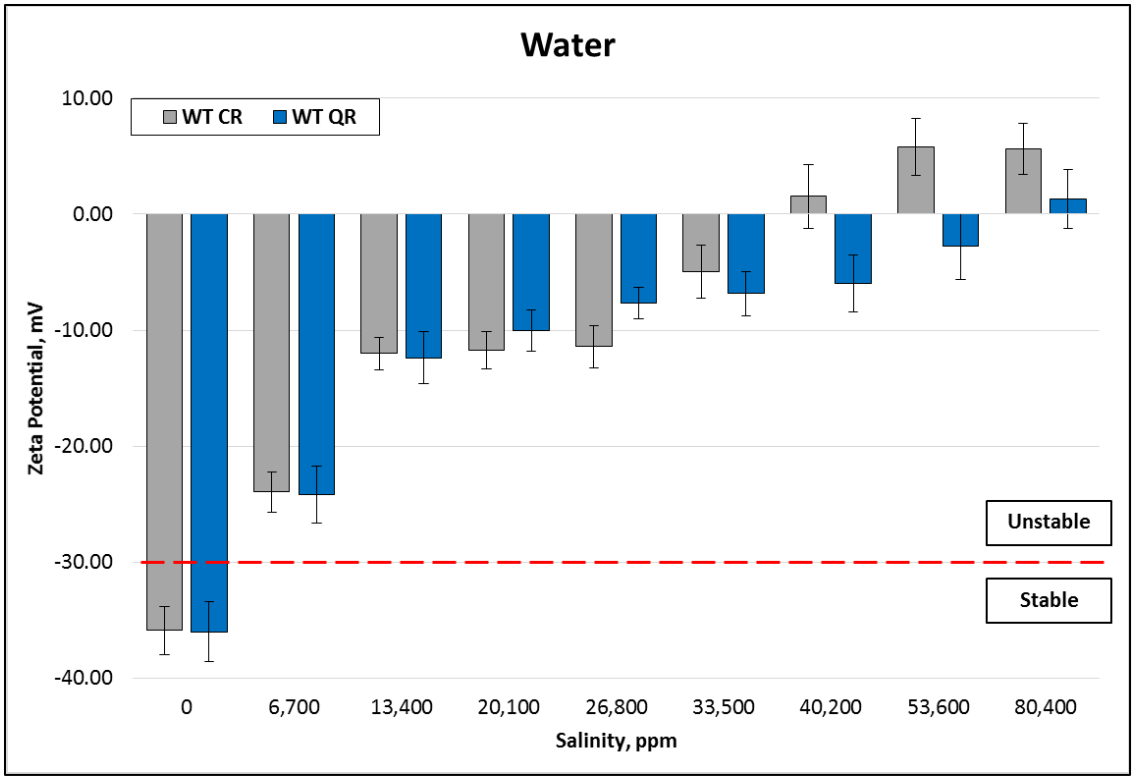

Fig. 32 – Zeta Potential Trend of Brine at Different Salinity

Table 10 – Zeta Potential Measurements of Nano-tech Fluid at Different Salinity

Zeta Potential*, mV				
Fluid	ppm	pH	Carbonate Rich	Quartz Rich
NF	0	7.18	-26.88	-40.42
	6,700	7.32	-18.76	-24.78
	13,400	7.47	-10.63	-9.14
	20,100	7.61	-8.69	-7.19
	26,800	7.76	-6.75	-5.23
	33,500	7.69	-3.00	-4.54
	40,200	7.63	0.75	-3.84
	53,600	7.51	1.08	-0.61
	80,400	7.33	3.22	3.58
* Standard Deviation: < 3.00 mV				

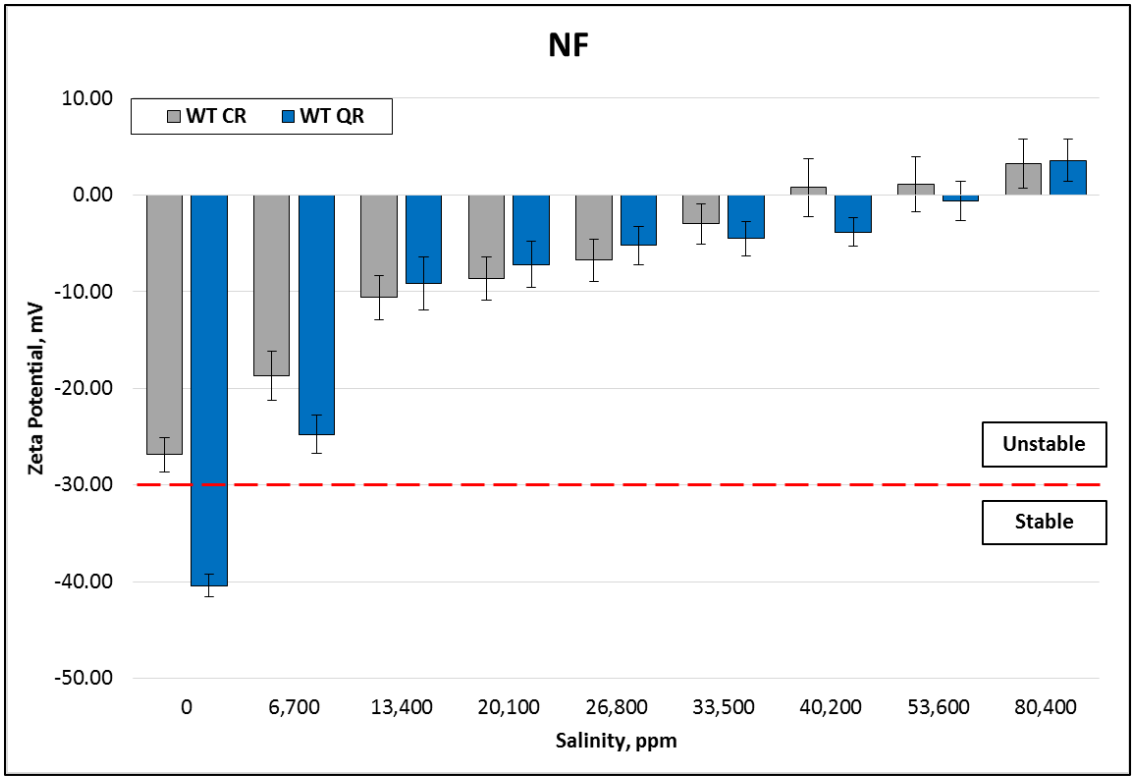

Fig. 33 – Zeta Potential Trend of Nano-tech Fluid at Different Salinity

Table 11 – Zeta Potential Measurements of Surfactant 01 at Different Salinity

Zeta Potential*, mV				
Fluid	**ppm**	**pH**	**Carbonate Rich**	**Quartz Rich**
S01	0	6.90	-58.91	-56.84
	6,700	7.12	-39.13	-41.60
	13,400	7.34	-19.34	-26.35
	20,100	7.55	-21.42	-22.88
	26,800	7.76	-23.49	-19.41
	33,500	7.71	-16.79	-15.12
	40,200	7.66	-10.09	-10.83
	53,600	7.56	-6.80	-6.40
	80,400	7.51	-5.23	-9.48
* Standard Deviation: < 3.00 mV				

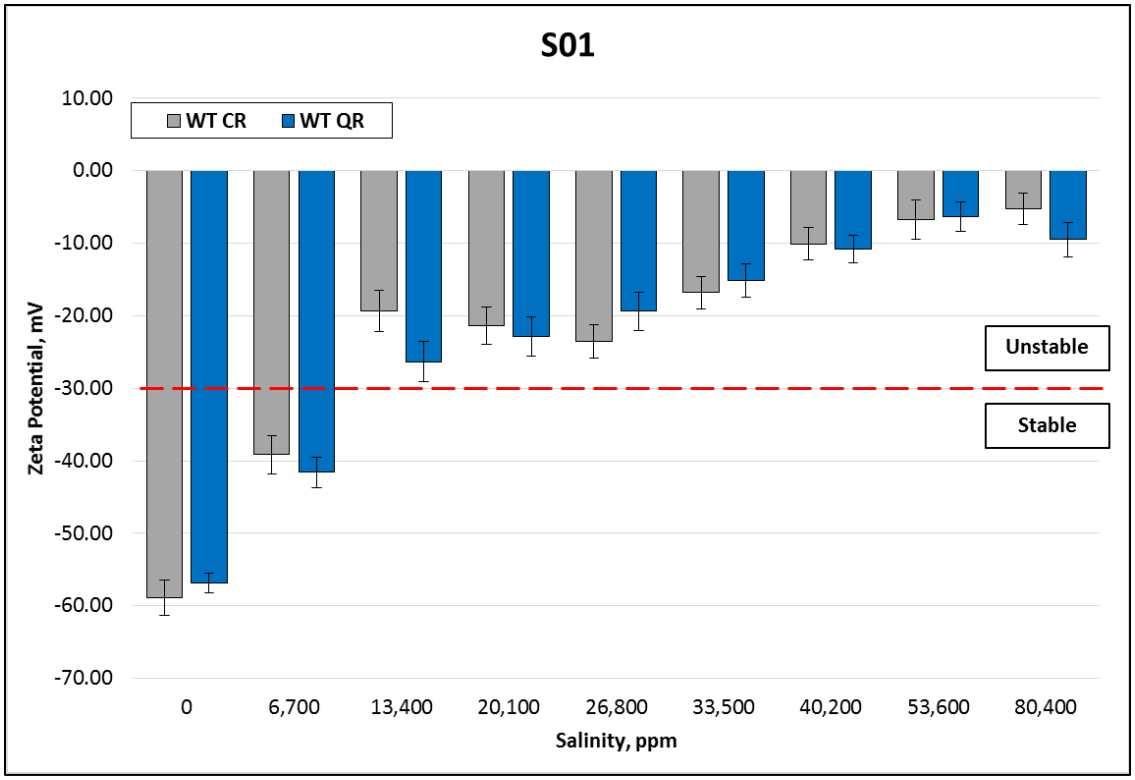

Fig. 34 – Zeta Potential Trend of Surfactant 01 at Different Salinity

Table 12 – Zeta Potential Measurements of Surfactant 02 at Different Salinity

Zeta Potential*, mV				
Fluid	ppm	pH	Carbonate Rich	Quartz Rich
S02	0	7.12	-42.63	-56.88
	6,700	7.29	-29.50	-36.43
	13,400	7.47	-16.36	-15.98
	20,100	7.64	-11.91	-12.95
	26,800	7.81	-7.46	-9.92
	33,500	7.73	-6.66	-9.11
	40,200	7.65	-5.86	-8.30
	53,600	7.49	-4.25	-6.68
	80,400	7.51	-4.89	-2.79
* Standard Deviation: < 3.00 mV				

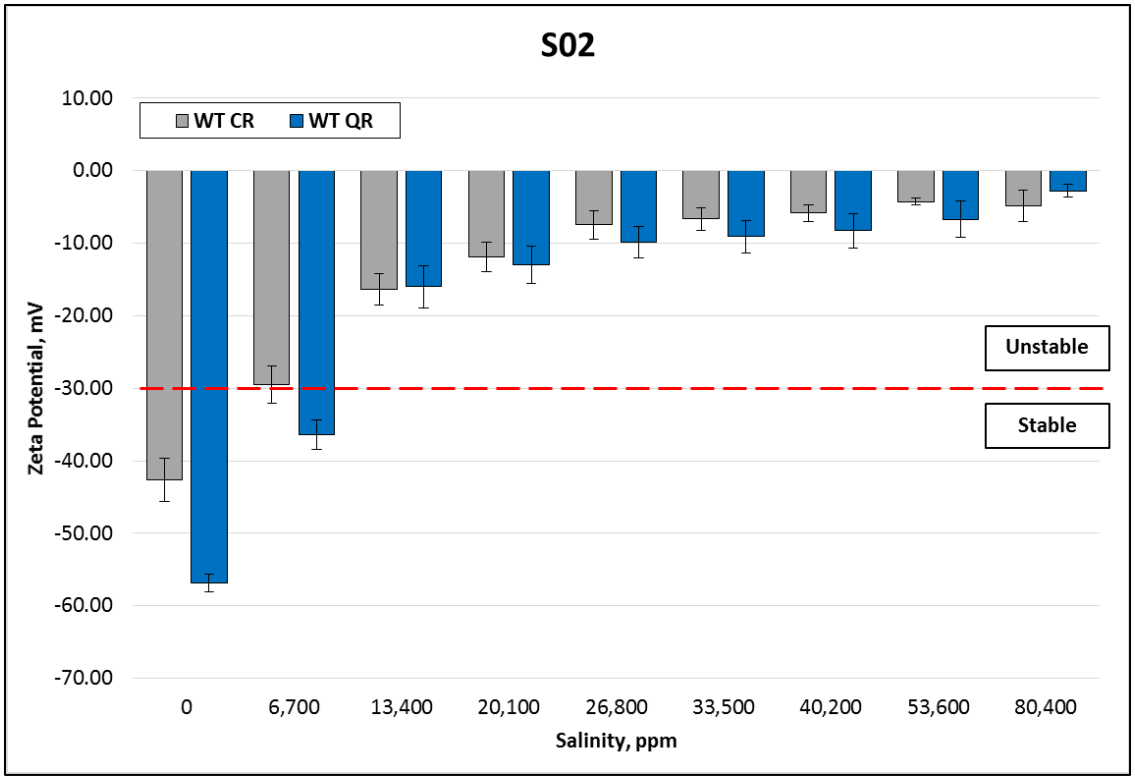

Fig. 35 – Zeta Potential Trend of Surfactant 02 at Different Salinity

Table 13 – Zeta Potential Measurements of Surfactant 03 at Different Salinity

Zeta Potential*, mV				
Fluid	ppm	pH	Carbonate Rich	Quartz Rich
S03	0	6.06	-34.11	-58.81
	6,700	6.46	-25.33	-41.13
	13,400	6.86	-16.55	-23.45
	20,100	7.26	-12.15	-17.16
	26,800	7.67	-7.74	-10.87
	33,500	7.63	-7.54	-9.78
	40,200	7.59	-7.34	-8.69
	53,600	7.51	-6.94	-6.51
	80,400	7.45	-6.06	-0.47
* Standard Deviation: < 3.00 mV				

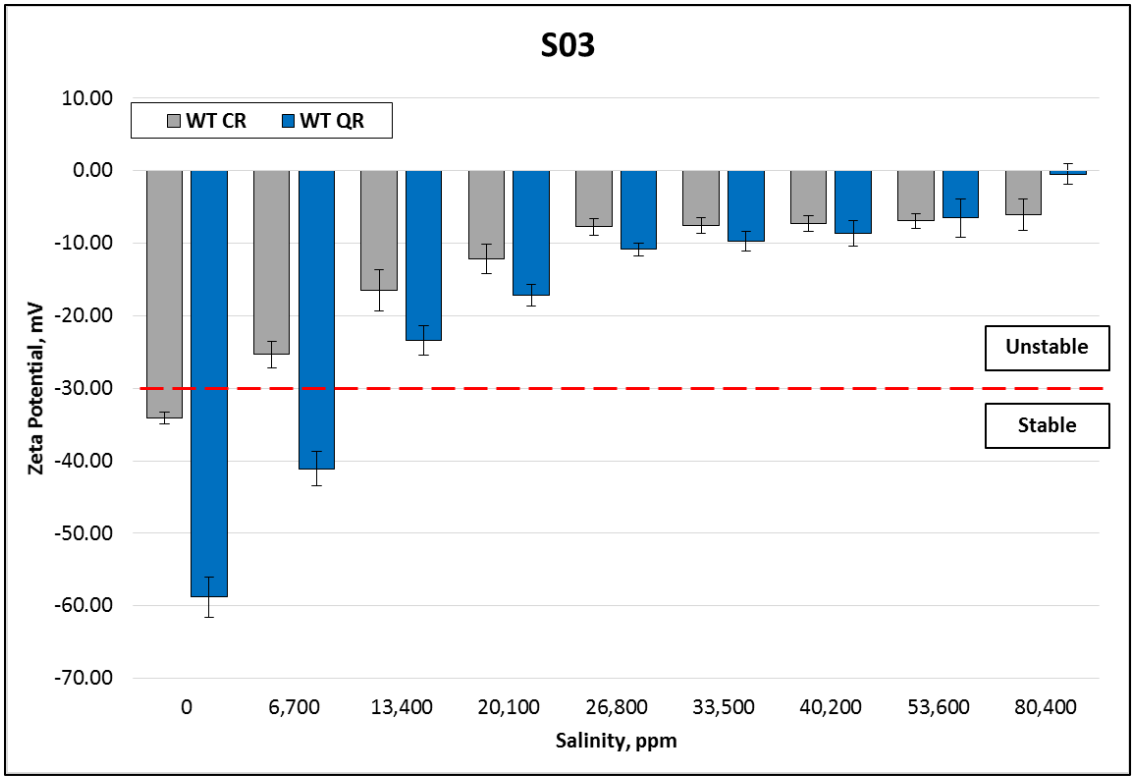

Fig. 36 – Zeta Potential Trend of Surfactant 03 at Different Salinity

Table 14 – Zeta Potential Measurements of Surfactant 04 at Different Salinity

Zeta Potential*, mV				
Fluid	**ppm**	**pH**	**Carbonate Rich**	**Quartz Rich**
S04	0	5.98	-33.79	-53.07
	6,700	6.42	-20.67	-30.37
	13,400	6.85	-7.54	-7.66
	20,100	7.29	-7.12	-7.89
	26,800	7.73	-6.69	-8.11
	33,500	7.68	-5.57	-6.46
	40,200	7.64	-4.45	-4.81
	53,600	7.56	-2.21	-1.50
	80,400	7.31	4.70	0.65
* Standard Deviation: < 3.00 mV				

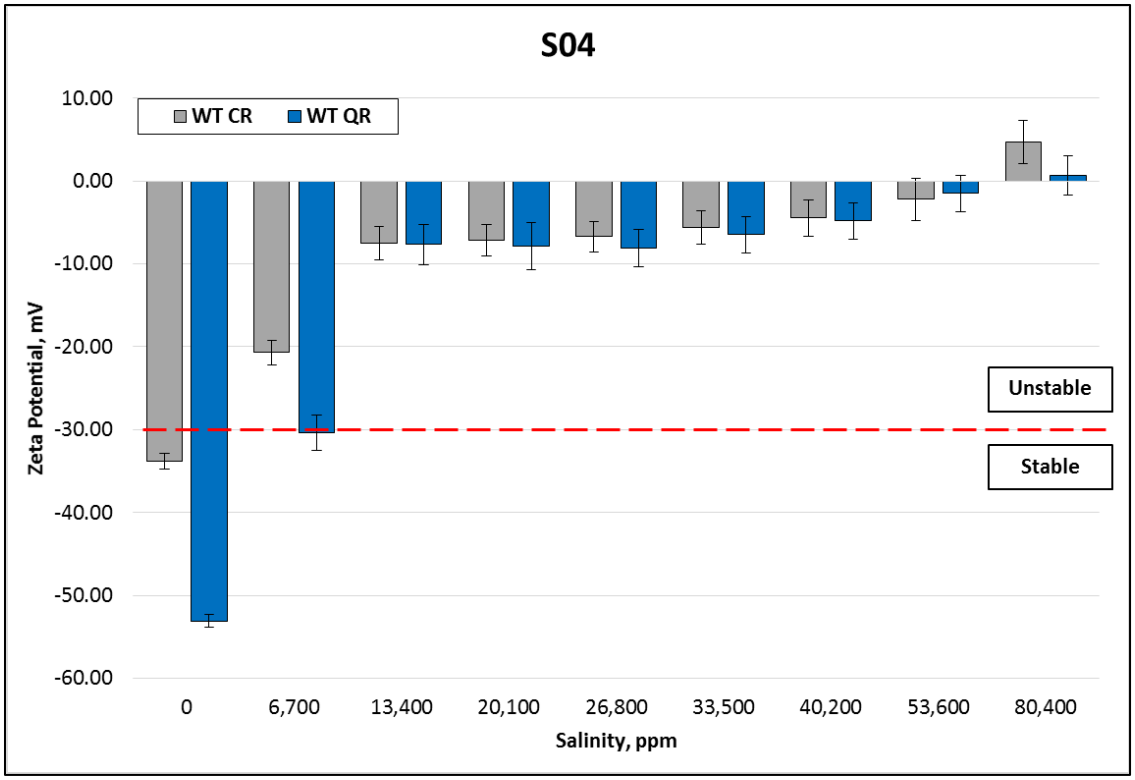

Fig. 37 – Zeta Potential Trend of Surfactant 04 at Different Salinity

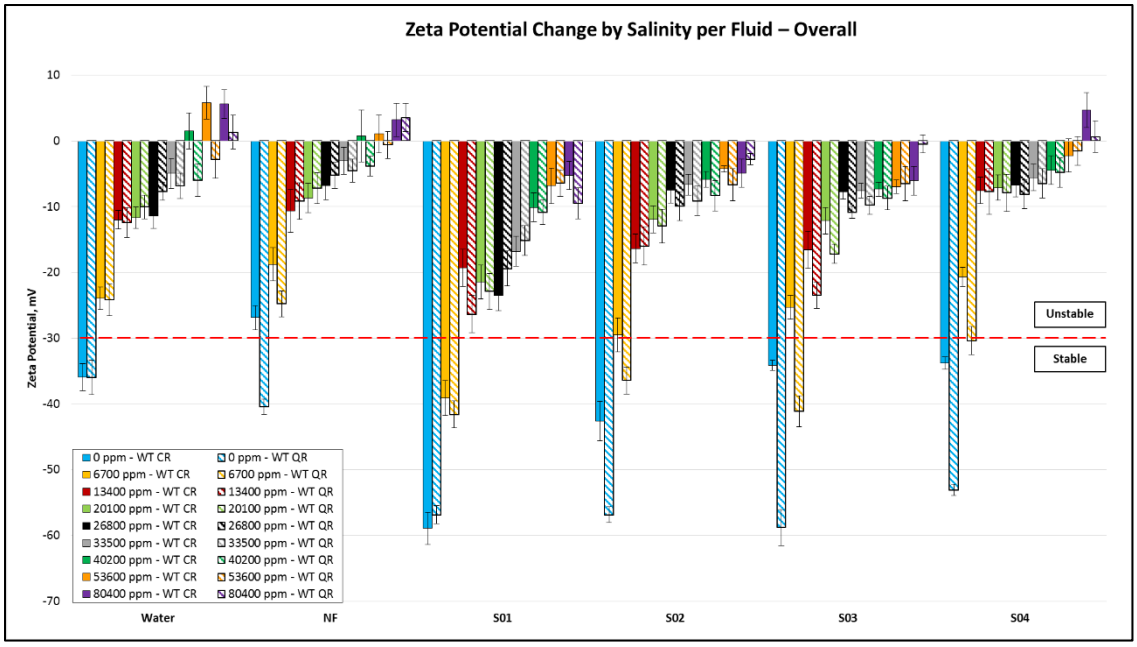

Fig. 38 – The Overall Comparison of Zeta Potential for All Cases

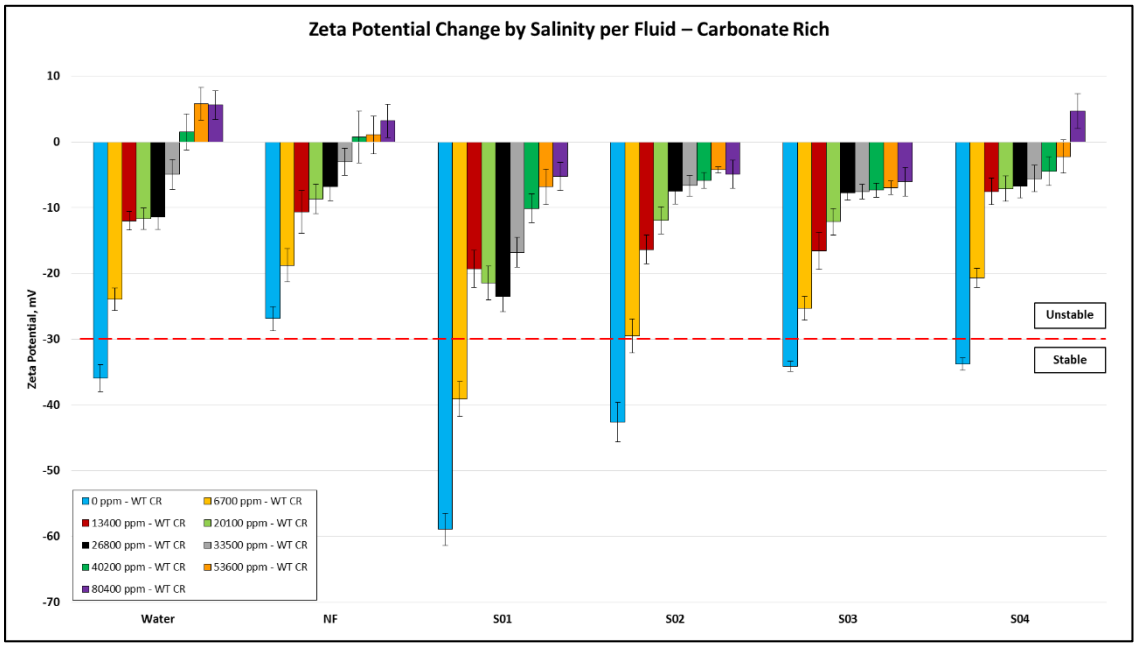

Fig. 39 – The Overall Comparison of Zeta Potential Trend for WT CR Particles

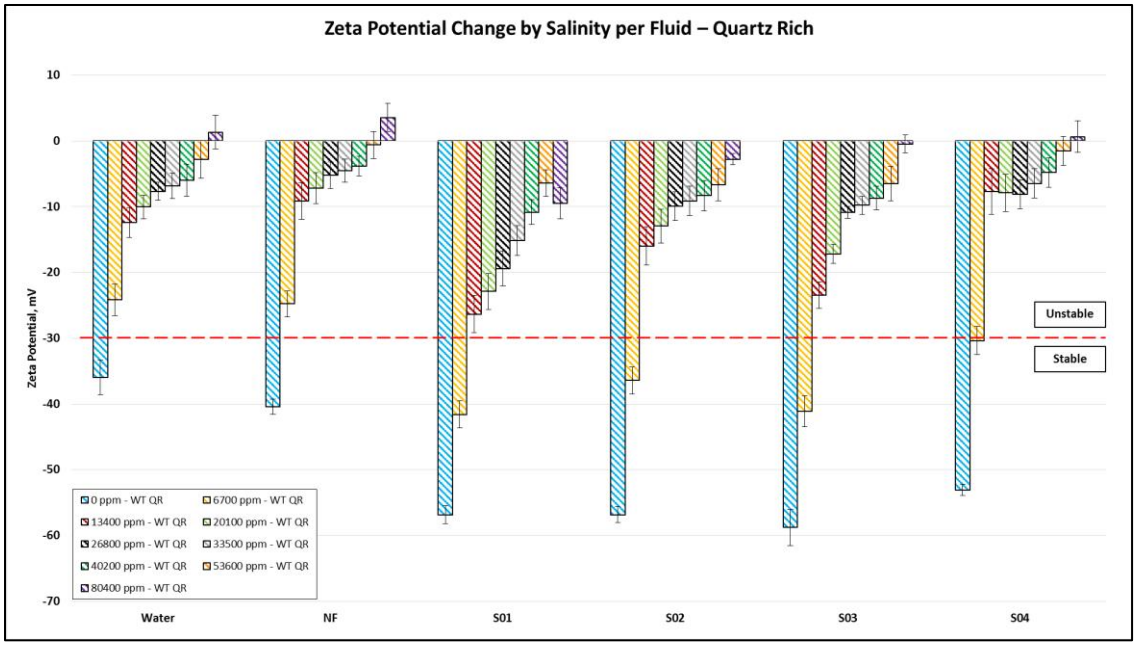

Fig. 40 – The Overall Comparison of Zeta Potential Trend for WT QR Particles

5.2 Interfacial Tension

Interfacial tension between crude oil and fifty four cases of aqueous phase solution was measured. Unlike zeta potential, IFT for two lithology was not necessary because the same crude oil was used for both rock types in this investigation.

It was observed that the interfacial tension is strongly affected by the presence of both surfactant and salt in the solutions. Initial IFT of no salinity water, distilled water, and crude oil was 24.66 mN/m, which is the highest IFT of all cases, but once surfactant was added at a concentration of 1 gpt, IFT was reduced to more than 50% of the initial value. Furthermore, with the addition of salinity, IFT reduced to even lower value of as low as 0.70 mN/m. For water without chemical additives, increasing salinity resulted in a

strong reduction of IFT. At low salinity of 6,700 ppm, IFT was reduced to 17.38 mN/m, and at even higher salinity of 26,800 ppm, IFT became 11.88 mN/m, more than a half of the initial IFT value. This behavior of IFT occurred throughout all solutions, as salinity and surfactant both have a strong ability to reduce IFT. However, the critical salt concentration (CSC) is reached at approximately 30,000 ppm, or 30 g/L for all solutions. Even though IFT reduction does occur furthermore at higher salinity level, the change of IFT after the CSC is not as significant as the lower salinity.

Among all fluids, Surfactant 01 showed the lowest initial IFT of 1.65 mN/m. This can be explained with the initial components of Surfactant 01, as it already contains sodium chloride in the chemical itself. Surfactant 02 and Surfactant 03 showed the highest reaction when exposed to salt, as the initial IFT of 16.81 mN/m for S02 was reduced to 9.90 mN/m even with 6,700 ppm salinity, and 15.28 mN/m to 9.27 mN/m for S03 with the same salinity. Throughout the experiment, the standard deviation for IFT was kept under 1.00 mN/m. The results of IFT for each fluid are shown in **Table 15** through **Table 20**, and **Fig. 41** through **Fig. 46**. The overall comparison of IFT for all fluids at different salinity is presented in **Fig. 47**, and the trend of IFT reduction to observe the similarity of all fluids can be found in **Fig. 48**.

As a result, Nano-technology Fluid and Surfactant 01 showed more stable IFT with the presence of salinity, while water, Surfactant 02, 03, and 04 showed more reactive and stronger impact on IFT reduction with salinity. This can be concluded that identifying the reactivity of surfactant and salinity for IFT is necessary to select proper chemicals to be blended with the type of water used for stimulation processes.

Table 15 – IFT Measurements of Water at Different Salinity

Fluid	ppm	IFT (mN/m)	Standard Deviation (mN/m)
Water	0	24.66	0.98
	6,700	17.38	0.78
	13,400	12.05	0.48
	20,100	11.97	0.22
	26,800	11.88	0.20
	33,500	11.85	0.19
	40,200	11.36	0.32
	53,600	10.73	0.26
	80,400	10.69	0.91

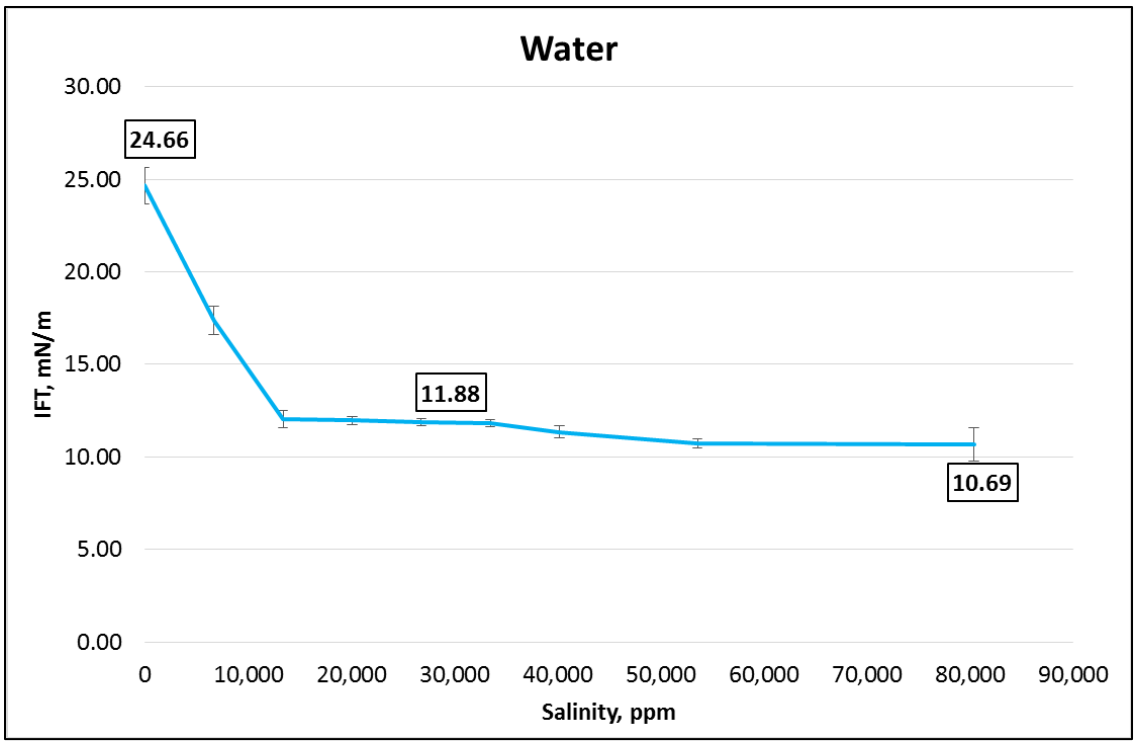

Fig. 41 – IFT Reduction Trend of Water at Different Salinity

Table 16 – IFT Measurements of Nano-technology Fluid at Different Salinity

Fluid	ppm	IFT (mN/m)	Standard Deviation (mN/m)
NF	0	10.68	0.52
	6,700	9.84	0.24
	13,400	8.82	0.13
	20,100	7.49	0.20
	26,800	6.56	0.39
	33,500	6.51	0.21
	40,200	6.33	0.25
	53,600	6.00	0.26
	80,400	4.85	0.19

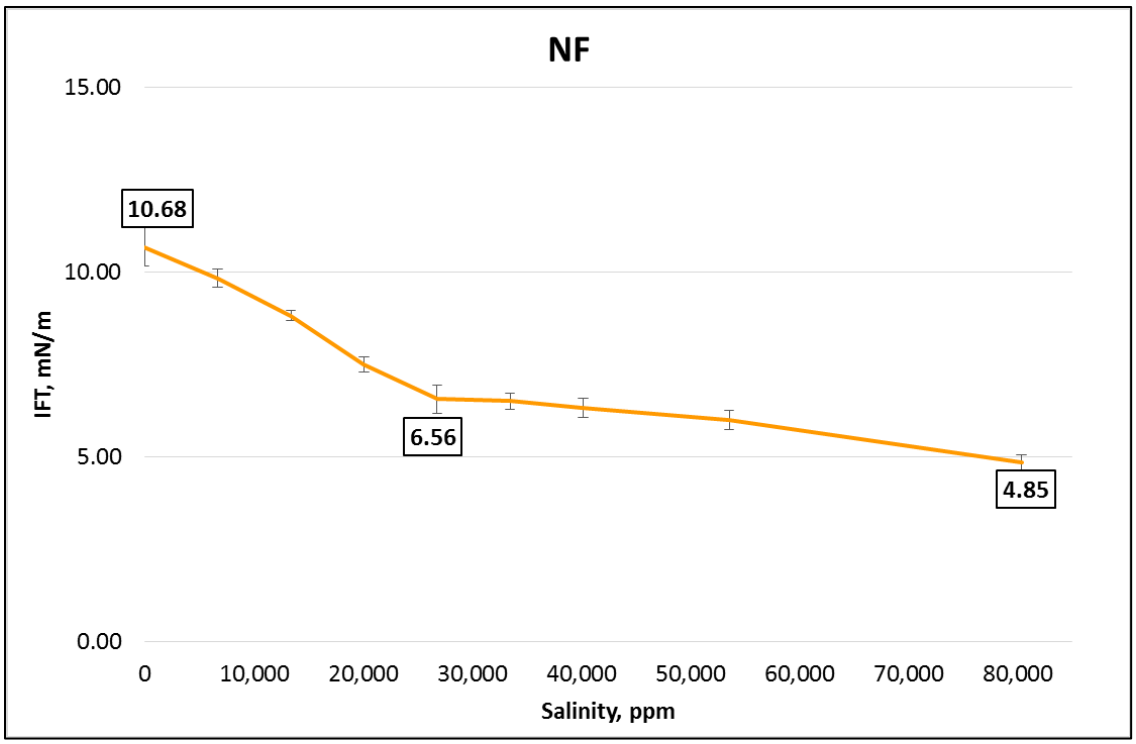

Fig. 42 – IFT Reduction Trend of Nano-Technology Fluid at Different Salinity

Table 17 – IFT Measurements of Surfactant01 at Different Salinity

Fluid	ppm	IFT (mN/m)	Standard Deviation (mN/m)
S01	0	1.65	0.10
	6,700	1.52	0.13
	13,400	1.08	0.15
	20,100	1.03	0.16
	26,800	0.96	0.18
	33,500	0.96	0.13
	40,200	0.96	0.10
	53,600	0.94	0.08
	80,400	0.90	0.14

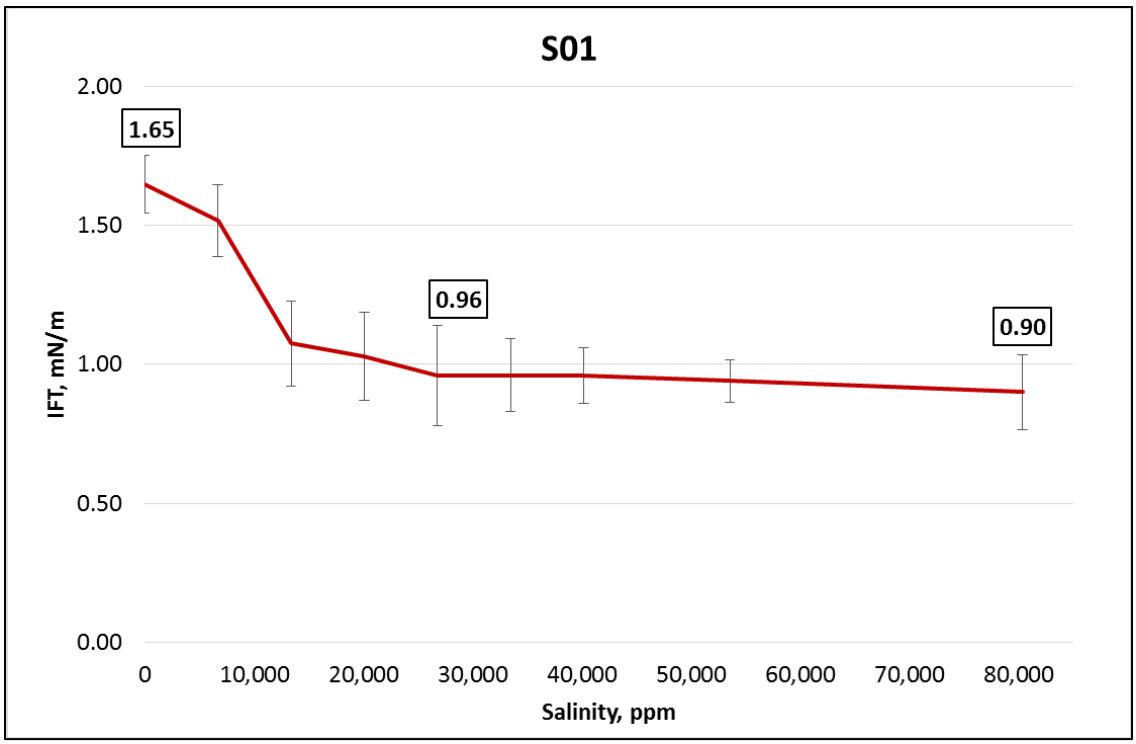

Fig. 43 – IFT Reduction Trend of Surfactant01 at Different Salinity

Table 18 – IFT Measurements of Surfactant02 at Different Salinity

Fluid	ppm	IFT (mN/m)	Standard Deviation (mN/m)
S02	0	16.81	0.54
	6,700	9.90	0.31
	13,400	3.01	0.52
	20,100	2.79	0.36
	26,800	2.35	0.58
	33,500	2.24	0.49
	40,200	1.76	0.74
	53,600	1.49	0.12
	80,400	0.81	0.14

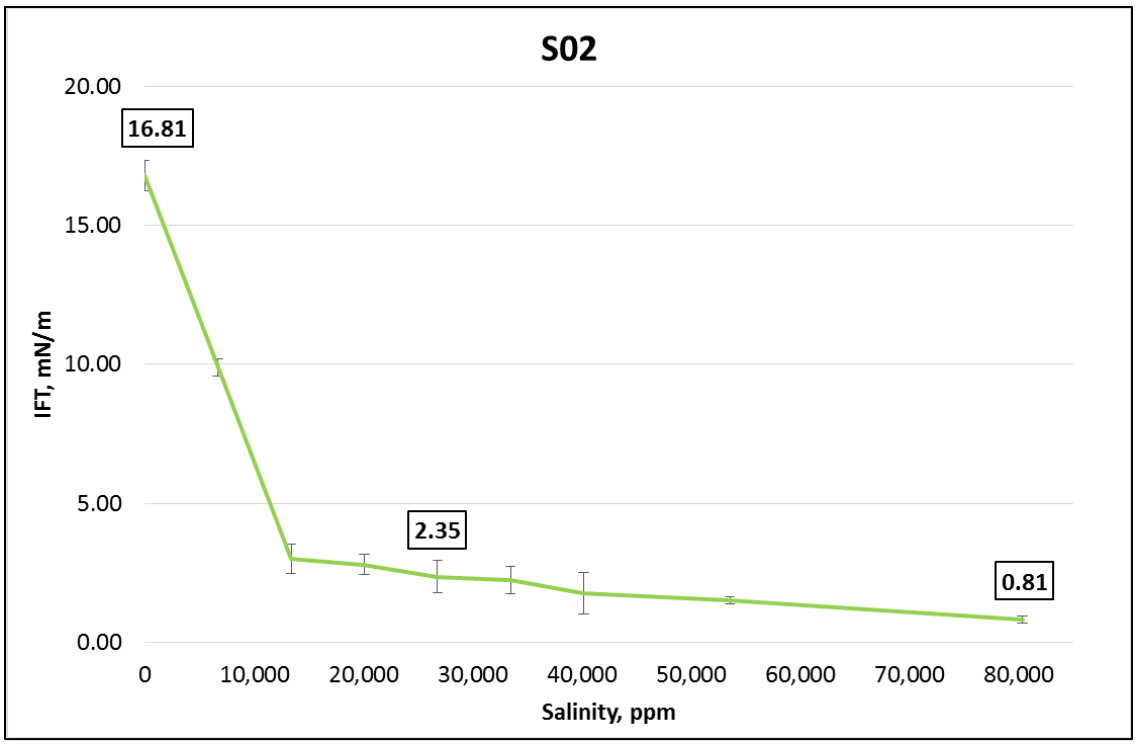

Fig. 44 – IFT Reduction Trend of Surfactant02 at Different Salinity

Table 19 – IFT Measurements of Surfactant03 at Different Salinity

Fluid	ppm	IFT (mN/m)	Standard Deviation (mN/m)
S03	0	15.28	0.82
	6,700	9.27	0.42
	13,400	2.01	0.09
	20,100	2.11	0.14
	26,800	1.82	0.25
	33,500	1.80	0.20
	40,200	1.60	0.15
	53,600	0.98	0.08
	80,400	0.70	0.33

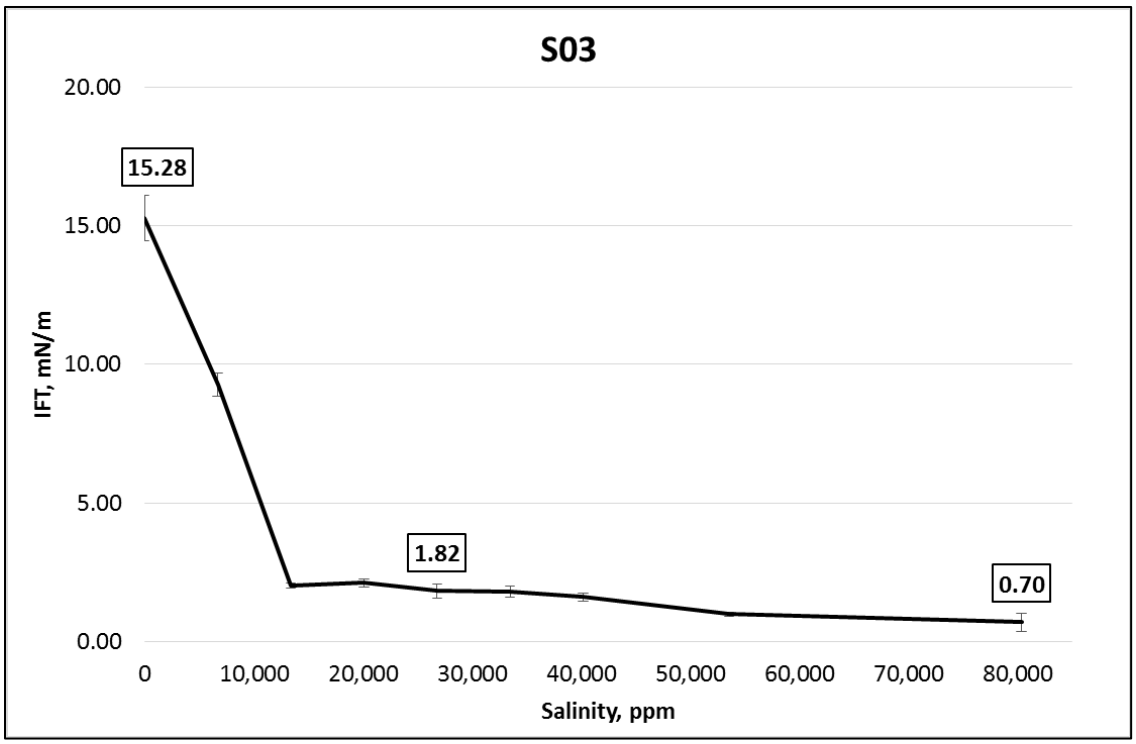

Fig. 45 – IFT Reduction Trend of Surfactant03 at Different Salinity

Table 20 – IFT Measurements of Surfactant04 at Different Salinity

Fluid	ppm	IFT (mN/m)	Standard Deviation (mN/m)
S04	0	17.95	0.60
	6,700	13.44	0.31
	13,400	9.36	0.19
	20,100	9.17	0.12
	26,800	8.97	0.14
	33,500	8.92	0.11
	40,200	8.86	0.09
	53,600	8.64	0.09
	80,400	6.91	0.46

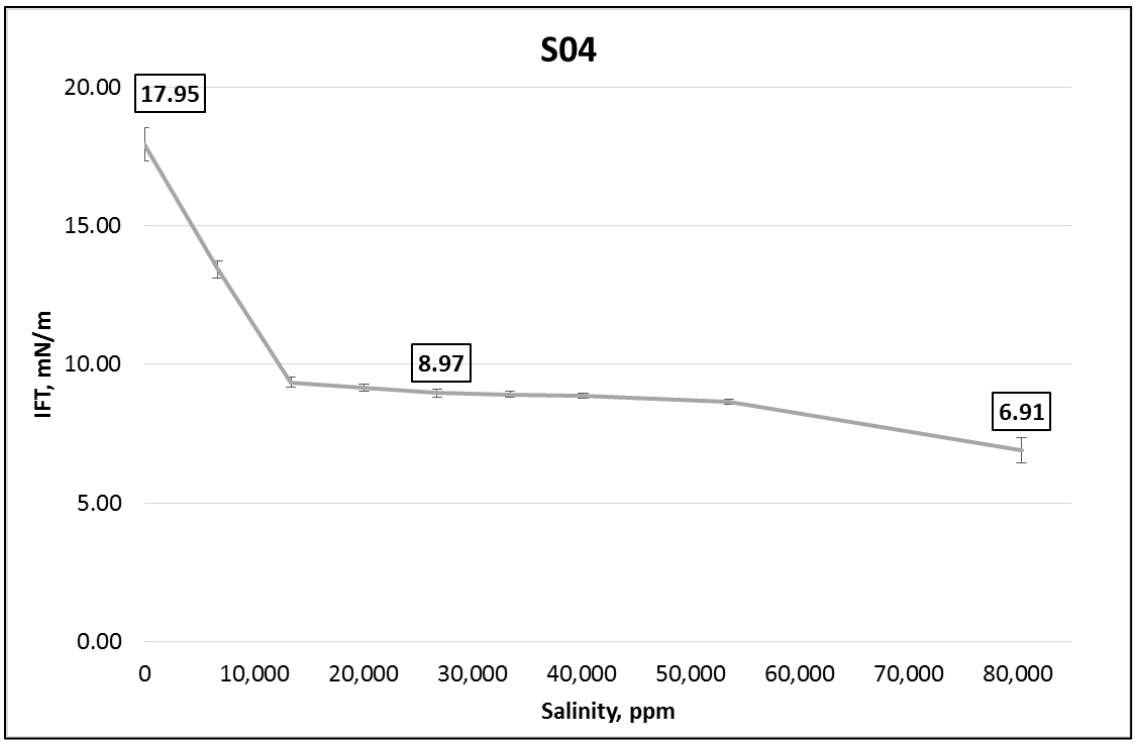

Fig. 46 – IFT Reduction Trend of Surfactant04 at Different Salinity

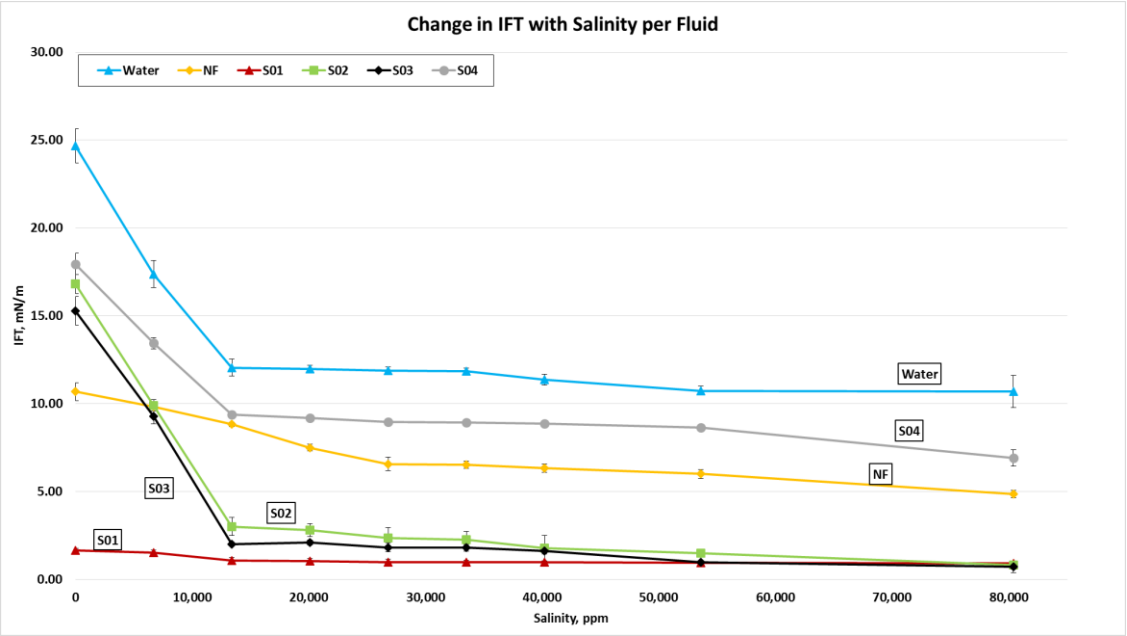

Fig. 47 – The Overall Comparison of IFT Reduction with Salinity

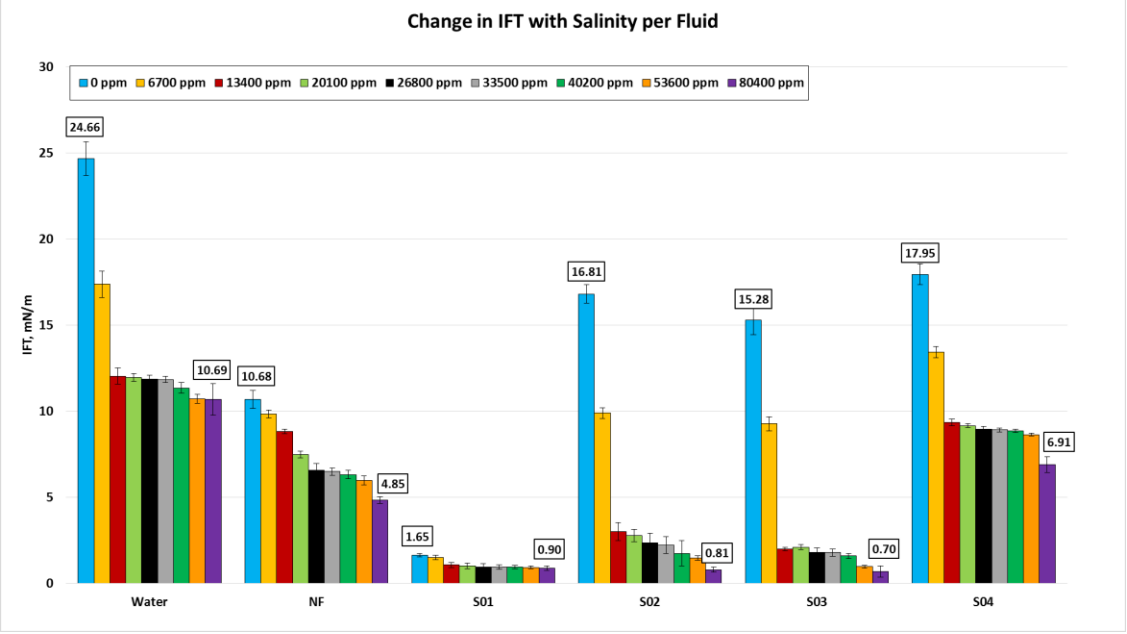

Fig. 48 – The Overall Comparison of IFT Reduction Trend for All Fluids

5.3 Contact Angle

Contact angle measurements identify the original wettability of the reservoir rocks and determine the ability of aqueous phase solutions to alter the surface wettability. All solutions were tested with both carbonate rich and quartz rich rocks to distinguish the difference in surface characteristics and the interactions with each other. Minimum of 5 rock chips were used and more than 10 attempts of measurements for each solution were conducted to accurately estimate the average static contact angle of each rock type, and to mitigate the standard deviation and errors.

As a result, all contact angle measurements were averaged, and standard deviations of all average contact angles were kept less than 5 degrees. Again, due to extreme heterogeneity of the formation, qualitative analysis and comparison to observe the general trends and interactions of surfactant, salinity, and each rock type are more important than the quantitative values of each contact angle.

The original wettability of the formation WT was determined to be in the oil-wet range. Especially, carbonate rich rocks showed strongly oil-wet surface with average contact angle of 132.25°, with standard deviation of 3.41°. Quartz rich also showed oil-wet surface but weakly, with average contact angle of 118.75°, at 4.42° of standard deviation. Adding chemical additives to this water without salinity showed wettability alteration to either intermediate or water-wet range, but at different levels, as shown in **Table 21**, **Fig. 49**, and **Fig. 50**.

Nano-technology Fluid, Surfactant01, and Surfactant03 altered the original wettability of both rock types to intermediate range. Surfactant03 also changed the

wettability of WT CR to intermediately wet surface, but showed the strongest interaction with WT QR, shifting its wettability to water-wet range. Surfactant04 did not create strong change in contact angle in carbonate rich rocks, but a small reduction of contact angle occurred for quartz rich. Overall, it was observed that all surfactants did not interact in a similar behavior with both rock types, and each rock type had its own preferred or more favorable surfactant additives for wettability alteration. This indicates that the ability of surfactants to alter wettability is based on the dominant lithology of the formation, and may vary by the properties of interacting rocks.

Table 21 – Change of Avg. Contact Angle with the Presence of Surfactants at the concentration of 1 gpt, and No Salinity for Both Rock Types

		WT CR		WT QR	
Fluid	**Salinity, ppm**	**CA, deg.**	**Wettability**	**CA, deg.**	**Wettability**
Water	0	138.15	Oil Wet	121.20	Oil Wet
NF		108.40	Intermediate	87.60	Intermediate
S01		97.60	Intermediate	89.95	Intermediate
S02		107.00	Intermediate	91.30	Intermediate
S03		105.65	Intermediate	65.00	Water Wet
S04		116.05	Oil Wet	102.90	Intermediate
* Standard Deviation < 5 Degrees					

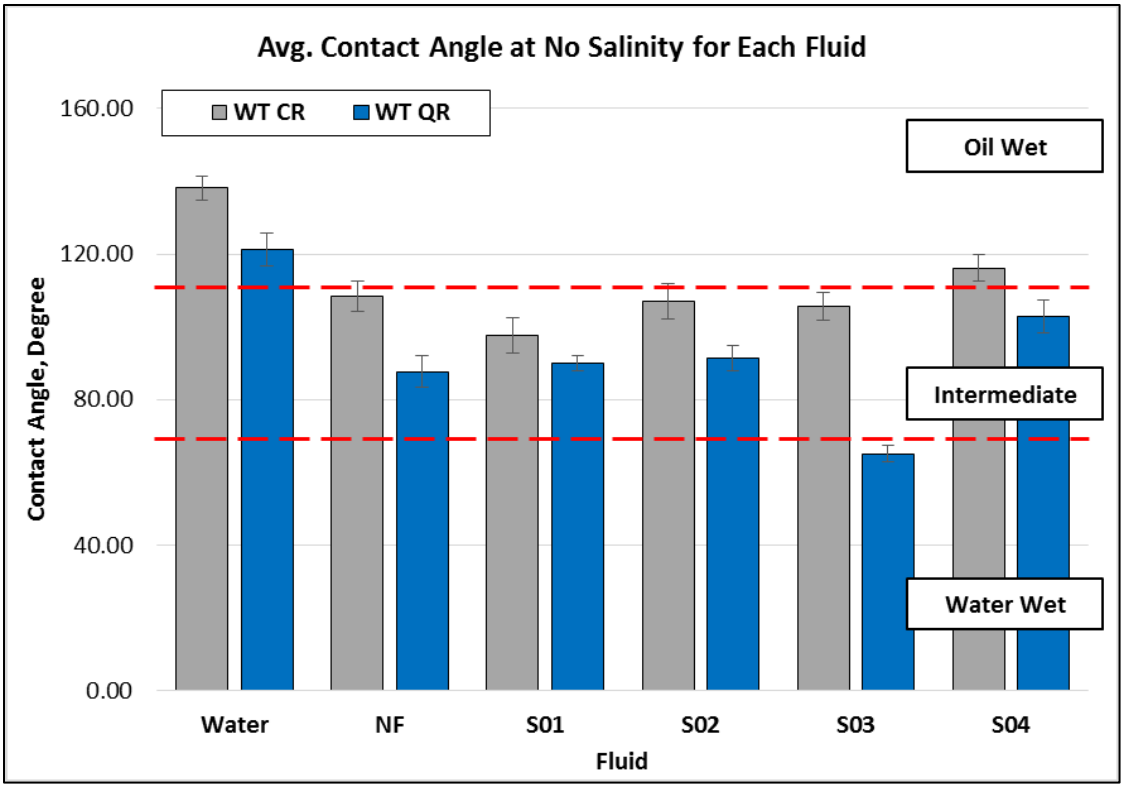

Fig. 49 – Change in Avg. Contact Angle with Chemical Additives at No Salinity

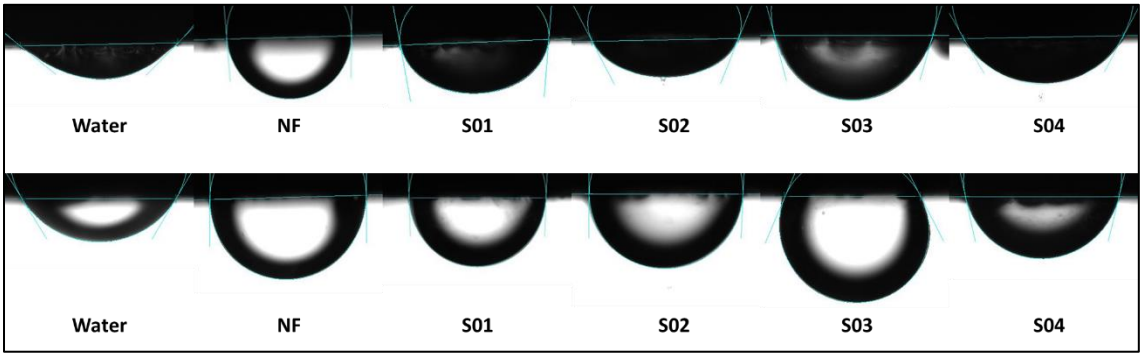

Fig. 50 – Wettability Alteration by the Presence of Chemical Additives at concentration of 1 gpt, and No Salinity: WT CR (Top), WT QR (Bottom)

Impact of salinity on contact angle showed similar trends and behaviors for all aqueous phase solutions. As salinity increases, contact angle started to decrease, even without the presence of chemical additives. For all fluids, the strongest change in wettability was observed at the salinity of 26,800 ppm, but considering the standard deviation and the small difference of average contact angle, wettability alteration occurs most effectively at the salinity level between 20,000 to 33,000 ppm. NF01, S01, and S02 showed the strongest reaction with the presence of salinity, while others showed insignificant sensitivity. Also, S03 showed the strongest wettability alteration with quartz rich rocks at any salinity level, making the surface wettability to water-wet throughout all salinity, but not as effective for carbonate rich rocks. Results of contact angle measurements for each fluid at different salinity can be found in **Table 22** through **Table 27,** and **Fig. 51** through **Fig. 56**. The overall results of average contact angle for all fluids in both lithology is shown in **Fig. 57**, and the results for each rock type to observe the similarity of trends for contact angle change is presented in **Fig. 58**, and **Fig. 59**. Additionally, **Table 28**, **Fig. 60**, and **Fig. 61** show the change of contact angle by addition of chemical additives at 26,800 ppm of salinity, where the highest wettability alteration was observed.

Consequently, the impact of salinity on wettability alteration is the highest at low salinity up to 33,500 ppm, and gradually decreases as salinity increases further. By observing the behavior of contact angle changes for all cases of aqueous phase solution, it can also be concluded that the interactions between surfactant and salinity may vary based on the dominant lithology of the formation that they interact with, because of the matrix

and electrical properties such as surface charge, which can be justified with the zeta potential measurements above. As the magnitude of zeta potential decreases with increasing salinity, electrical double layer surrounding the rock particles becomes thinner, making the surface of the rock more hydrophobic. Having stronger hydrophobic surface leads surfactant-added brines to not effectively adsorb on the surface and create wettability alteration. However, the magnitude of zeta potential is higher at no salinity, compared to zeta potential at low salinity fluid. This explains that aqueous phase solutions at low salinity create change in surface wettability through ion exchanges of salts and surface, which can lead to more effective adsorption of both surfactant and salt without making the surface extremely hydrophobic. Therefore, the optimum or the most favorable salinity of 20,000 to 30,000 ppm is recommended for designing completion fluids in ULR.

Table 22 – Avg. Contact Angle for Water at Different Salinity for Both Rock Types

Fluid	ppm	WT CR		WT QR	
		CA, Deg.	Wettability	CA, Deg.	Wettability
Water	0	132.25	Oil Wet	118.75	Oil Wet
	6,700	132.80	Oil Wet	118.73	Oil Wet
	13,400	130.70	Oil Wet	117.70	Oil Wet
	20,100	119.20	Oil Wet	109.30	Intermediate
	26,800	107.75	Intermediate	101.00	Intermediate
	33,500	113.65	Intermediate	105.60	Intermediate
	40,200	119.60	Oil Wet	110.40	Intermediate
	53,600	123.30	Oil Wet	116.65	Oil Wet
	80,400	126.90	Oil Wet	119.35	Oil Wet
*Standard Deviation: < 5 Degree					

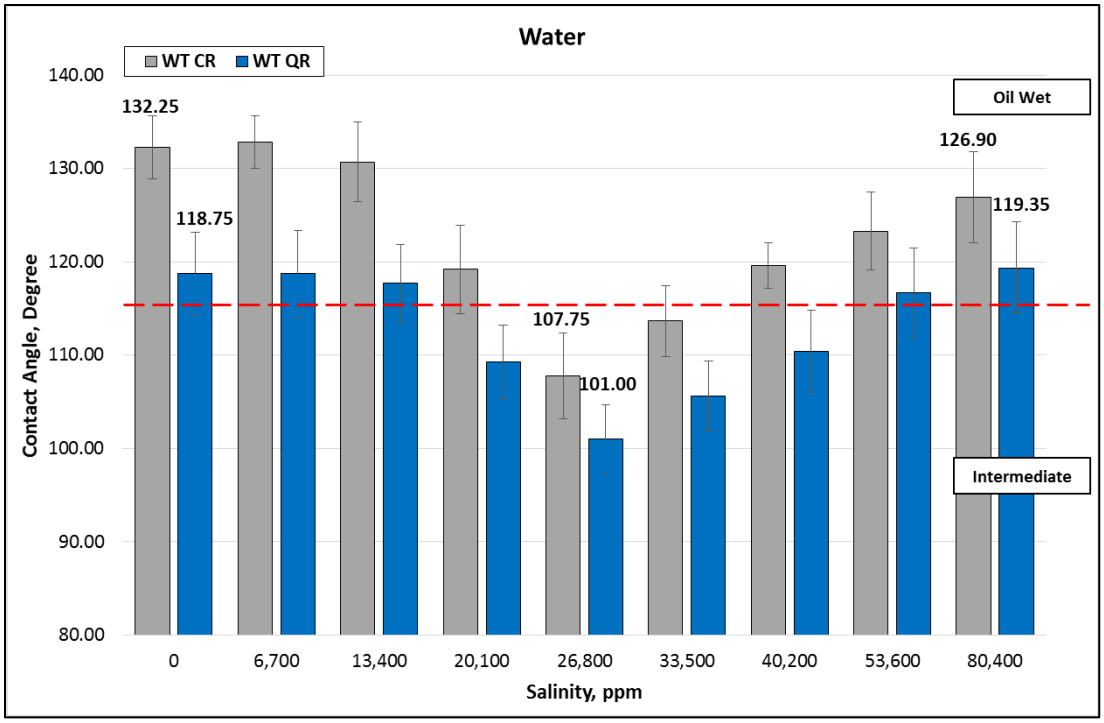

Fig. 51 – Change in Avg. Contact Angle for Water at Different Salinity for Both Rock Types

Table 23 – Avg. Contact Angle for Nano-Technology Fluid at Different Salinity for Both Rock Types

Fluid	ppm	WT CR		WT QR	
		CA, Deg.	Wettability	CA, Deg.	Wettability
NF	0	108.40	Intermediate	87.60	Intermediate
	6,700	100.45	Intermediate	82.30	Intermediate
	13,400	92.55	Intermediate	75.00	Intermediate
	20,100	88.90	Intermediate	72.05	Water Wet
	26,800	85.30	Intermediate	69.10	Water Wet
	33,500	89.95	Intermediate	73.45	Water Wet
	40,200	94.70	Intermediate	76.90	Intermediate
	53,600	102.10	Intermediate	82.80	Intermediate
	80,400	108.50	Intermediate	86.30	Intermediate
*Standard Deviation: < 5 Degree					

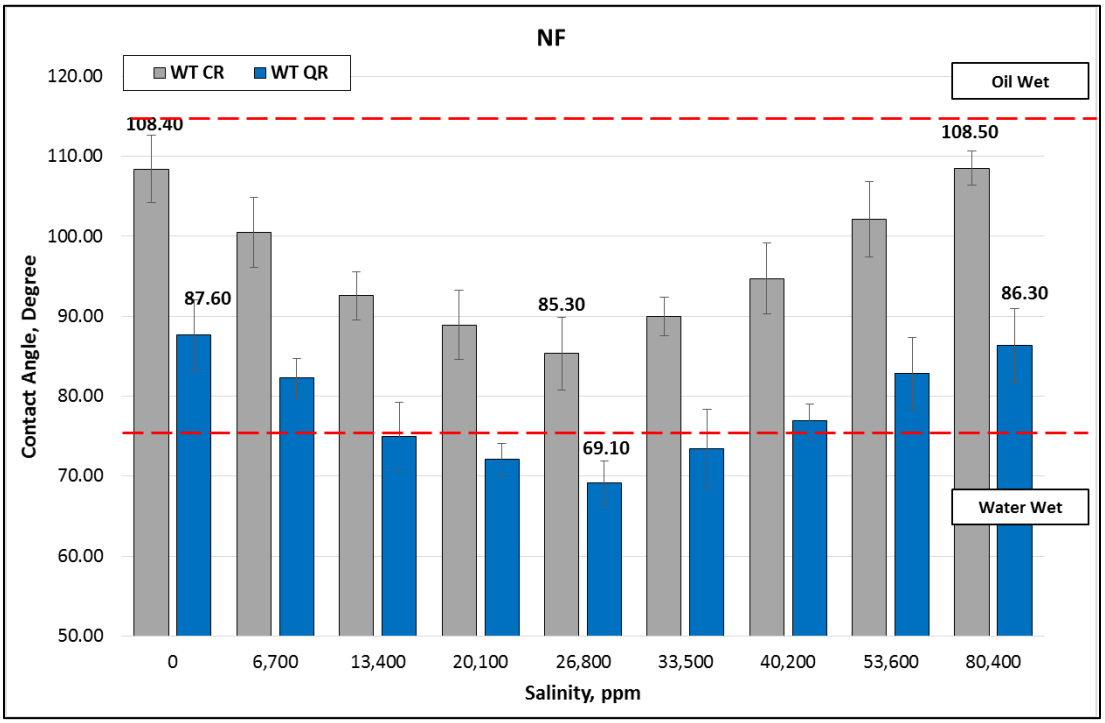

Fig. 52 – Change in Avg. Contact Angle for Nano-Technology Fluid at Different Salinity for Both Rock Types

Table 24 – Avg. Contact Angle for Surfactant01 at Different Salinity for Both Rock Types

Fluid	ppm	Carbonate Rich		Quartz Rich	
		Angle, Deg.	Wettability	Angle, Deg.	Wettability
S01	0	97.60	Intermediate	89.95	Intermediate
	6,700	92.55	Intermediate	84.90	Intermediate
	13,400	87.55	Intermediate	79.90	Intermediate
	20,100	80.65	Intermediate	75.60	Intermediate
	26,800	73.80	Water Wet	71.25	Water Wet
	33,500	77.05	Intermediate	72.60	Water Wet
	40,200	80.30	Intermediate	73.90	Water Wet
	53,600	85.20	Intermediate	76.55	Intermediate
	80,400	90.75	Intermediate	78.65	Intermediate
*Standard Deviation: < 5 Degree					

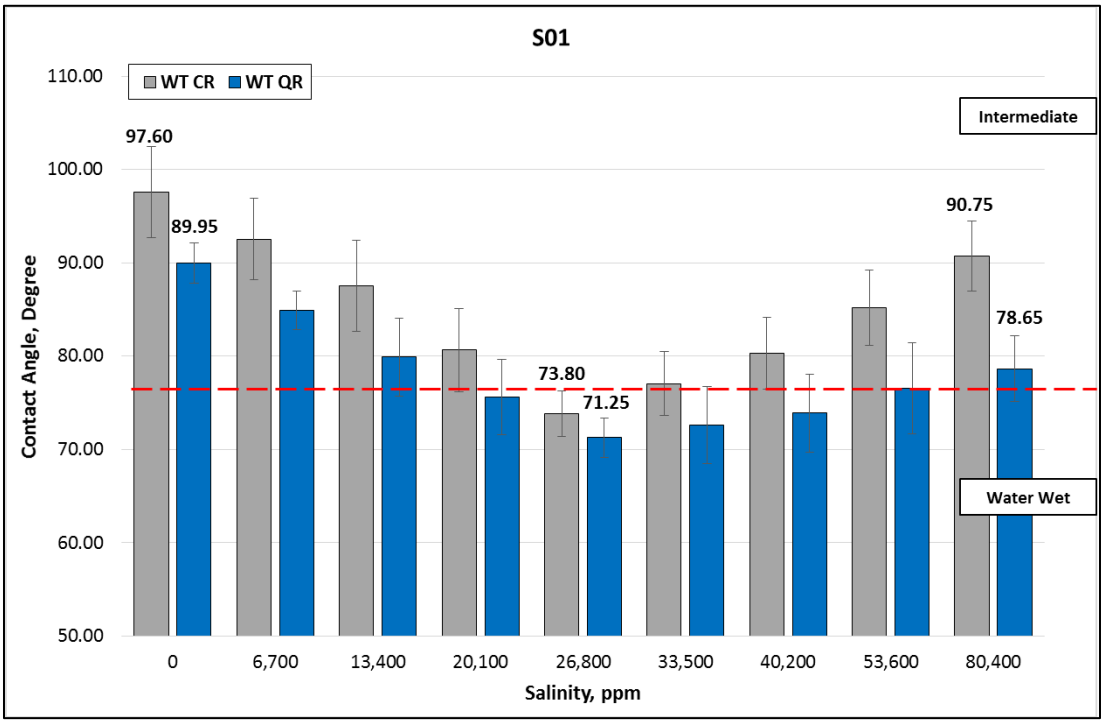

Fig. 53 – Change in Avg. Contact Angle for Surfactant01 at Different Salinity for Both Rock Types

Table 25 – Avg. Contact Angle for Surfactant02 at Different Salinity for Both Rock Types

Fluid	ppm	Carbonate Rich		Quartz Rich	
		Angle, Deg.	Wettability	Angle, Deg.	Wettability
S02	0	107.00	Intermediate	91.30	Intermediate
	6,700	98.90	Intermediate	83.90	Intermediate
	13,400	90.80	Intermediate	76.60	Intermediate
	20,100	89.20	Intermediate	73.85	Intermediate
	26,800	87.65	Intermediate	71.10	Intermediate
	33,500	89.05	Intermediate	73.20	Intermediate
	40,200	90.50	Intermediate	75.25	Intermediate
	53,600	93.35	Intermediate	79.45	Intermediate
	80,400	104.25	Intermediate	82.65	Intermediate
*Standard Deviation: < 5 Degree					

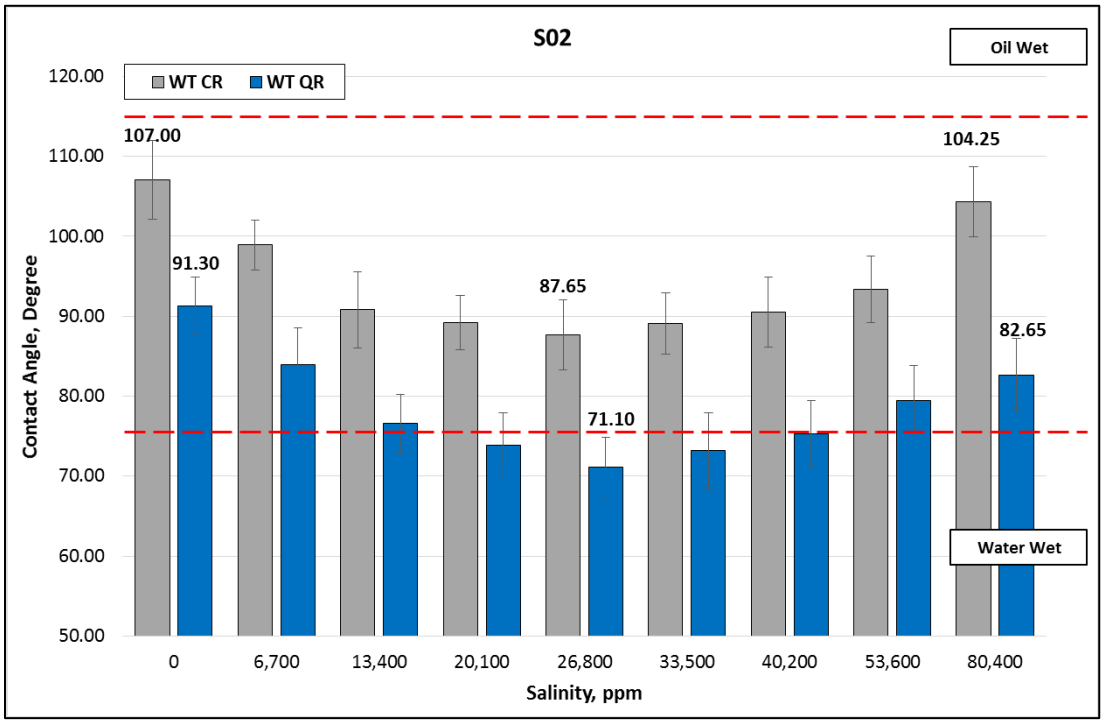

Fig. 54 – Change in Avg. Contact Angle for Surfactant02 at Different Salinity for Both Rock Types

Table 26 – Average Contact Angle for Surfactant03 at Different Salinity for Both Rock Types

Fluid	ppm	Carbonate Rich		Quartz Rich	
		Angle, Deg.	Wettability	Angle, Deg.	Wettability
S03	0	105.65	Intermediate	65.00	Water Wet
	6,700	99.30	Intermediate	63.25	Water Wet
	13,400	93.00	Intermediate	61.55	Water Wet
	20,100	81.40	Intermediate	60.90	Water Wet
	26,800	69.85	Water Wet	60.30	Water Wet
	33,500	72.15	Intermediate	60.55	Water Wet
	40,200	74.53	Intermediate	60.75	Water Wet
	53,600	79.20	Intermediate	61.25	Water Wet
	80,400	89.25	Intermediate	63.10	Water Wet
*Standard Deviation: < 5 Degree					

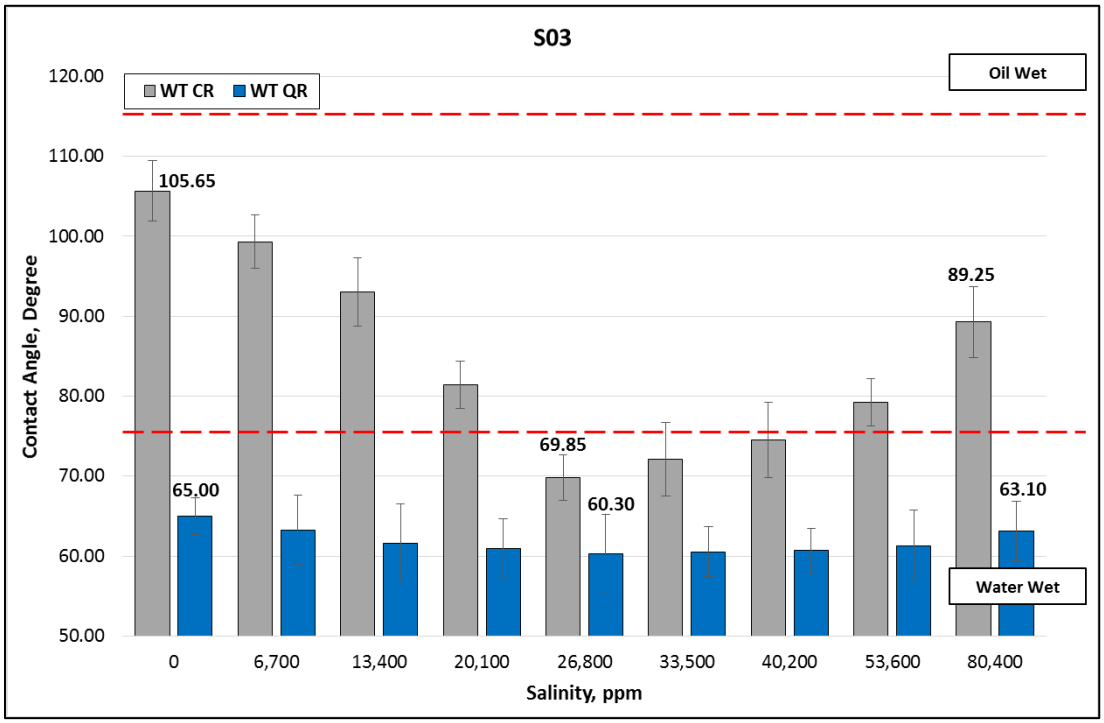

Fig. 55 – Change in Avg. Contact Angle for Surfactant03 at Different Salinity for Both Rock Types

Table 27 – Average Contact Angle for Surfactant04 at Different Salinity for Both Rock Types

Fluid	ppm	Carbonate Rich		Quartz Rich	
		Angle, Deg.	Wettability	Angle, Deg.	Wettability
S04	0	116.05	Oil Wet	102.90	Intermediate
	6,700	115.60	Oil Wet	101.10	Intermediate
	13,400	115.20	Oil Wet	99.35	Intermediate
	20,100	110.35	Oil Wet	97.35	Intermediate
	26,800	105.50	Intermediate	95.40	Intermediate
	33,500	105.90	Intermediate	96.30	Intermediate
	40,200	106.35	Intermediate	97.15	Intermediate
	53,600	107.20	Intermediate	98.95	Intermediate
	80,400	112.75	Oil Wet	104.05	Intermediate
*Standard Deviation: < 5 Degree					

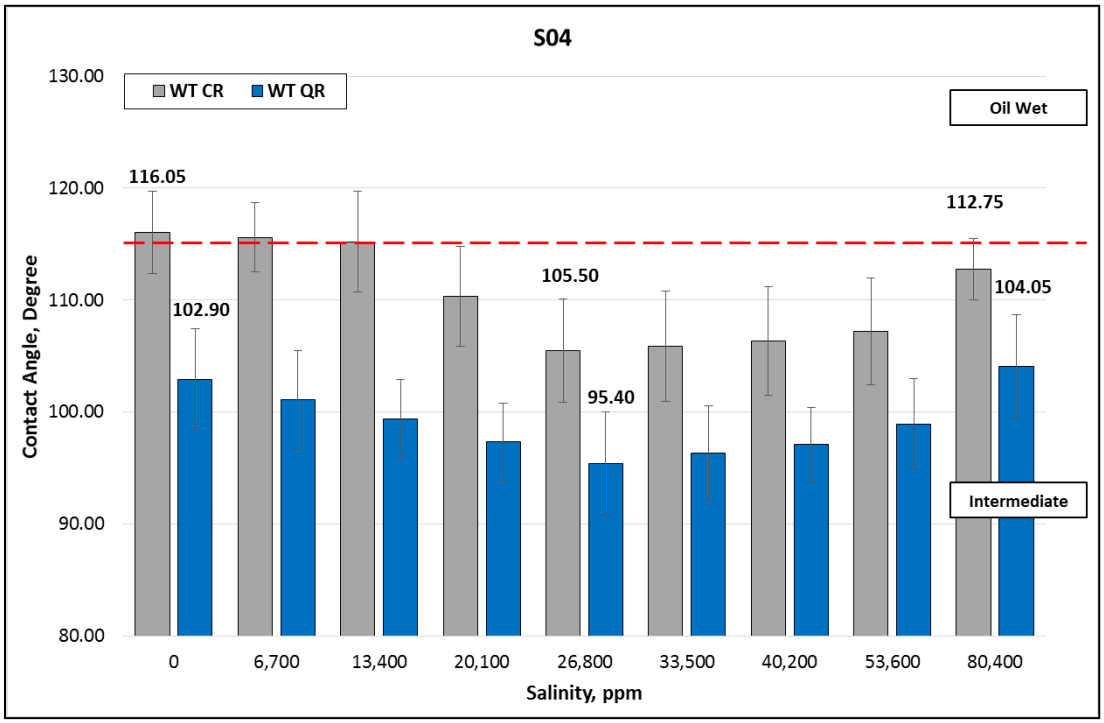

Fig. 56 – Change in Avg. Contact Angle for Surfactant04 at Different Salinity for Both Rock Types

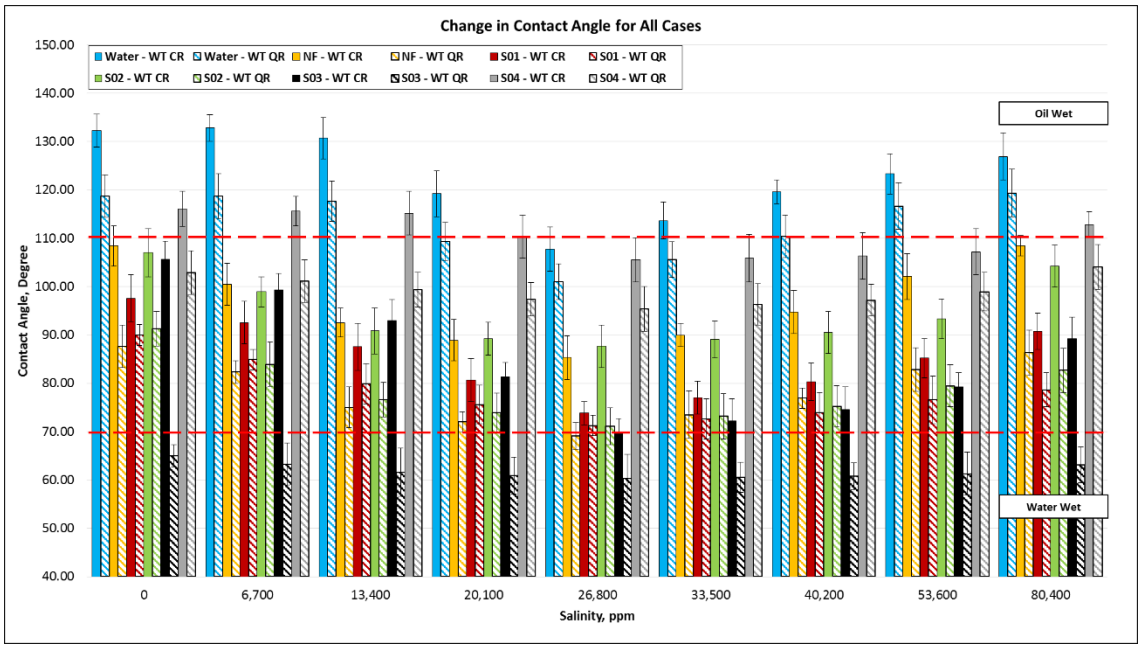

Fig. 57 – The Overall Comparison of Change in Avg. Contact Angle at Different Salinity for Both Rock Types

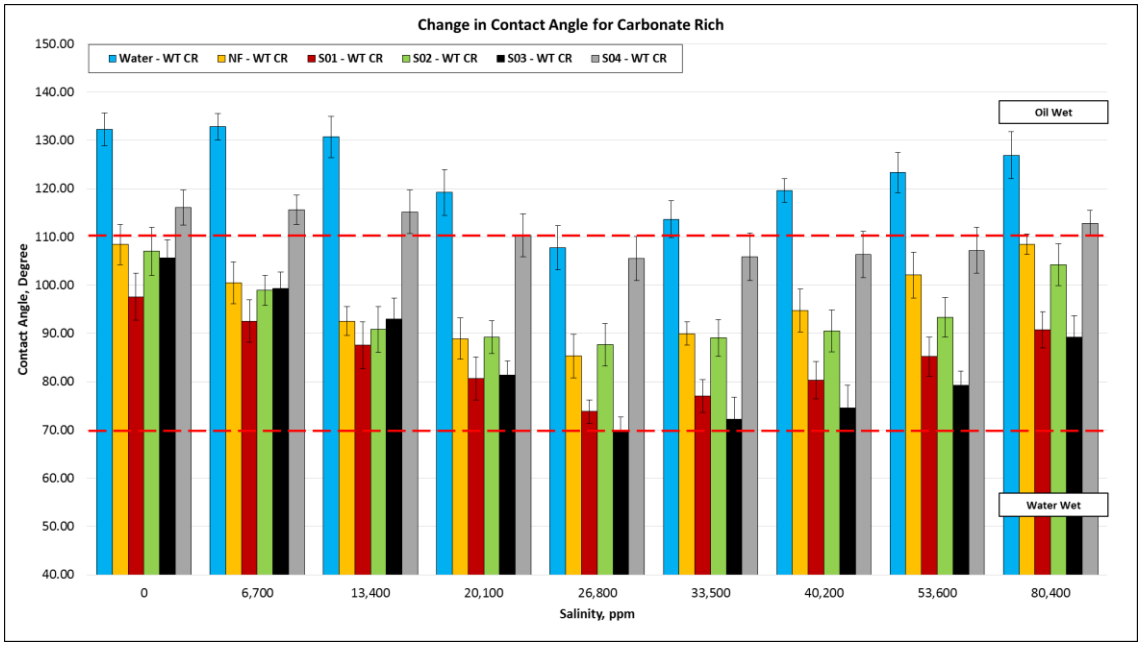

Fig. 58 – The Comparison of Change in Avg. Contact Angle at Different Salinity per Fluid for Carbonate Rich Rocks

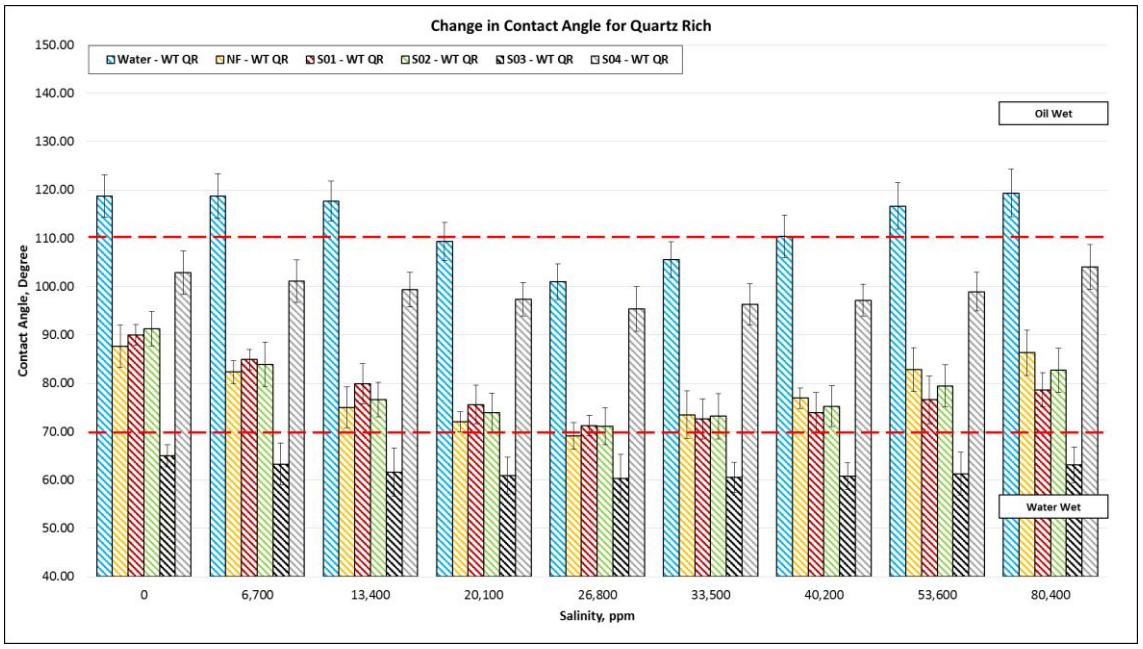

Fig. 59 – The Comparison of Change in Avg. Contact Angle at Different Salinity per Fluid for Quartz Rich Rocks

Table 28 – Change of Average Contact Angle with the Presence of Surfactants at the concentration of 1 gpt, and 26,800 ppm for Both Rock Types

		WT CR		WT QR	
Fluid	**Salinity, ppm**	**CA, deg.**	**Wettability**	**CA, deg.**	**Wettability**
Water	26,800	107.75	Intermediate	101.00	Intermediate
NF		85.30	Intermediate	69.10	Water Wet
S01		73.80	Water Wet	71.25	Water Wet
S02		87.65	Intermediate	71.10	Water Wet
S03		69.85	Water Wet	60.30	Water Wet
S04		105.50	Intermediate	95.40	Intermediate
* Standard Deviation < 5 Degrees					

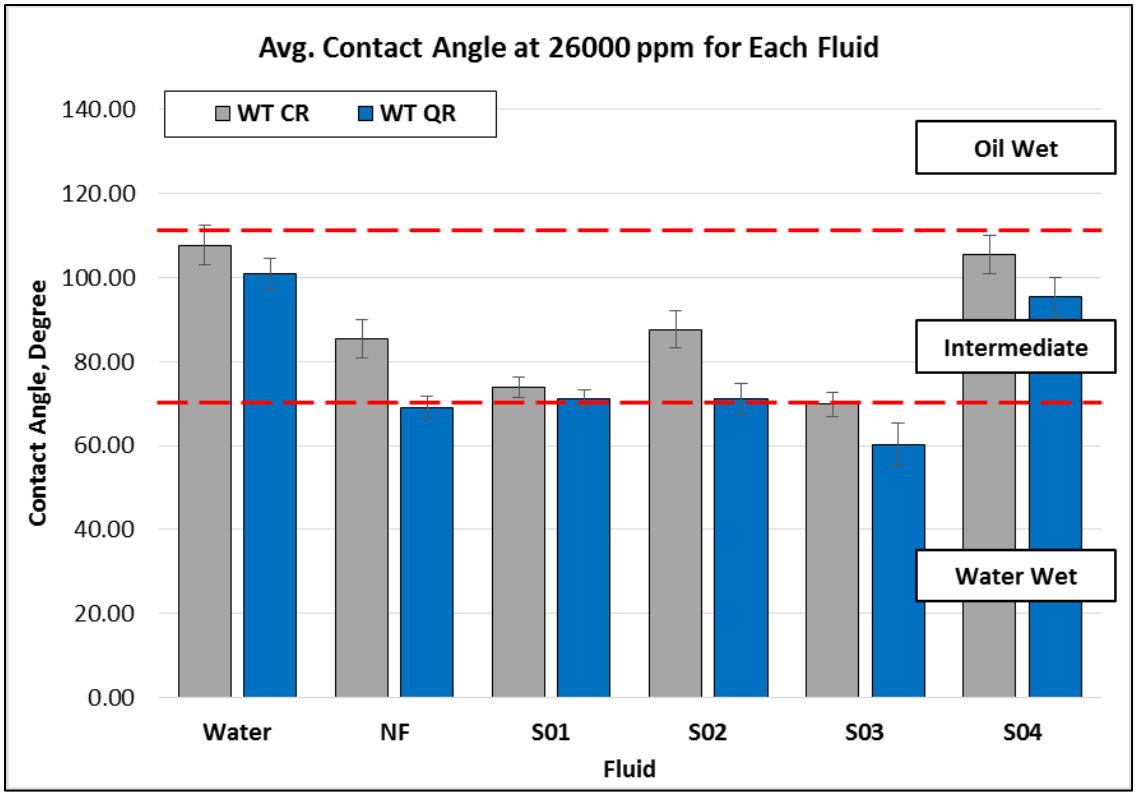

Fig. 60 – Change in Avg. Contact Angle with Chemical Additives at 26,800 ppm

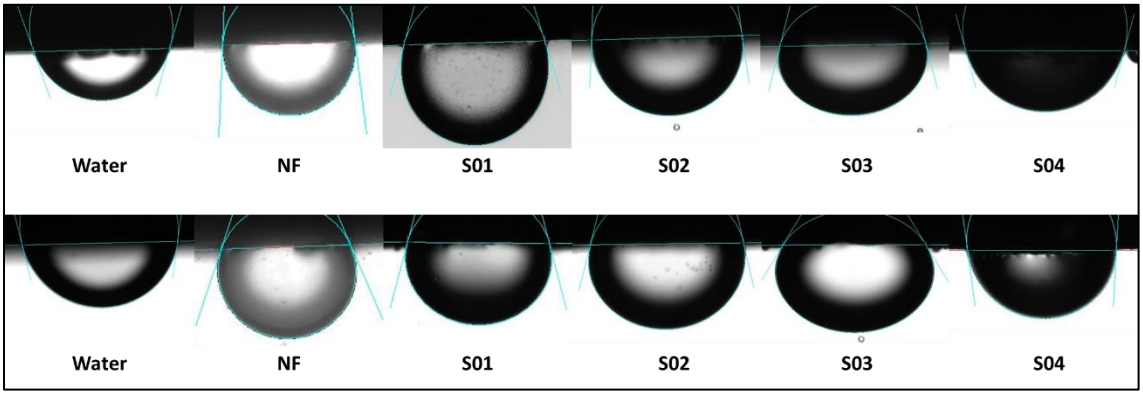

Fig. 61 – Wettability Alteration with the Presence of Chemical Additives at 26,800 ppm: WT CR (Top), WT QR (Bottom)

5.4 Spontaneous Imbibition and CT Scan Analysis

A few screening criteria for surfactant and salinity selection were established: having a low to intermediate, and stable interfacial tension, strong ability to alter wettability for different lithology, and tolerance to salinity.

As discussed in the earlier section, IFT measurements indicated that every surfactant has the ability to effectively reduce IFT between crude oil and aqueous phase solutions. Among all surfactants tested, S01 and NF reduced the IFT the most at no salinity. Also, NF and S01 showed fairly stable IFT regardless of the salinity, while S02, S03, and S04 showed strong sensitivity with the presence of salt in the solution. Contact Angle measurements determined that all surfactant-added solutions altered the wettability of rock surface to intermediate or water-wet range, but differently for each rock type. NF, S01 and S03 changed the surface wettability most effectively for carbonate rich rocks, and NF, S01, S02, and S03 for quartz rich rocks. However, a significant difference of wettability altering ability between two lithology occurred with S02 and S03. They did not change the average contact angle of carbonate rich rocks as effectively as they did for quartz rich rocks.

Based on the analysis above, NF and S01 satisfied the screening criteria with low IFT, stable IFT with salinity, and strong ability to alter wettability for both rock types. Both surfactants were blended at the concentration of 1 gpt, and water without chemical additive was also used to inspect the performance improvement of surfactant-added completion fluids. Also, to compare the effect of salinity on overall imbibition process, three salinity levels were selected, which are 0 ppm, 26800 ppm, and 80400 ppm. 0 ppm

brine represents the fresh water from natural resources with negligible salinity, 26800 ppm brine is the most favorable frac water, and 80400 ppm brine is a representation of high salinity produced water. This combination makes total of nine cases of aqueous phase solution for spontaneous imbibition, shown in **Table 29**, and the same set of fluids was used on both carbonate rich and quartz rich core samples. Also, during the spontaneous imbibition experiment, timely CT scan and CT image analyses were conducted to visually inspect the fluid penetration and change in density within the core samples. To enhance the contrast of aqueous phase solutions in these scans, 4 wt. % potassium iodide (KI) was added to all fluids as a doping agent.

Table 29 – Types of Aqueous Phase Solutions Used for Spontaneous Imbibition

No.	Fluid Name	Description
1	DW_C, Q	Distilled Water (0 ppm) + 4 wt % KI
2	FW_C, Q	Frac Water (26,800 ppm) + 4 wt % KI
3	PW_C, Q	Produced Water (80,400 ppm) + 4 wt % KI
4	D_NF_C, Q	Distilled Water + 1 gpt of Nano-Technology Fluid + 4 wt % KI
5	F_NF_C, Q	Frac Water + 1 gpt of Nano-Technology Fluid+ 4 wt % KI
6	P_NF_C, Q	Produced Water + 1 gpt of Nano-Technology Fluid+ 4 wt % KI
7	D_S01_C, Q	Distilled Water + 1 gpt of Surfactant01 + 4 wt % KI
8	F_S01_C, Q	Frac Water + 1 gpt of Surfactant01 + 4 wt % KI
9	P_S01_C, Q	Produced Water + 1 gpt of Surfactant01 + 4 wt % KI

As mentioned in section 3.2, core samples were trimmed to form a cylindrical shape for volumetric calculation. Diameter and length of cores were measured to calculate the bulk volume, and porosity value of 8% was used for all cores to find the pore volume of each core. Detailed values for each core used in this experiment is in **Table 30** and

Table 31. Also, throughout the experiment, it was assumed that all cores are fully saturated with oil, with S_w (water saturation) = 0, and S_o (oil saturation) = 1. Then, the oil produced during the imbibition experiment was measured through graduated cylinder part of the modified Amott cell, **Fig. 62**, regularly to accurately observe the imbibition rate and oil recovery. **Eq. 8, Eq. 9 and Eq. 10** shows the necessary calculations used for this quantification procedures.

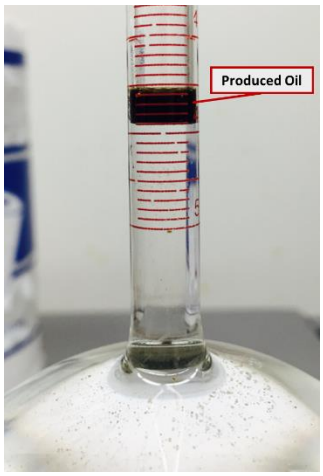

Fig. 62 – Example of Measurement for Produced Oil from a Modified Amott Cell

Table 30 – Dimension and Volumetric Measurements of Each Carbonate Rich Core Sample and the Corresponding Fluid Tested

#	Zone/Type	Fluid Tested	D, in	L, in	V, cu-in	V, ml	Porosity	Vpore, ml
1	WT CR	DW_C	0.97	2.59	1.92	31.44	0.08	2.52
2		FW_C	0.97	2.63	1.94	31.73		2.54
3		PW_C	0.99	2.59	2.01	32.91		2.63
4		D_NF_C	1.00	2.73	2.12	34.75		2.78
5		F_NF_C	0.97	2.72	2.00	32.83		2.63
6		P_NF_C	1.00	2.54	1.97	32.33		2.59
7		D_S01_C	1.00	2.78	2.16	35.42		2.83
8		F_S01_C	0.97	2.51	1.84	30.22		2.42
9		P_S01_C	1.00	2.65	2.07	33.94		2.72

Table 31 – Dimension and Volumetric Measurements of Each Quartz Rich Core Sample and the Corresponding Fluid Tested

#	Zone/Type	Fluid Tested	D, in	L, in	V, cu-in	V, ml	Porosity	Vpore, ml
1	WT QR	DW_Q	1.00	2.68	2.08	34.11	0.08	2.73
2		FW_Q	1.00	2.69	2.10	34.45		2.76
3		PW_Q	1.00	2.68	2.08	34.11		2.73
4		D_NF_Q	0.97	2.65	1.95	31.99		2.56
5		F_NF_Q	0.99	1.26	0.98	16.02		1.28
6		P_NF_Q	0.97	2.65	1.95	31.93		2.55
7		D_S01_Q	0.97	2.00	1.48	24.32		1.95
8		F_S01_Q	1.00	2.62	2.03	33.35		2.67
9		P_S01_Q	0.97	2.52	1.86	30.40		2.43

$$V_{bulk} = \frac{\pi}{4} * D^2 * L \quad \cdots\cdots (8)$$

$$V_{pore} = V_{bulk} * \phi * (1 - S_w) \quad \cdots\cdots (9)$$

$$Recovery\ Factor\ (\%) = \frac{V_{oil,produced}}{V_{pore}} * 100 \quad \cdots\cdots (10)$$

5.4.1 Spontaneous Imbibition for WT Carbonate Rich

Oil recovery factor of WT carbonate rich rock from spontaneous imbibition ranged from 5 % to 15 %. First of all, for three cases of water without chemical additives, FW with low salinity produced the most oil of 8.3%, compared to DW with no salinity or PW with high salinity, having RF of 8.0 % and 5.7 %, respectively. The overall comparison of imbibition rate and ultimate oil recovery for three cases is shown in **Fig. 63**, and detailed results for each case with timely images of produced oil along with important experimented parameters can be found in **Fig. 64** to **Fig. 66**. Although FW showed slightly

higher recovery factor than DW, the difference is very minor that the presence of salinity is almost negligible for brine without chemicals. However, it is clear that high salinity brine leads to lower recovery factor, which can be caused by a hydrophobic surface, lacking ability to alter wettability, and scaling tendency of salt components in a high reservoir temperature. Similar behaviors of imbibition performance were observed for aqueous phase solutions with Nano-technology Fluid and Surfactant01. 1 gpt of each surfactant blended in low salinity brine resulted in the highest recovery factor compared to other salinity brines. All results are shown in **Fig. 67** through **Fig. 74.**

In addition to the imbibition results, timely CT image analyses and measurements of average CT number of a whole core for each case were performed to inspect the penetration ability of fluids, mentioned in section 4.6. Average CT number showed that not a significant volume of brines penetrated into the core, resulting in a small penetration magnitude. It was also observed from the cross-sectional CT images that the saturation and density changes within the core occurred strongly in the bottom, center part of the core, indicating that gravity drainage is working as one of the oil recovery mechanisms. Low value of penetration magnitude can be also verified by the change in weight, having not much differences in weight of cores before and after imbibition experiments. All timely cross-sectional CT images, penetration magnitude analyses, and other results are presented in **Fig. 75** through **Fig. 92**, and **Table 32**.

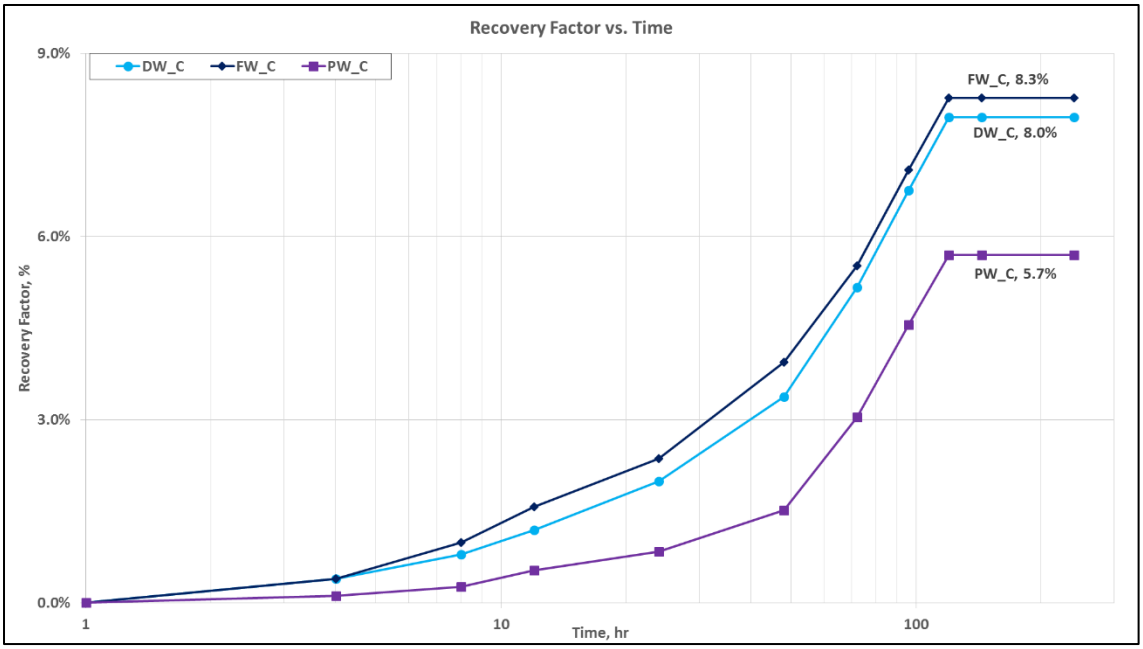

Fig. 63 – Overall Comparison of Imbibition Performances for Water in WT CR

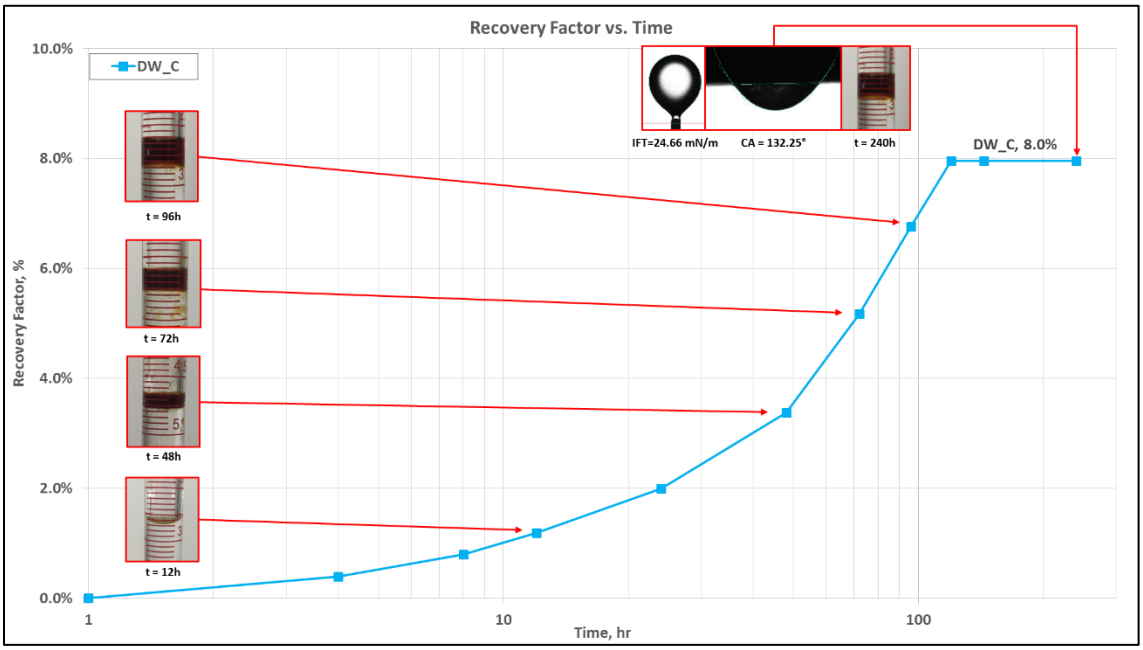

Fig. 64 – Imbibition Performance of DW in WT CR

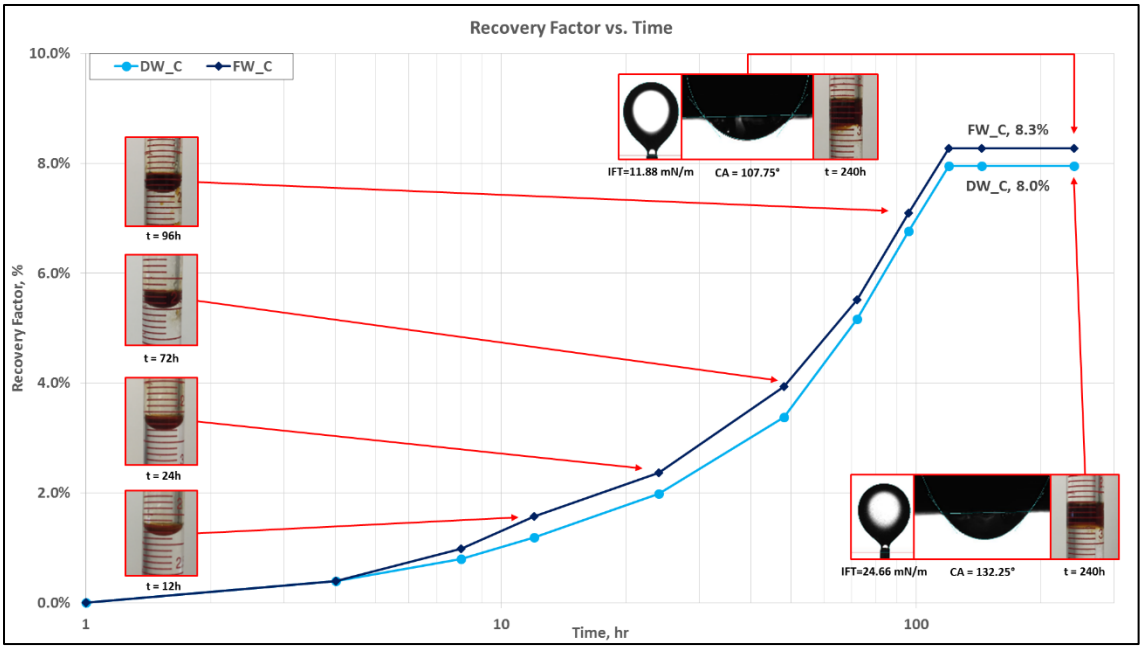

Fig. 65 – Imbibition Performance of FW compared to DW in WT CR

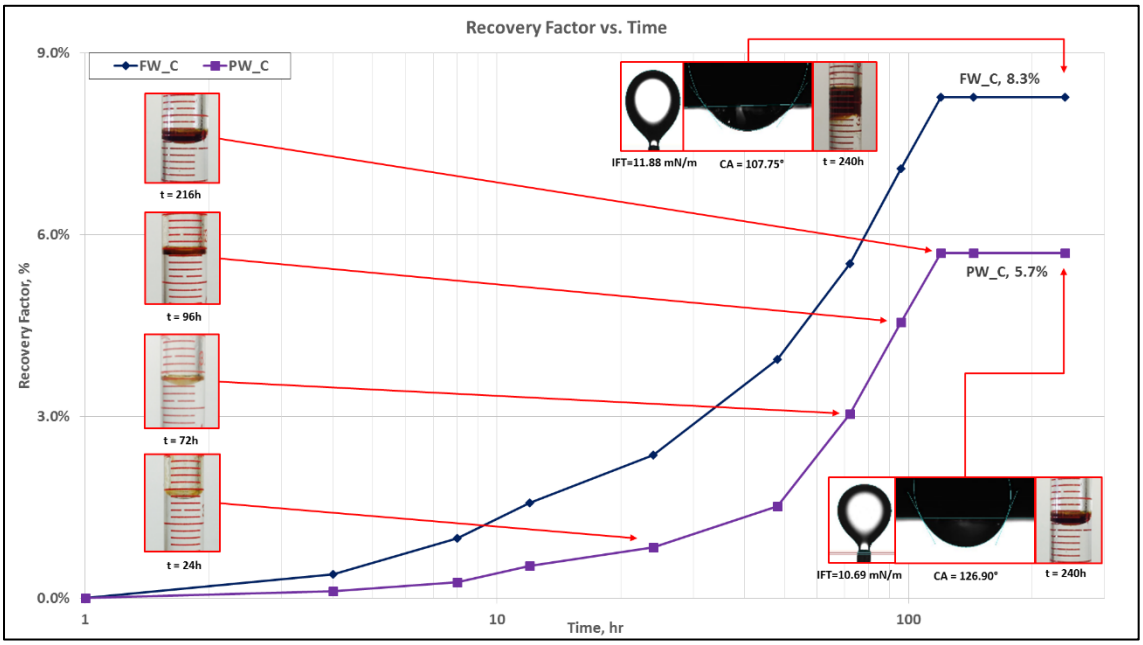

Fig. 66 - Imbibition Performance of HW compared to FW in WT CR

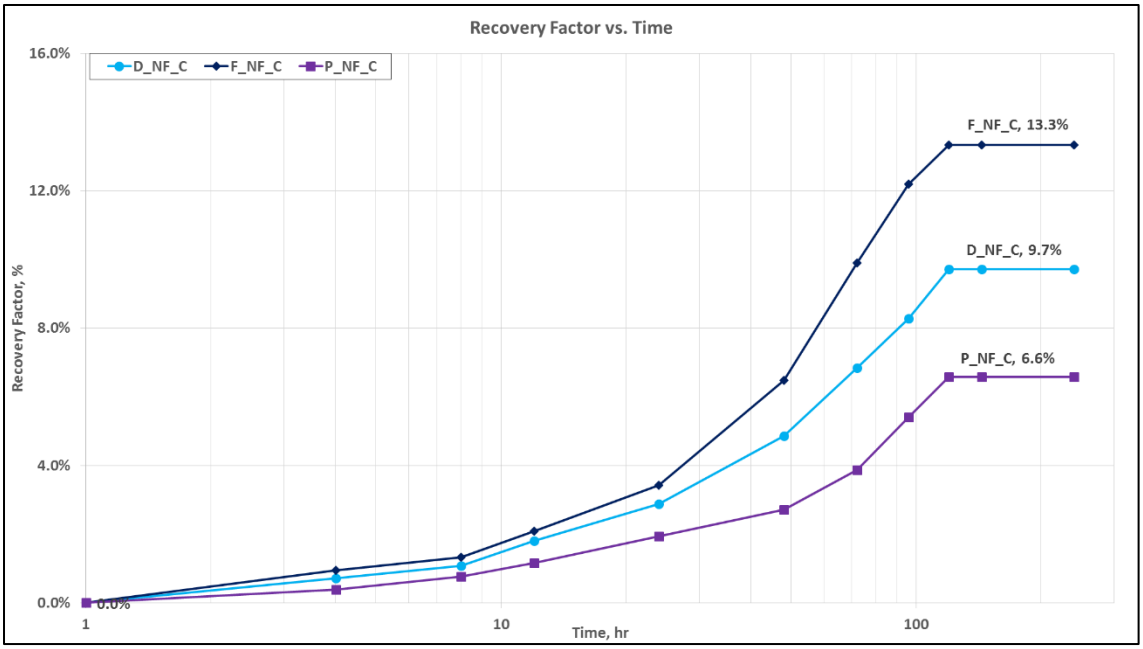

Fig. 67 – Overall Comparison of Imbibition Performances for Nano-Technology Fluid in WT CR

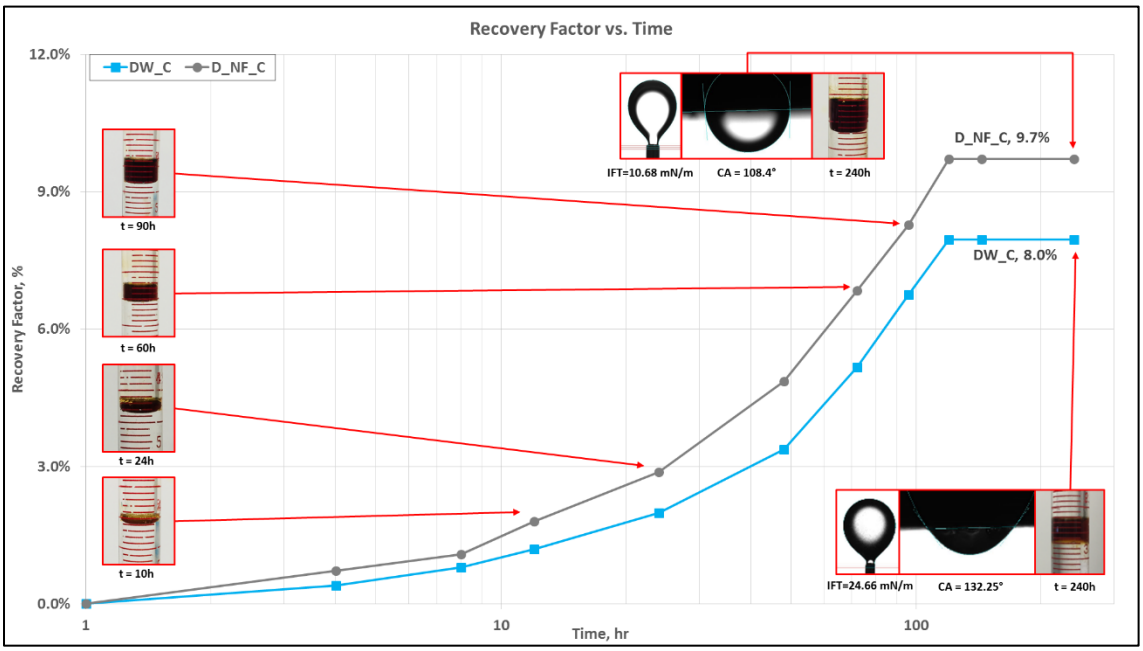

Fig. 68 – Imbibition Performance of D_NF compared to DW in WT CR

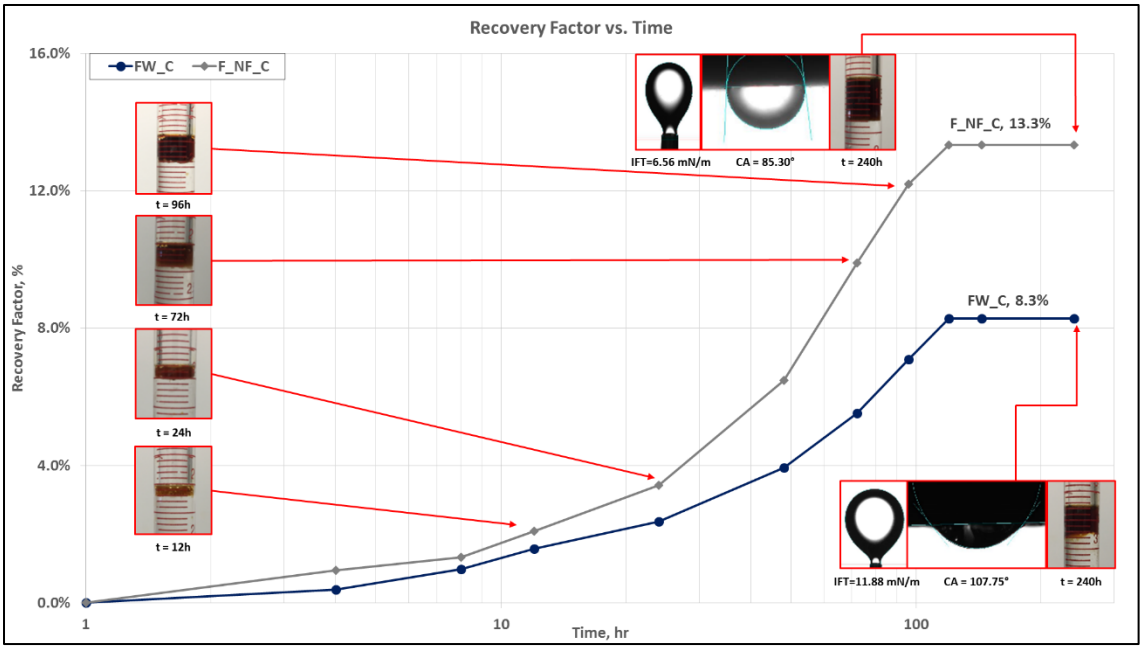

Fig. 69 – Imbibition Performance of F_NF compared to FW in WT CR

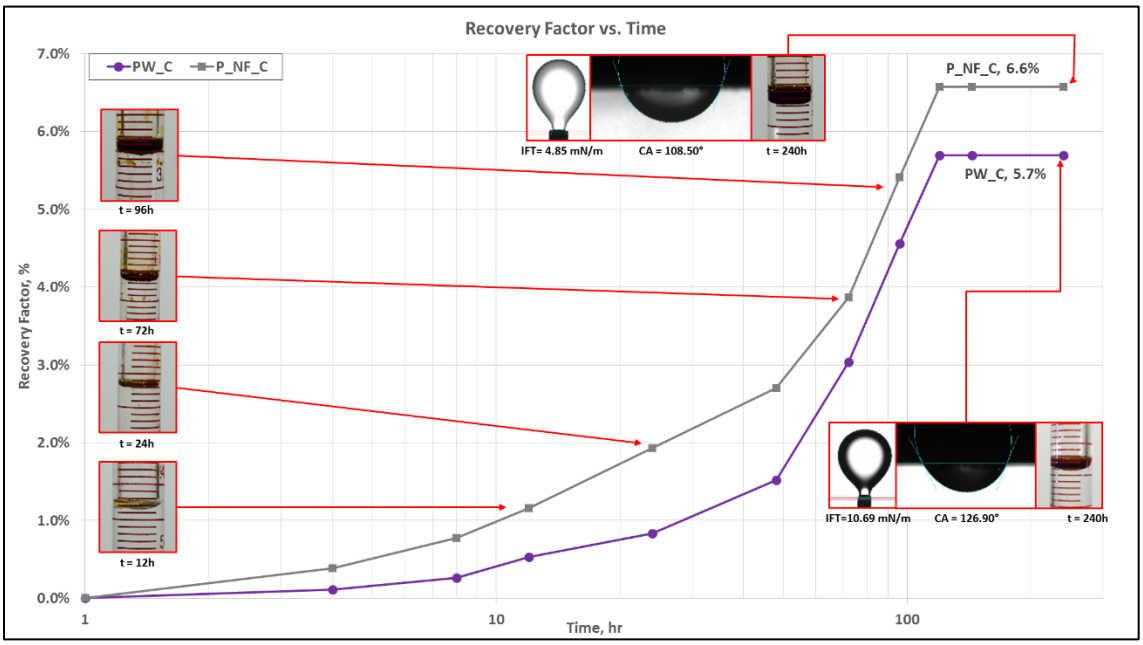

Fig. 70 - Imbibition Performance of P_NF compared to PW in WT CR

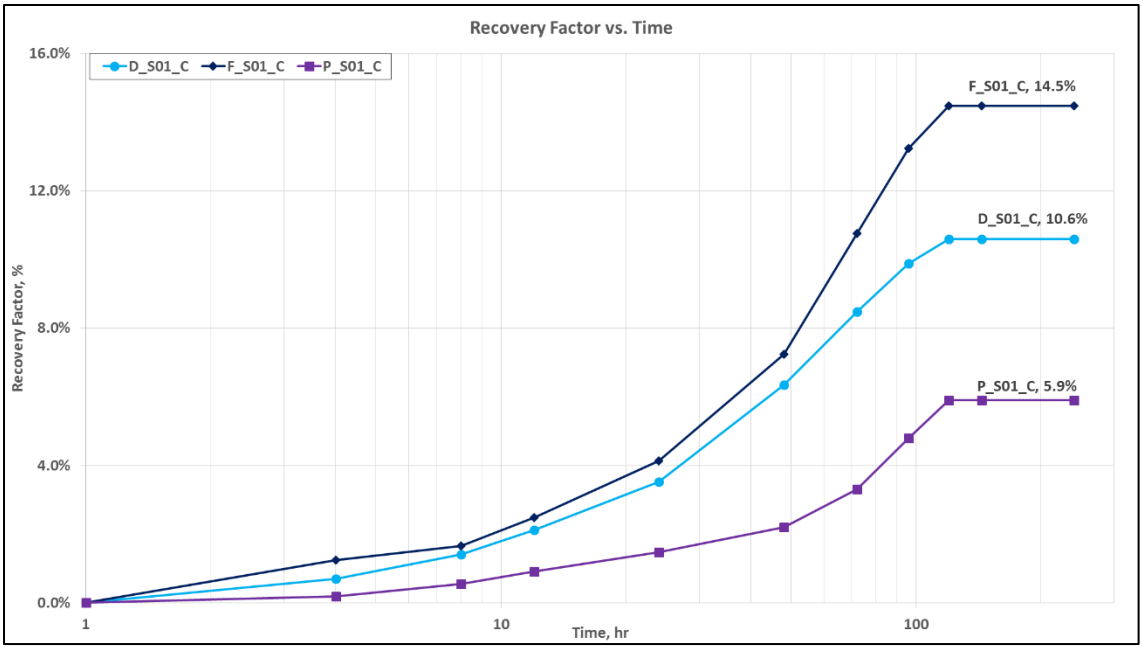

Fig. 71 – Overall Comparison of Imbibition Performance for Surfactant01 in WT CR

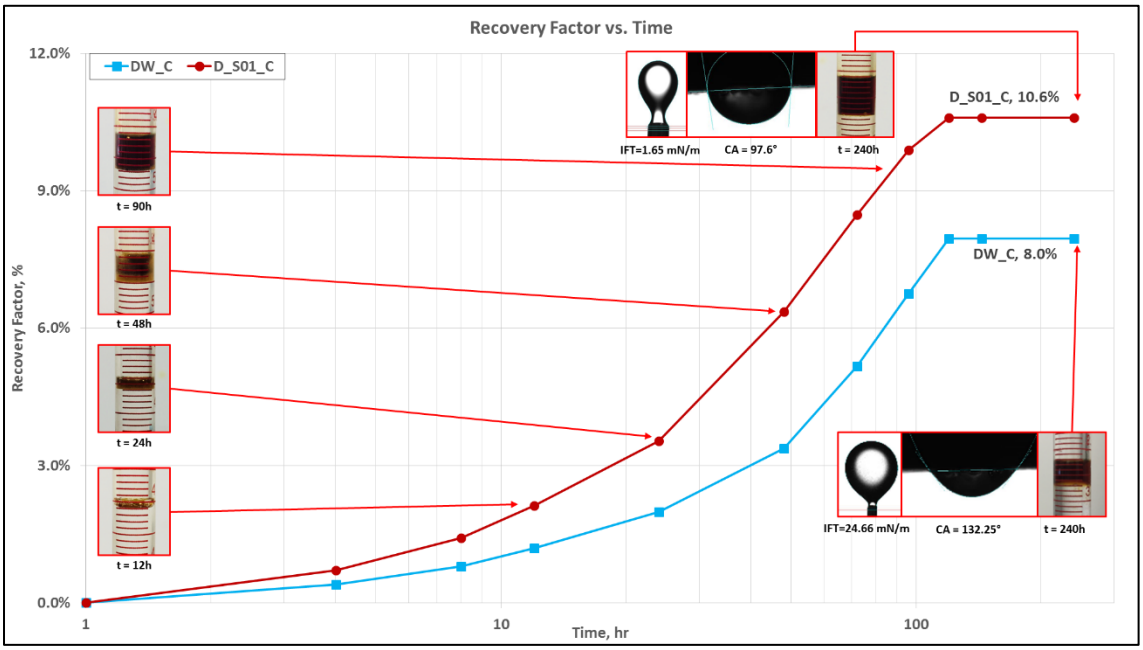

Fig. 72 – Imbibition Performance of D_S01 compared to DW in WT CR

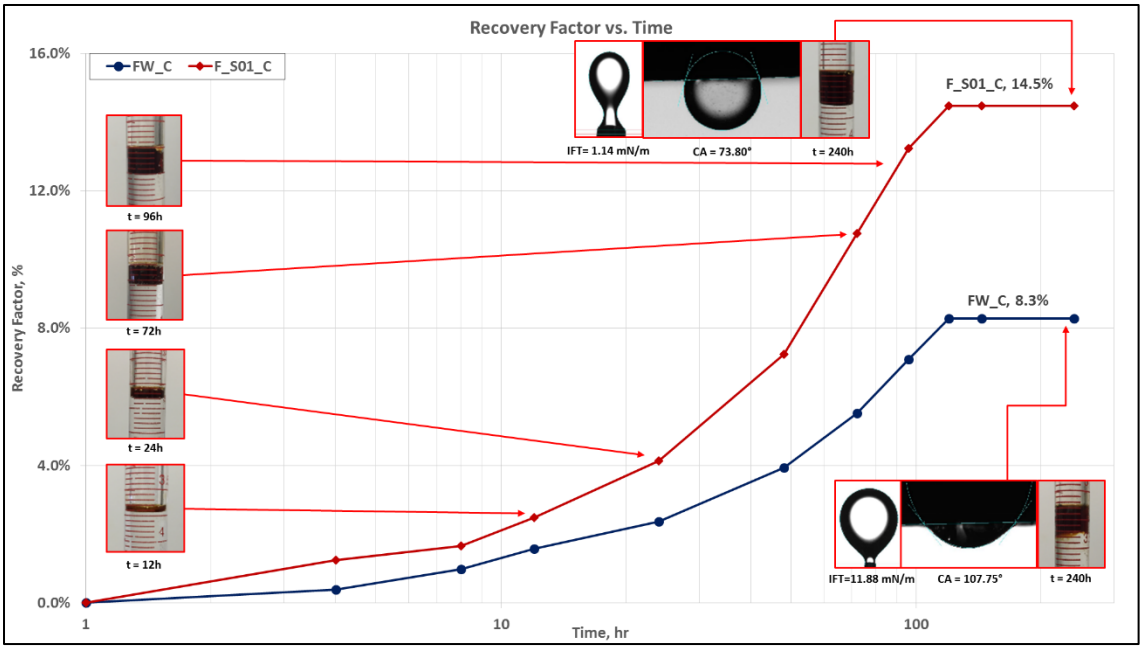

Fig. 73 – Imbibition Performance of F_S01 compared to FW in WT CR

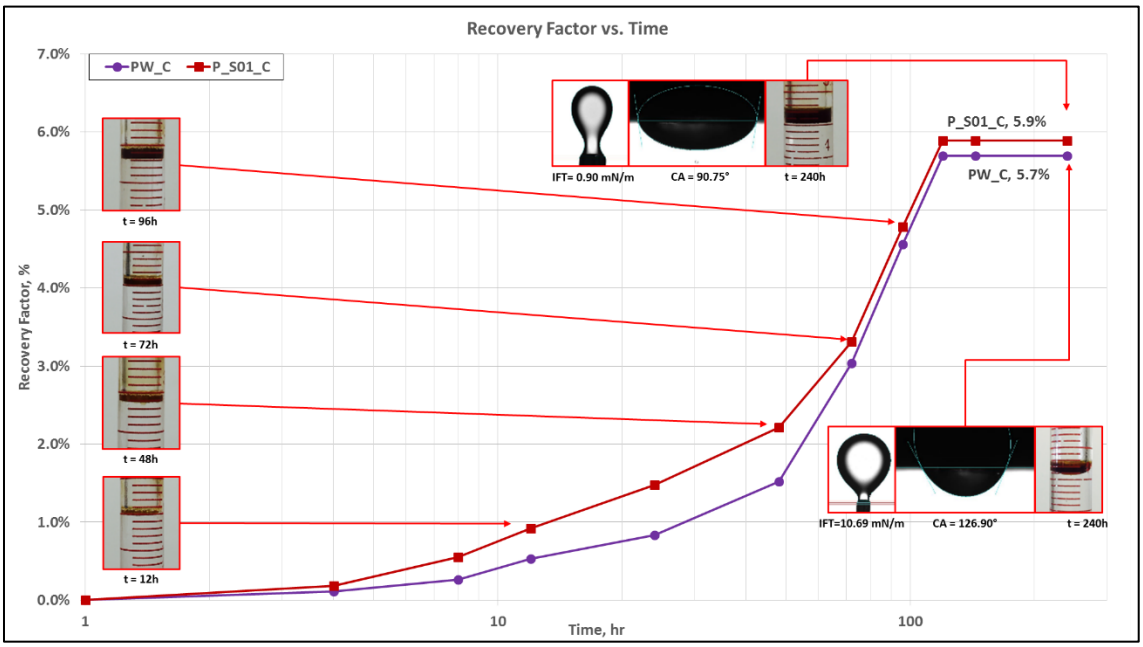

Fig. 74 – Imbibition Performance of P_S01 compared to PW in WT CR

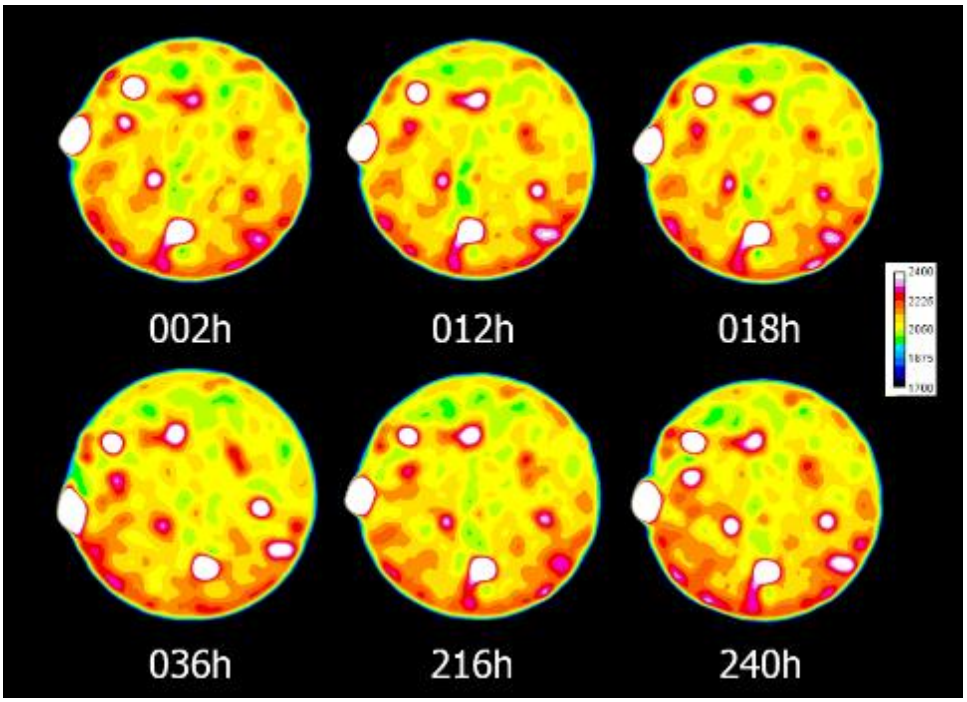

Fig. 75 – Timely Cross-sectional CT Images of a Core for DW in WT CR

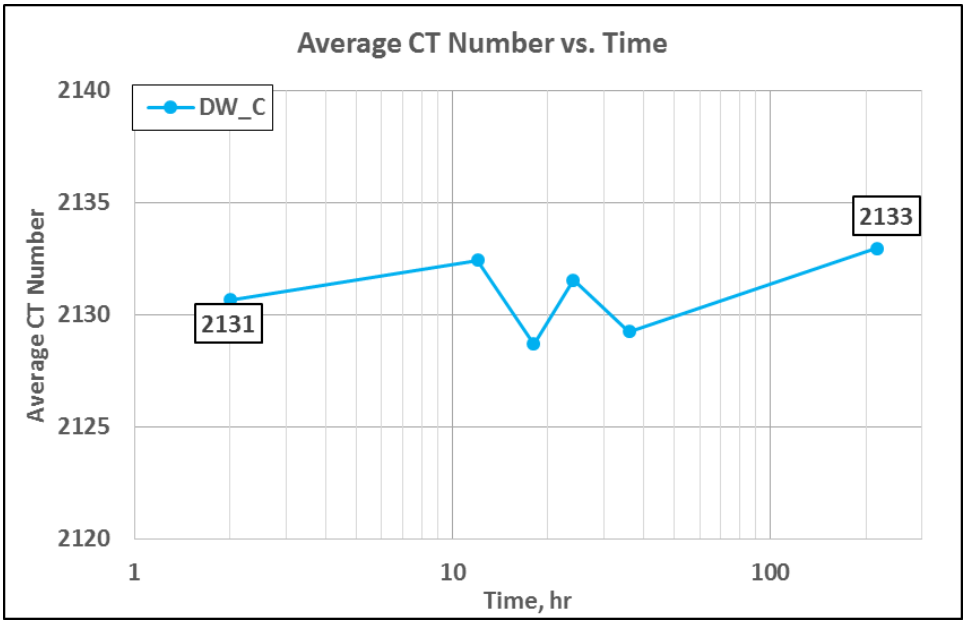

Fig. 76 – Change in Avg. CT Number for DW in WT CR

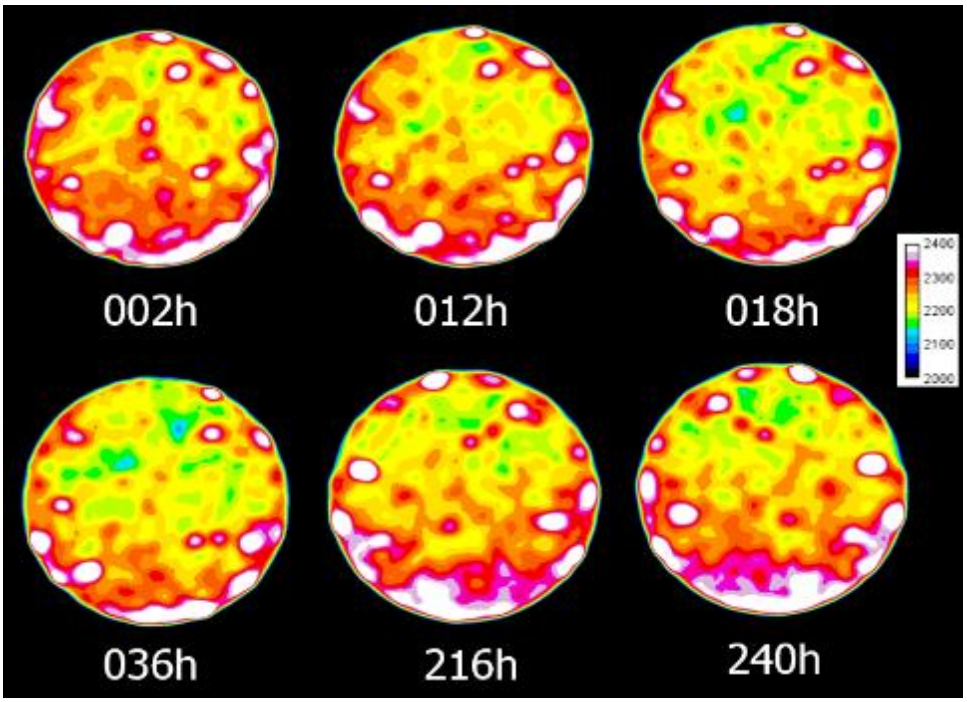

Fig. 77 – Timely Cross-sectional CT Images of a Core for FW in WT CR

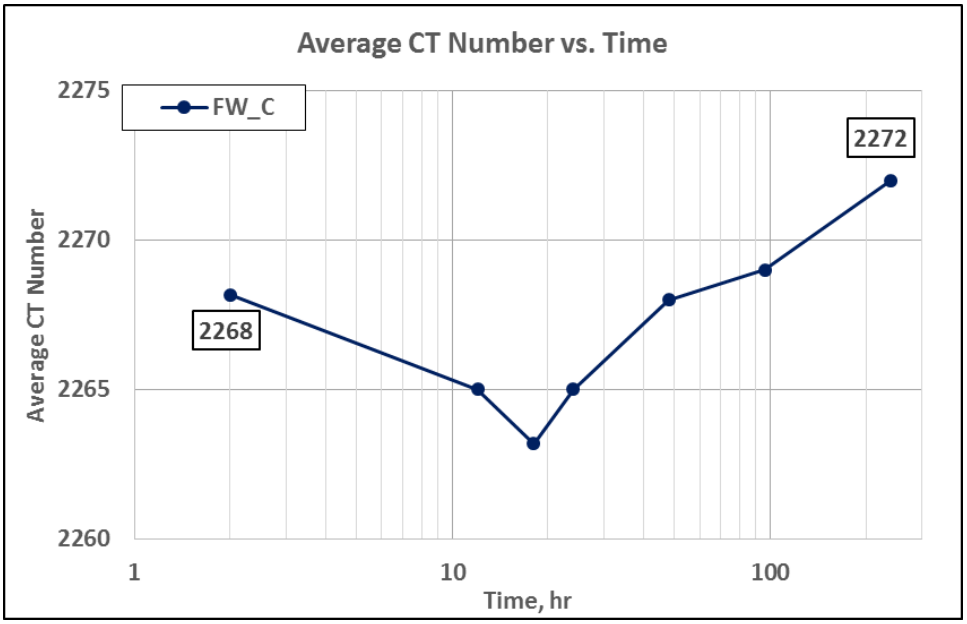

Fig. 78 – Change in Avg. CT Number for FW in WT CR

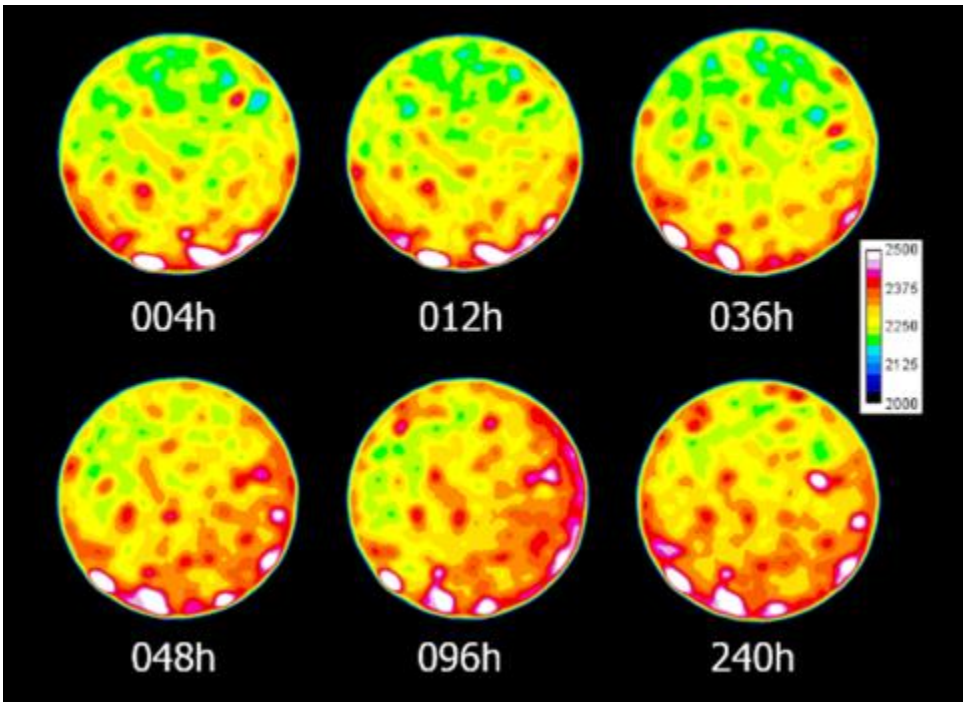

Fig. 79 – Timely Cross-sectional CT Images of a Core for PW in WT CR

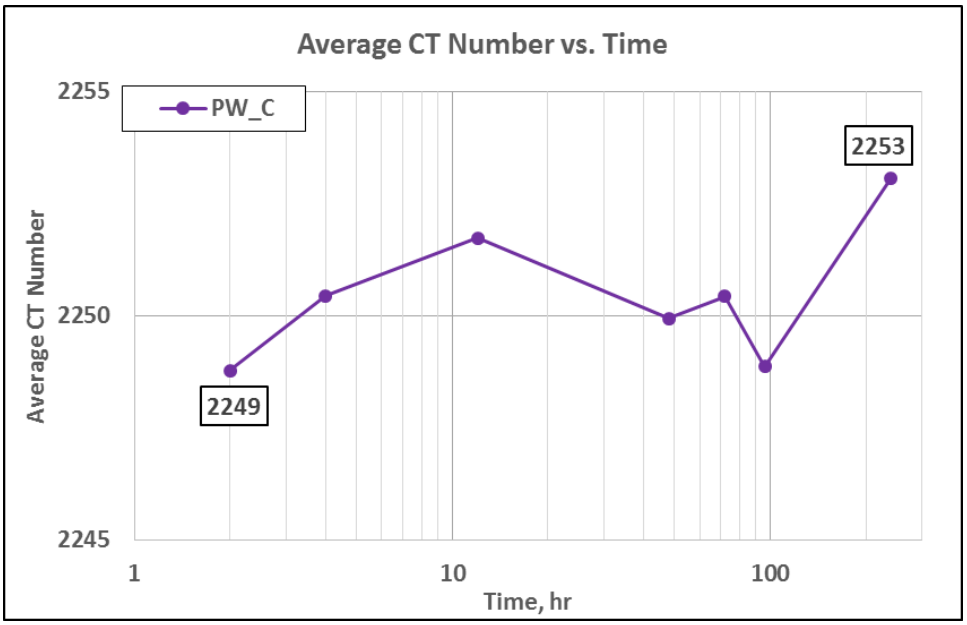

Fig. 80 – Change in Avg. CT Number for PW in WT CR

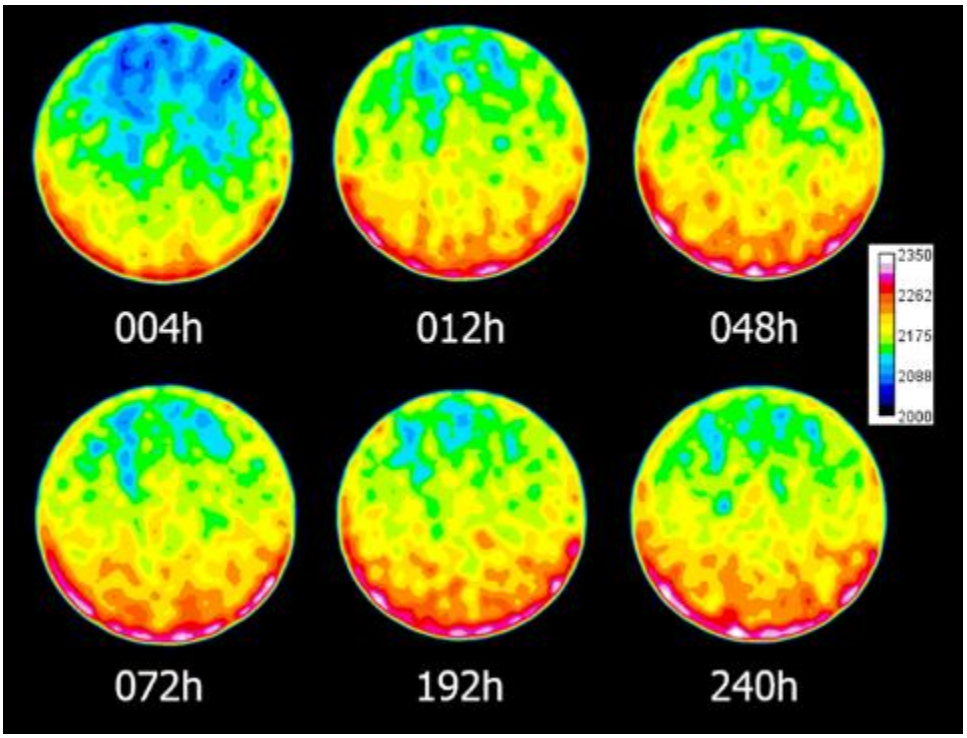

Fig. 81 – Timely Cross-sectional CT Images of a Core for D_NF in WT CR

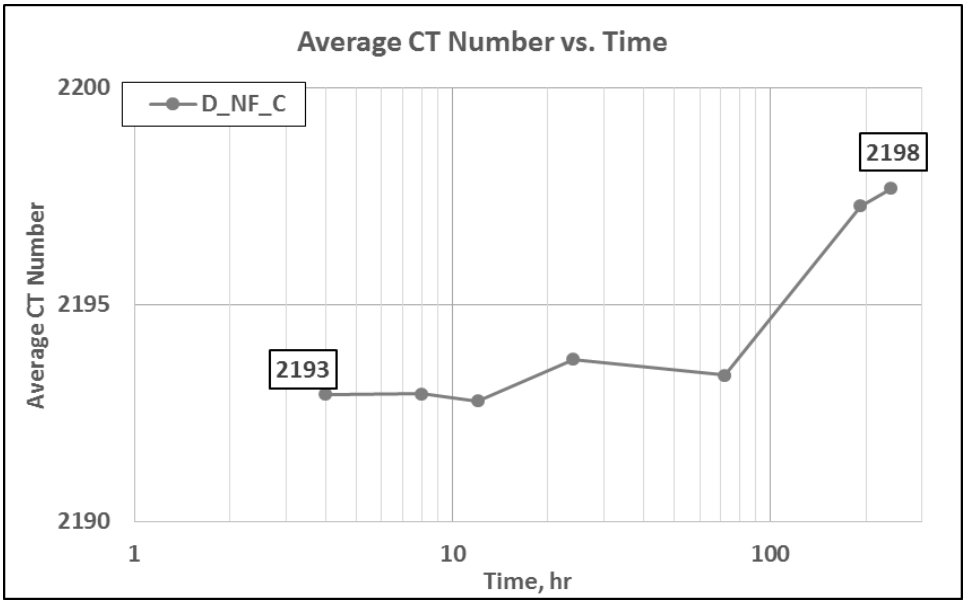

Fig. 82 – Change in Avg. CT Number for D_NF in WT CR

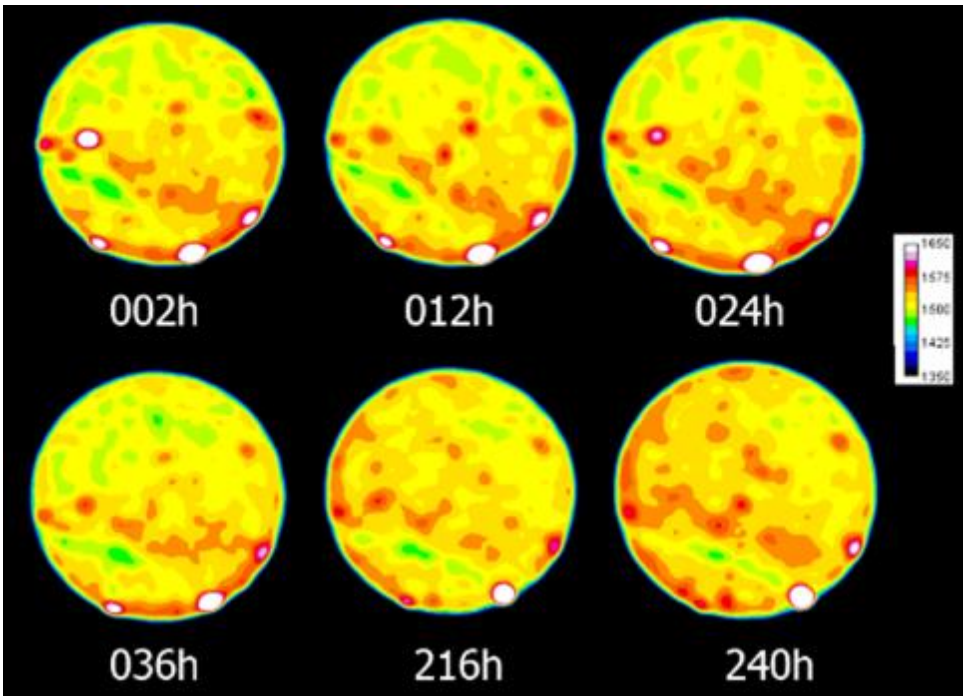

Fig. 83 – Timely Cross-sectional CT Images of a Core for F_NF in WT CR

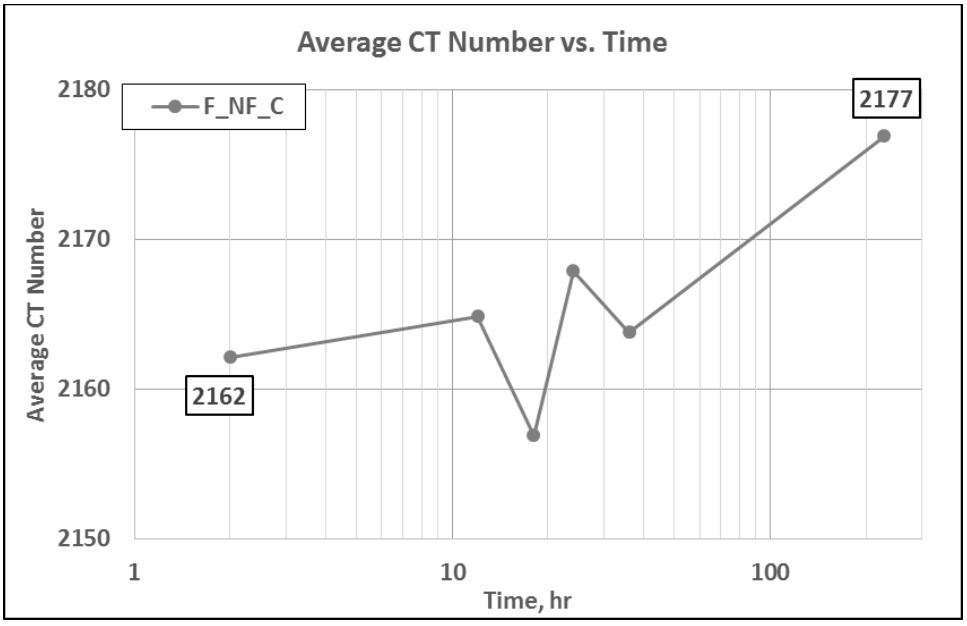

Fig. 84 – Change in Avg. CT Number for F_NF in WT CR

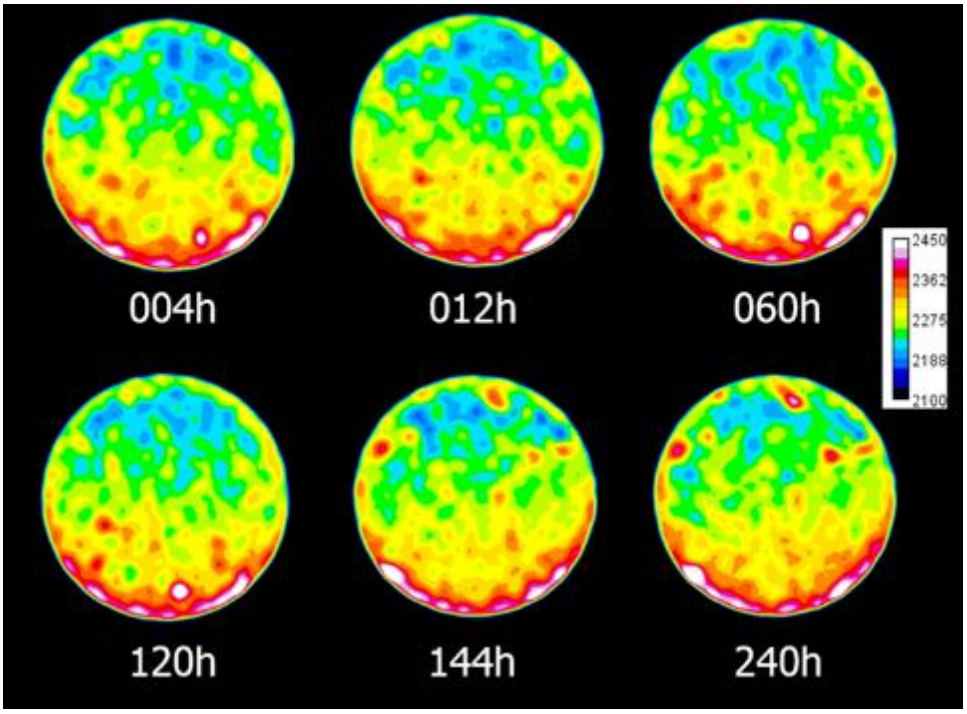

Fig. 85 – Timely Cross-sectional CT Images of a Core for P_NF in WT CR

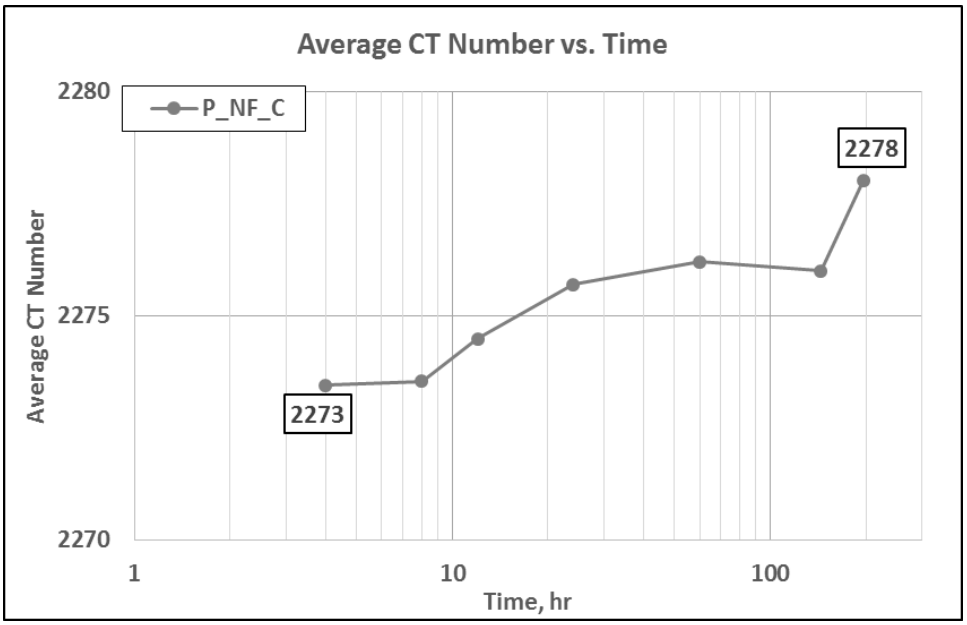

Fig. 86 – Change in Avg. CT Number for P_NF in WT CR

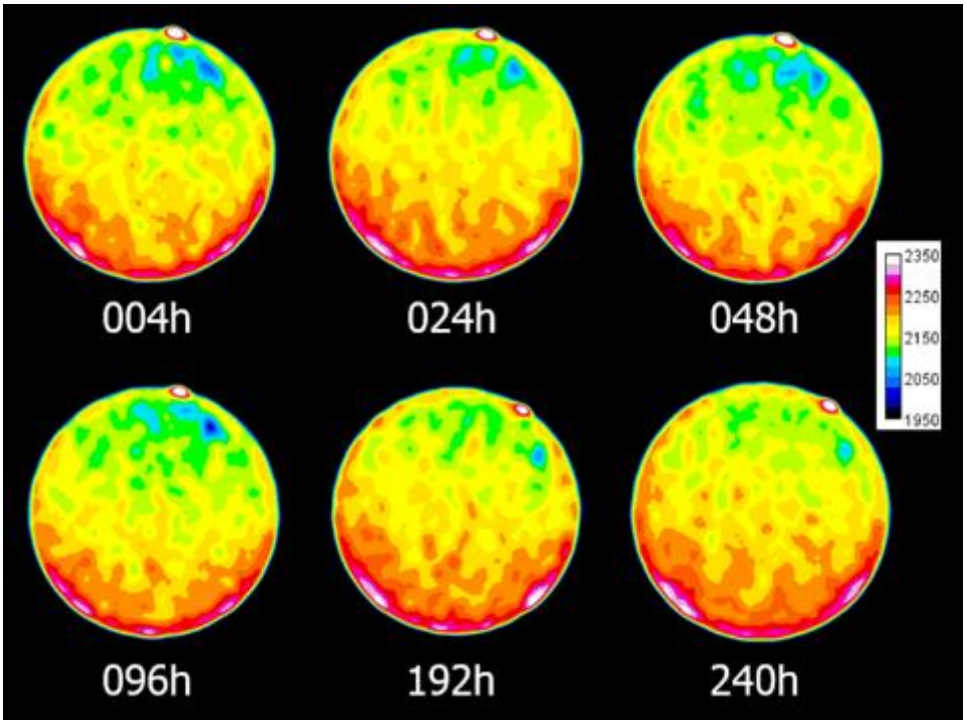

Fig. 87 - Timely Cross-sectional CT Images of a Core for D_S01 in WT CR

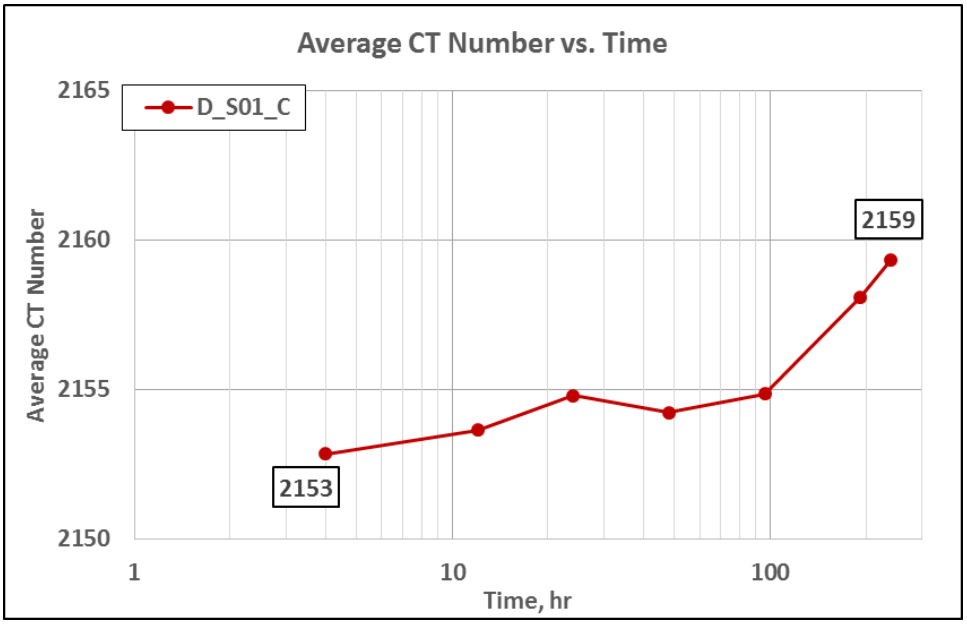

Fig. 88 – Change in Avg. CT Number for D_S01 in WT CR

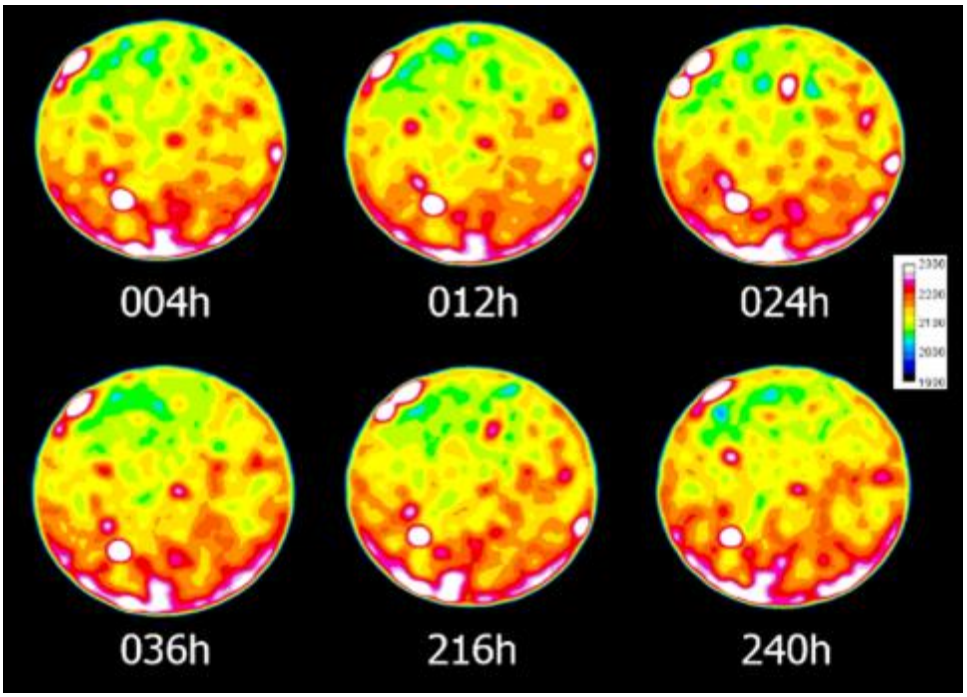

Fig. 89 – Timely Cross-sectional CT Images of a Core for F_S01 in WT CR

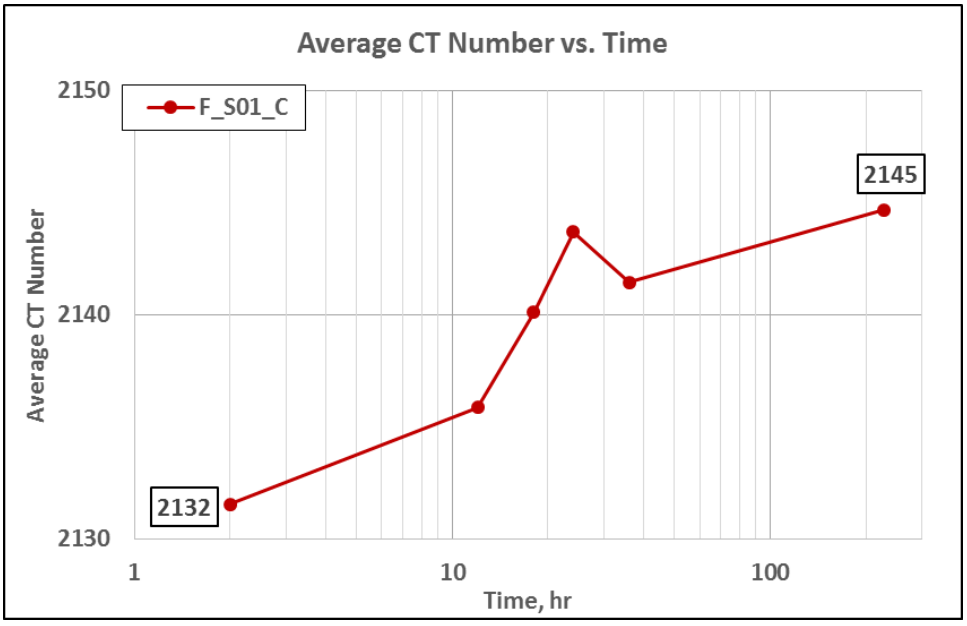

Fig. 90 – Change in Avg. CT Number for F_S01 in WT CR

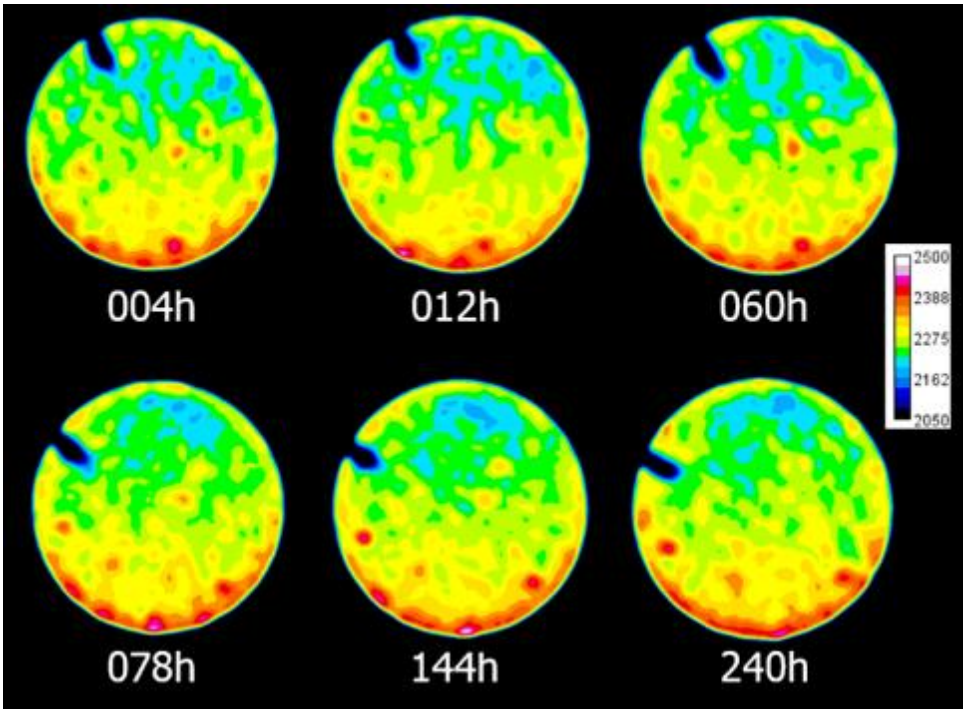

Fig. 91 – Timely Cross-sectional CT Images of a Core for P_S01 in WT CR

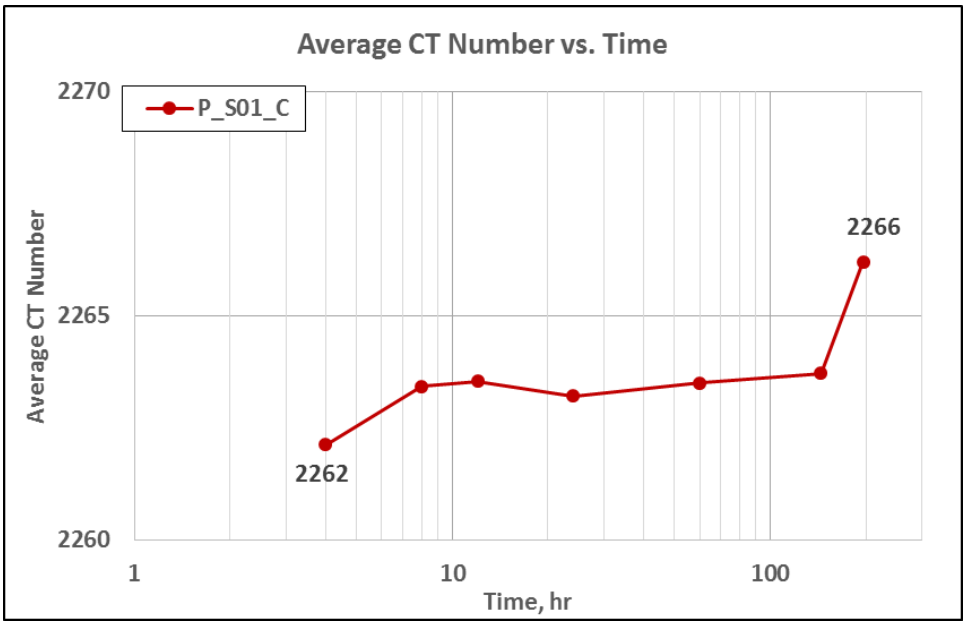

Fig. 92 – Change in Avg. CT Number for P_S01 in WT CR

Table 32 – Results of CT Image, and Weight Analyses for All Fluids in WT CR

Fluid	Initial Ave. CT #	Final Ave. CT #	Penetration Magnitude	Initial Weight, g	Final Weight, g	ΔWeight, g	RF, %
DW_C	2131	2133	2	80.83	80.96	0.13	8.0 %
FW_C	2268	2272	4	83.26	83.35	0.09	8.3 %
PW_C	2249	2253	4	86.62	86.70	0.08	5.7%
D_NF_C	2193	2198	5	91.16	91.22	0.06	9.7%
F_NF_C	2162	2177	15	84.99	85.15	0.16	13.3 %
P_NF_C	2273	2278	5	86.02	86.14	0.11	6.6%
D_S01_C	2153	2159	6	92.89	92.98	0.09	10.6%
F_S01_C	2132	2145	13	78.41	78.54	0.14	14.5 %
P_S01_C	2262	2266	4	89.71	89.80	0.09	5.9%

5.4.2 Spontaneous Imbibition for WT Quartz Rich

Compared to WT carbonate rich rocks, oil recovery from WT quartz rich rock was much higher, ranging from 11 % to 34 %, and the imbibition rate was also faster. Like the results in the previous section, recovery factor was the highest with low salinity aqueous phase solutions regardless of the presence of surfactants. However, in contrast to imbibition results with carbonate rich cores, solutions with high salinity produced more oil than fluids with no salinity, but at slower rate.

For three cases of water without chemical additives, FW, again, had the highest recovery factor of 13.1 %, compared to DW or PW with 11.0 % and 11.7 %, respectively. Interestingly, PW with high salinity showed higher recovery factor than DW with no salinity, producing at much slower rate. This may indicate that even though PW is lacking the ability to alter wettability compared to DW, lower IFT between crude oil and PW causes gravity drainage to occur more effectively in comparably more homogeneous and

more porous quartz rich cores. However, like the conclusion from the imbibition with carbonate rich rocks, the difference of recovery factor for all three is not major, and it can be concluded the impact of salinity on plain water is almost negligible.

Aqueous phase solutions with Nano-technology Fluid or Surfactant01 showed similar behaviors of imbibition performance. The highest recovery factor was obtained with 1 gpt of each surfactant in a low salinity brine. Also, surfactants mixed with high salinity brine outperformed no salinity brine with surfactants by a small margin, and at much slower rate. CT images and change in average CT number showed that higher penetration magnitude occurs when higher volume of oil is produced. Overall and individual results from spontaneous imbibition for nine aqueous phase solutions are shown from **Fig. 93** to **Fig. 104**.

Timely CT image analyses and measurements of average CT number of a whole core for each case were also performed. The change of average CT number was much clearer and more distinct in quartz rich cores, also resulting in higher penetration magnitude with higher recovery factor. This can be concluded that aqueous phase solutions are more effectively penetrating into the matrix and replacing oil retained in the pore space. Similarly, most change in saturation and contrast occurred in the lower center region of the cross-sectional CT images, which indicate the influence of gravity on oil recovery mechanism. Higher changes in weight were also observed, meaning more aqueous phase solutions with heavier density are flowing into the core while displacing oil at the same time. All cross-sectional CT images, average CT number measurements, and other important parameters are presented in **Fig. 105** through **Fig. 122**, and **Table 33**.

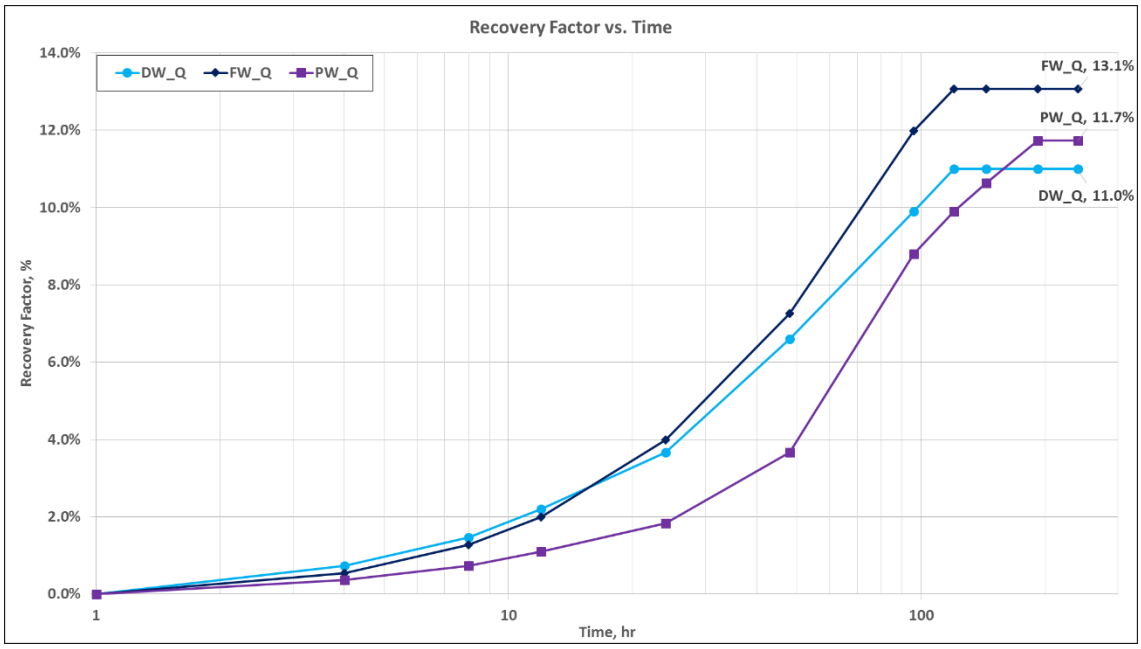

Fig. 93 – Overall Comparison of Imbibition Performances for Water in WT QR

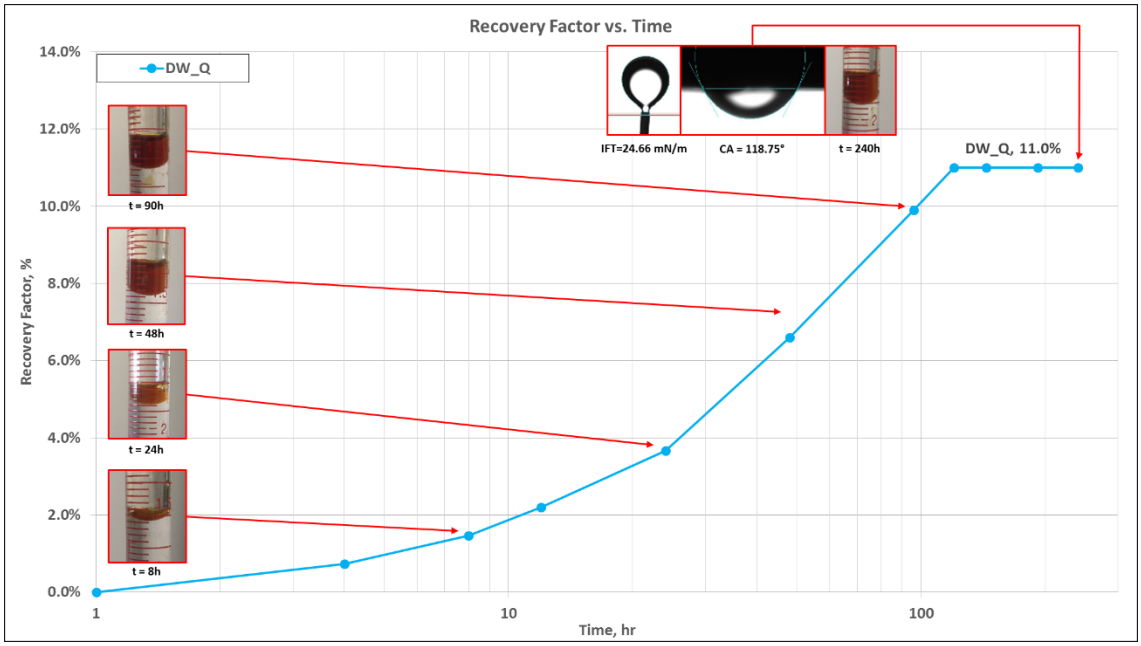

Fig. 94 - Imbibition Performance of DW in WT QR

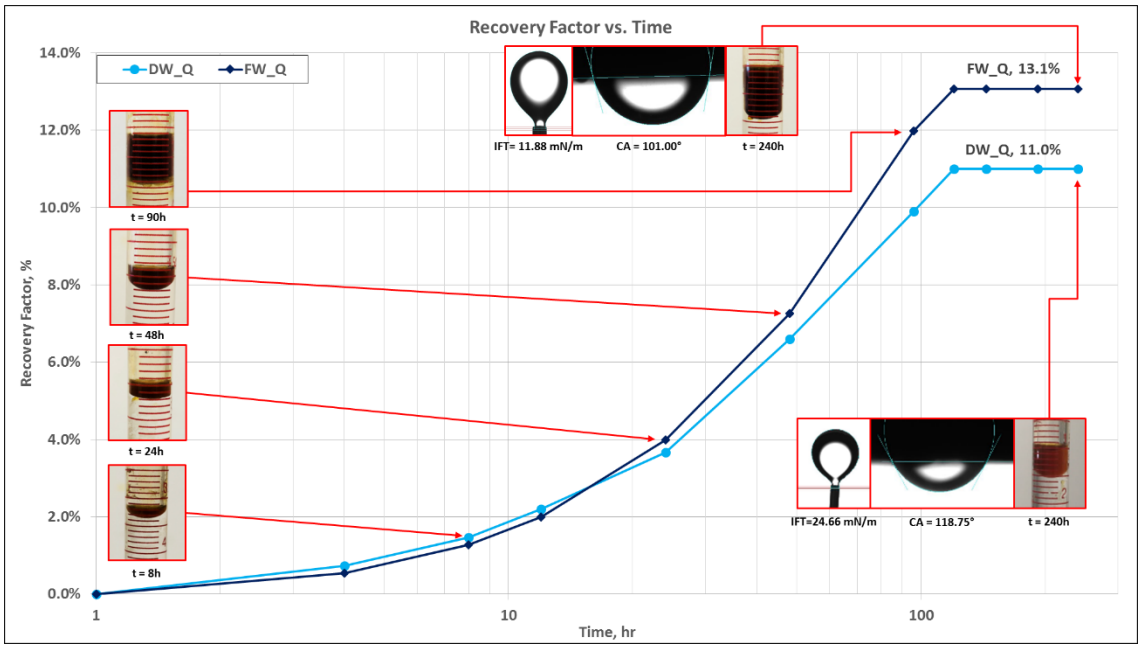

Fig. 95 – Imbibition Performance of FW compared to DW in WT QR

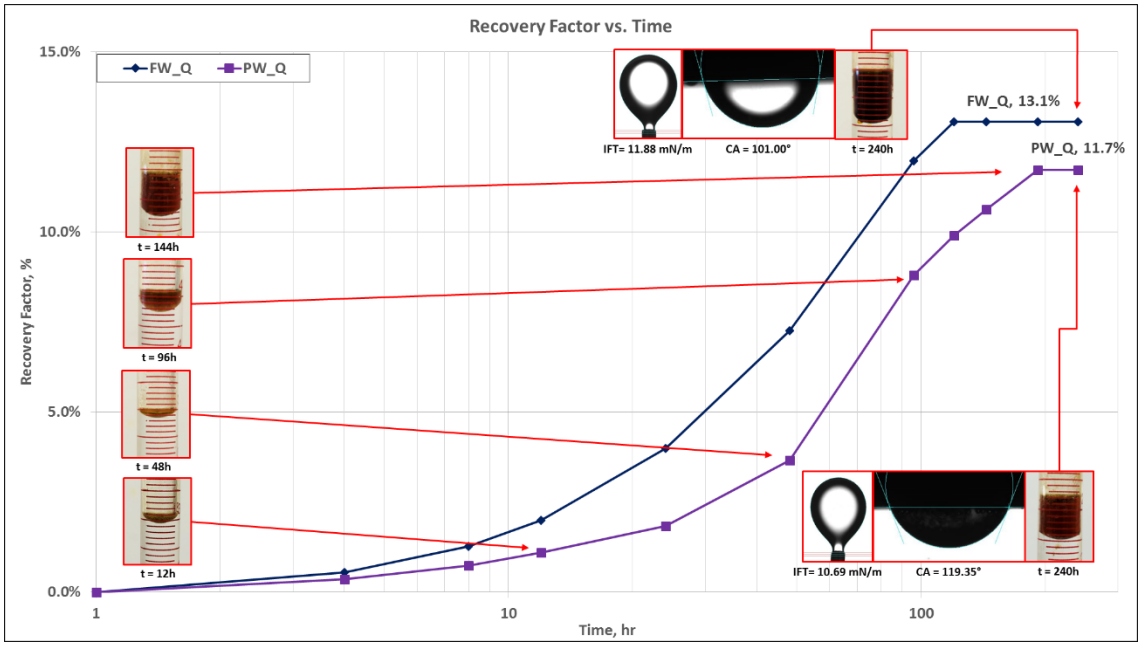

Fig. 96 – Imbibition Performance of PW compared to FW in WT QR

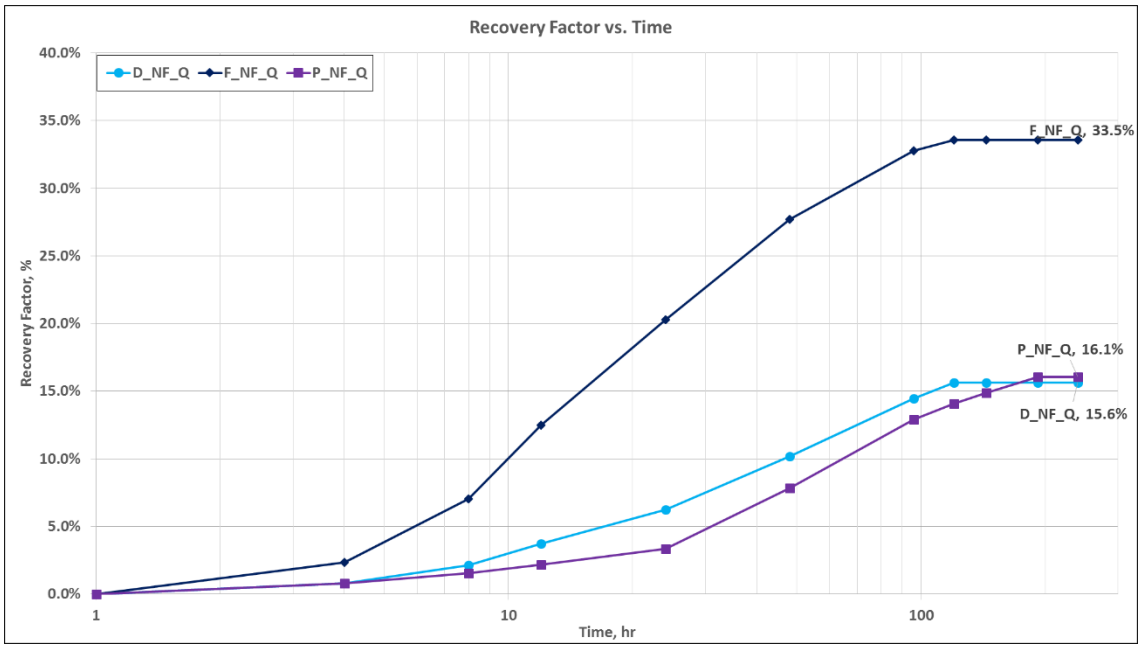

Fig. 97 - Overall Comparison of Imbibition Performances for Nano-Technology Fluid in WT CR

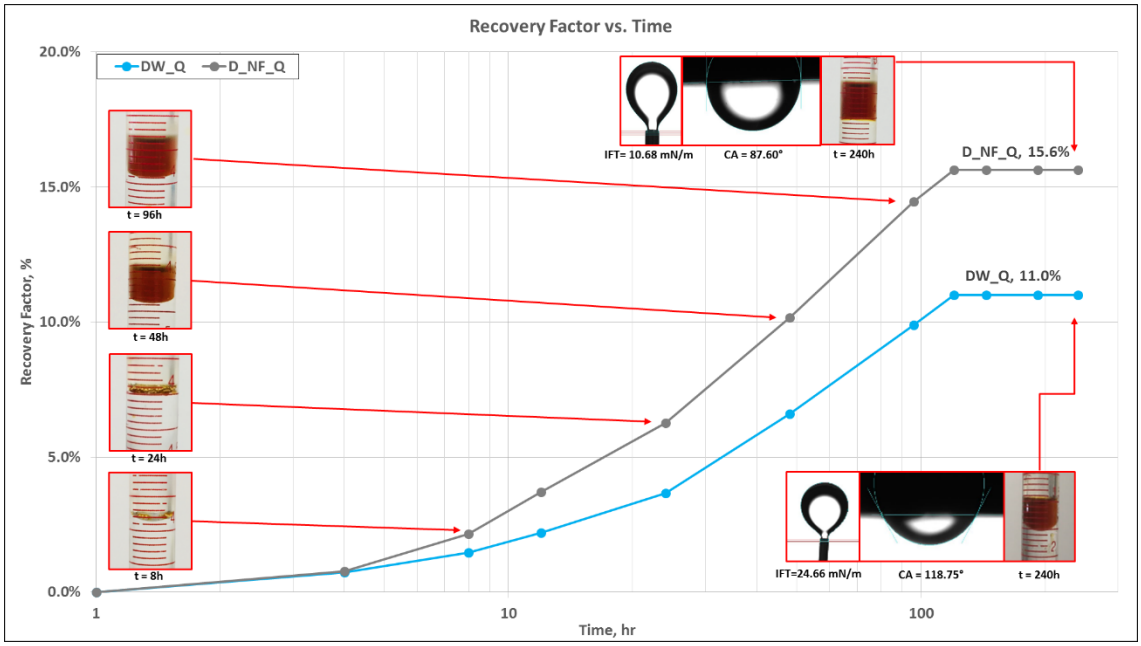

Fig. 98 – Imbibition Performance of D_NF compared to DW in WT QR

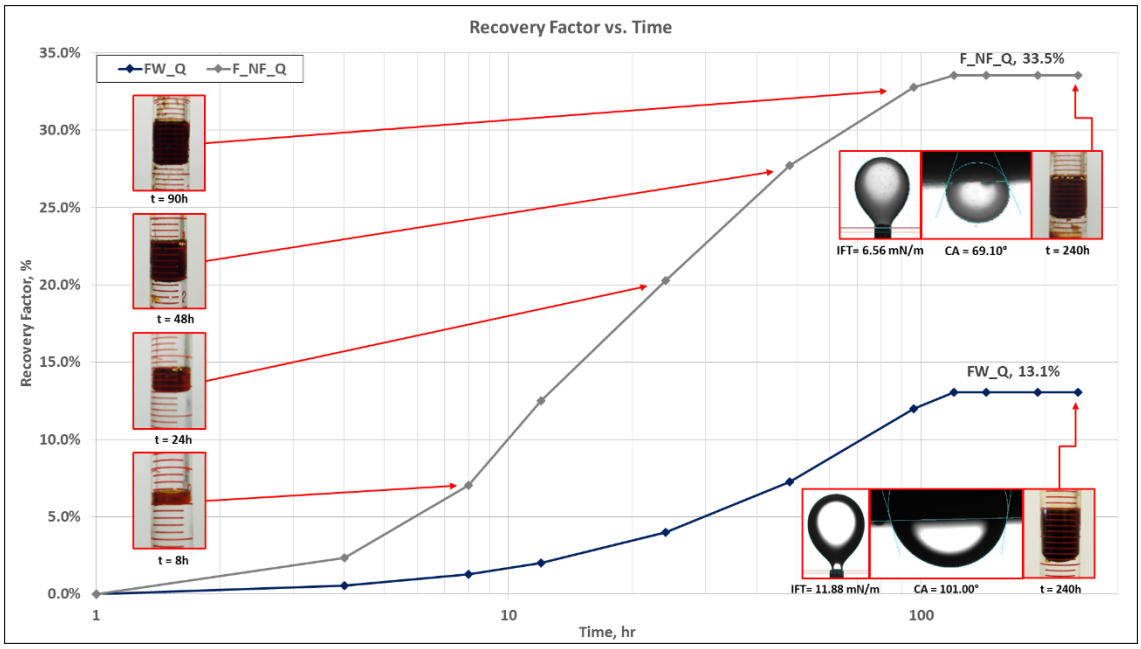

Fig. 99 – Imbibition Performance of F_NF compared to FW in WT QR

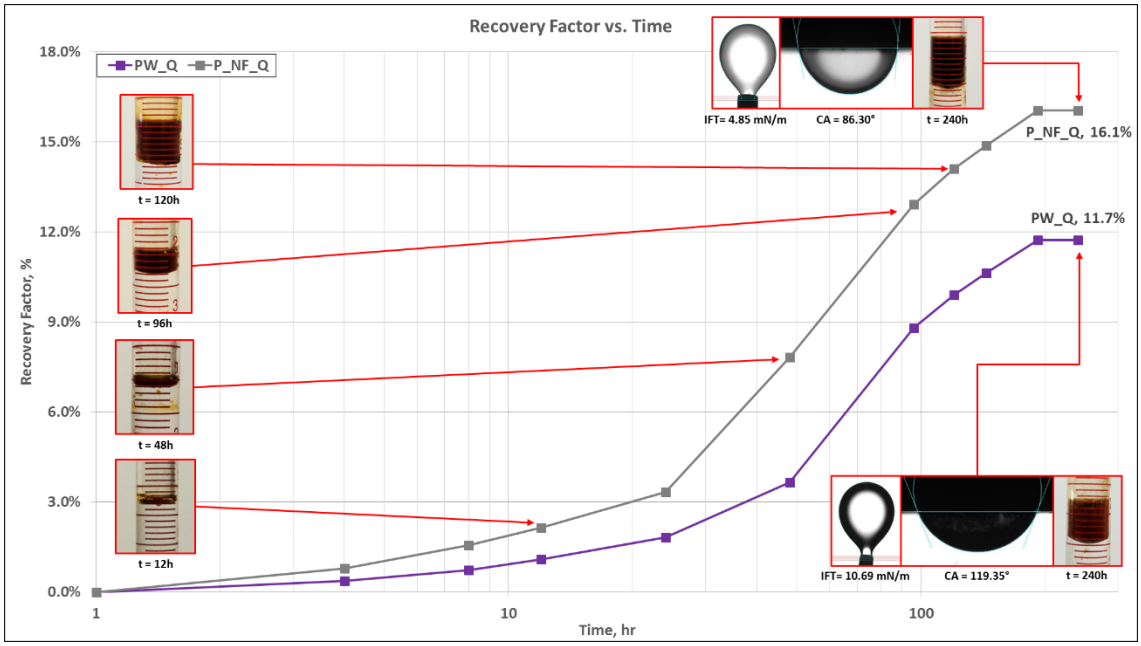

Fig. 100 – Imbibition Performance of P_NF compared to PW in WT QR

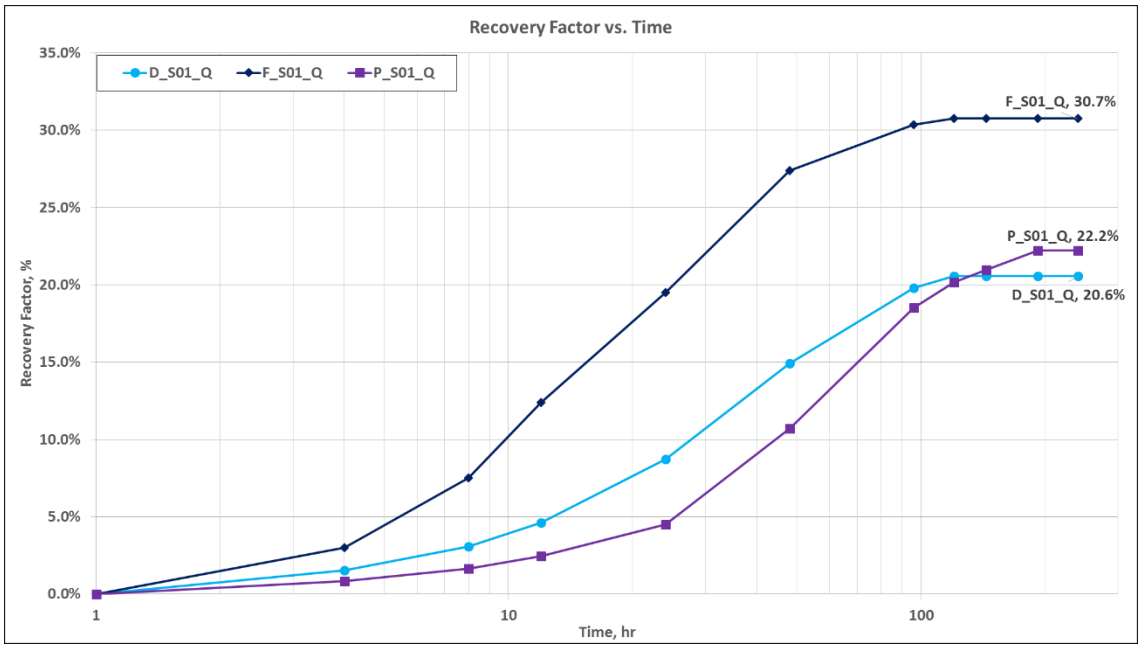

Fig. 101 – Overall Comparison of Imbibition Performances for Surfactant01 in WT QR

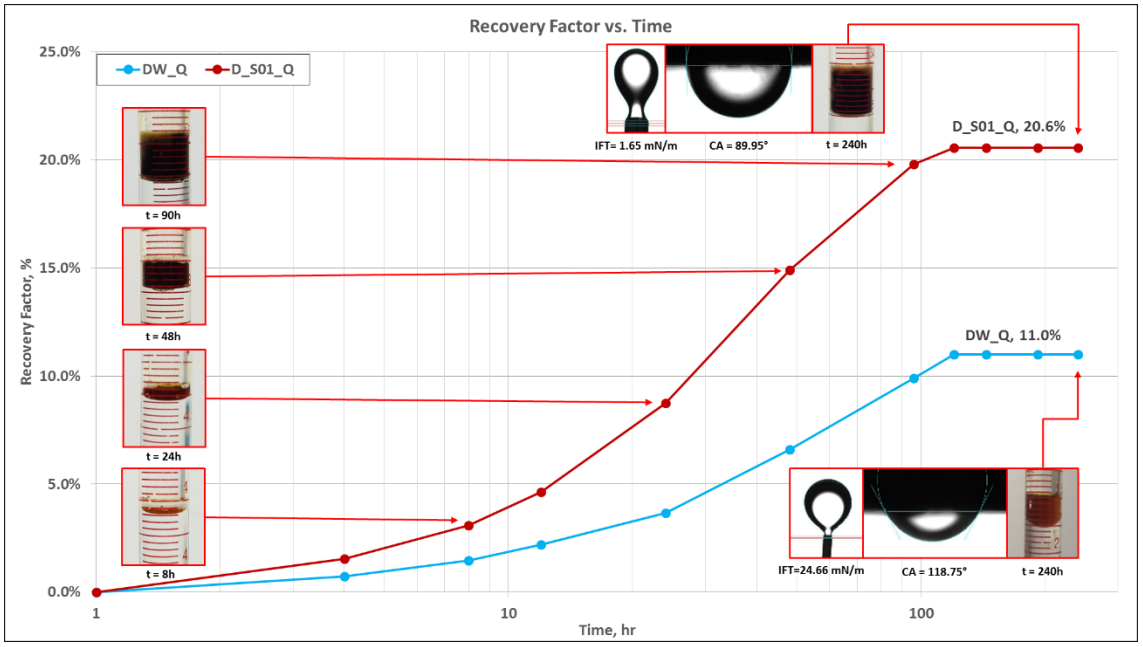

Fig. 102 – Imbibition Performance of D_S01 compared to DW in WT CR

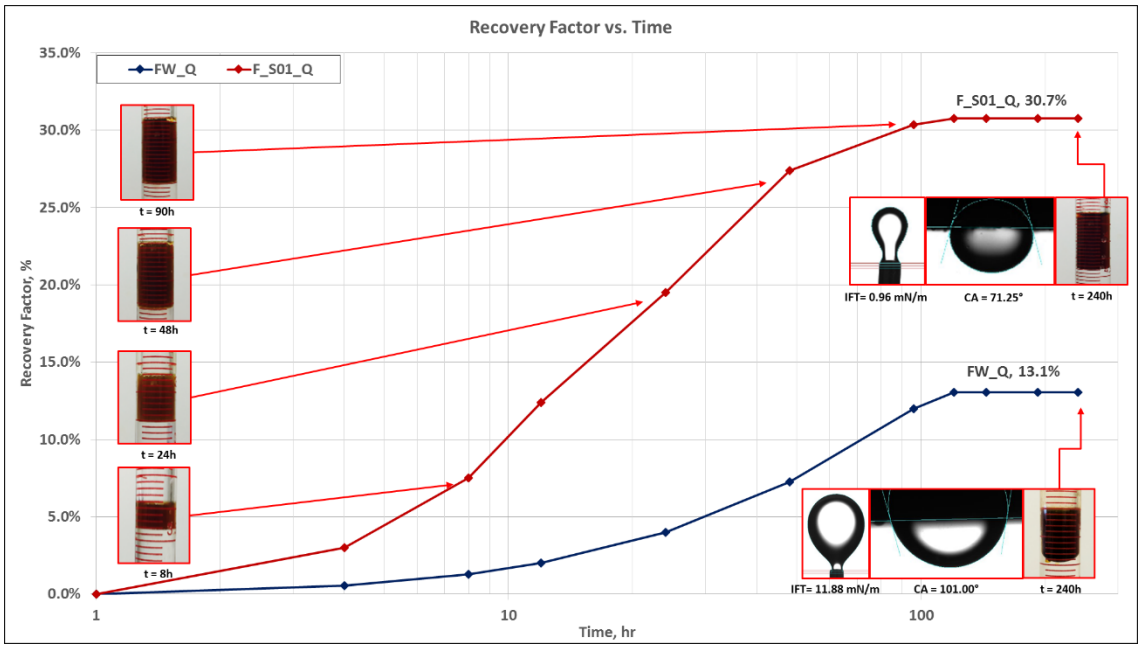

Fig. 103 - Imbibition Performance of F_S01 compared to FW in WT QR

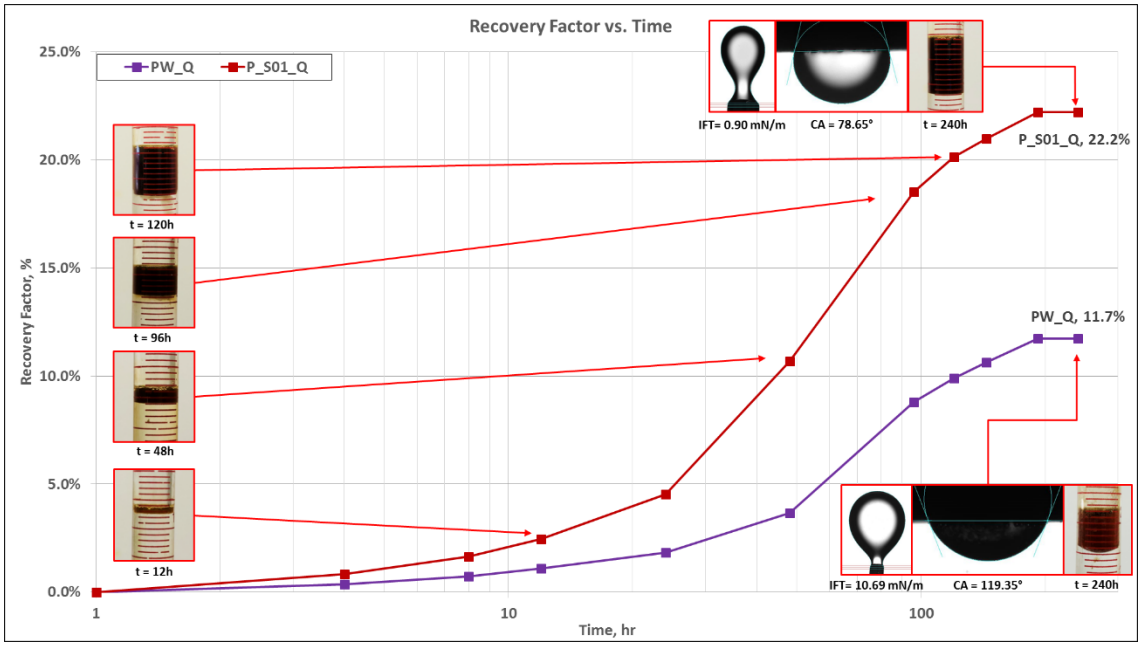

Fig. 104 - Imbibition Performance of P_S01 compared to PW in WT QR

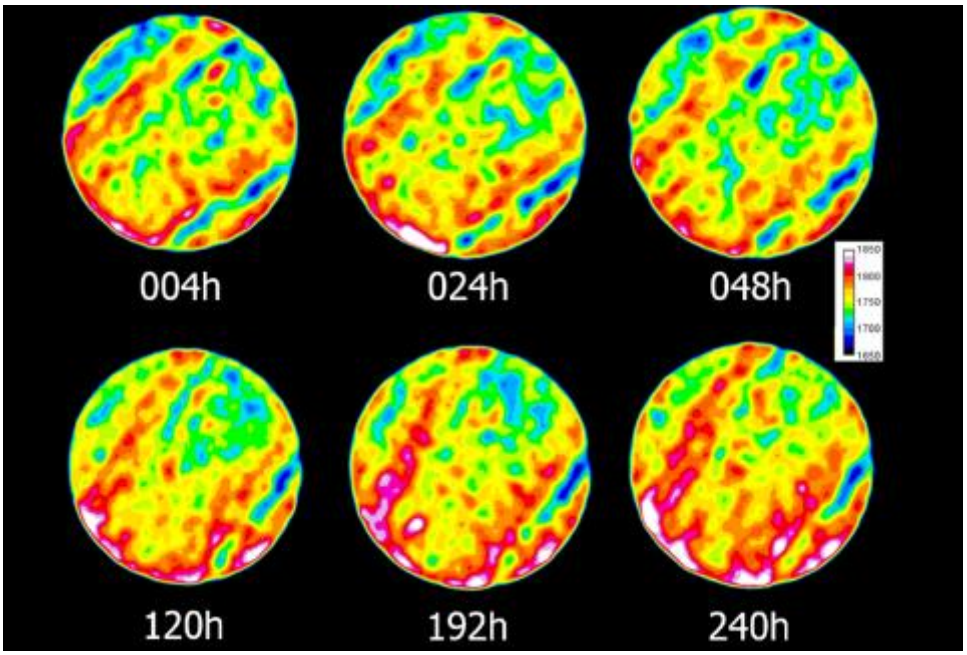

Fig. 105 – Timely Cross-sectional CT Images of a Core for DW in WT QR

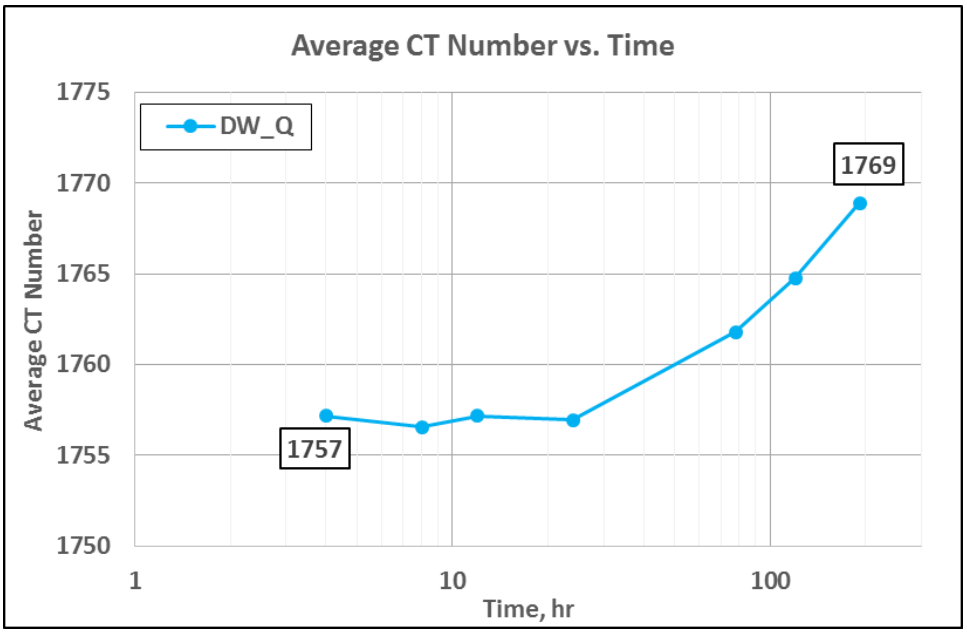

Fig. 106 – Change in Avg. CT Number for DW in WT QR

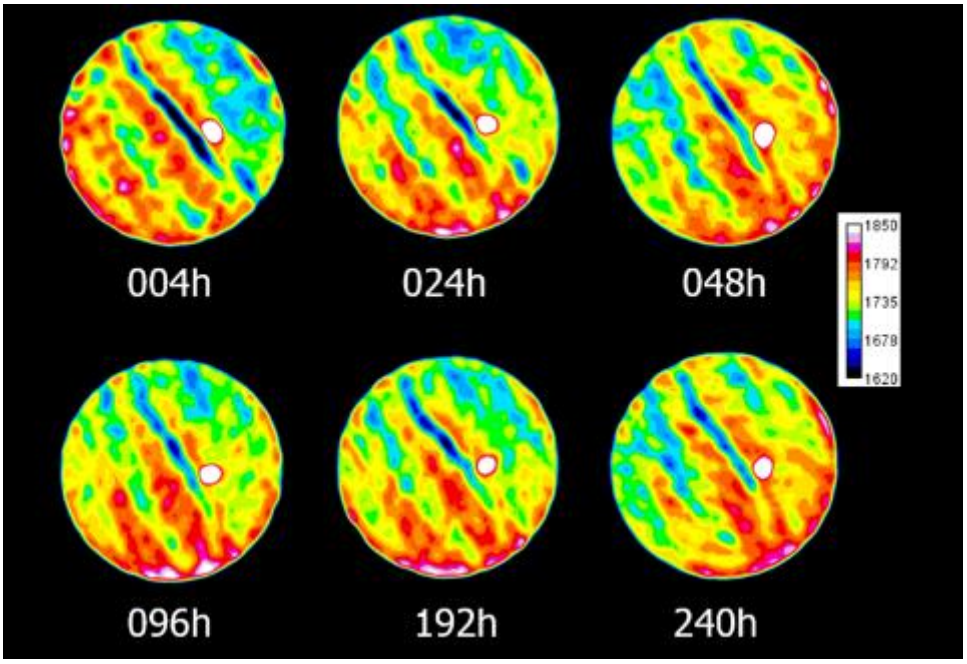

Fig. 107 – Timely Cross-sectional CT Images of a Core for FW in WT QR

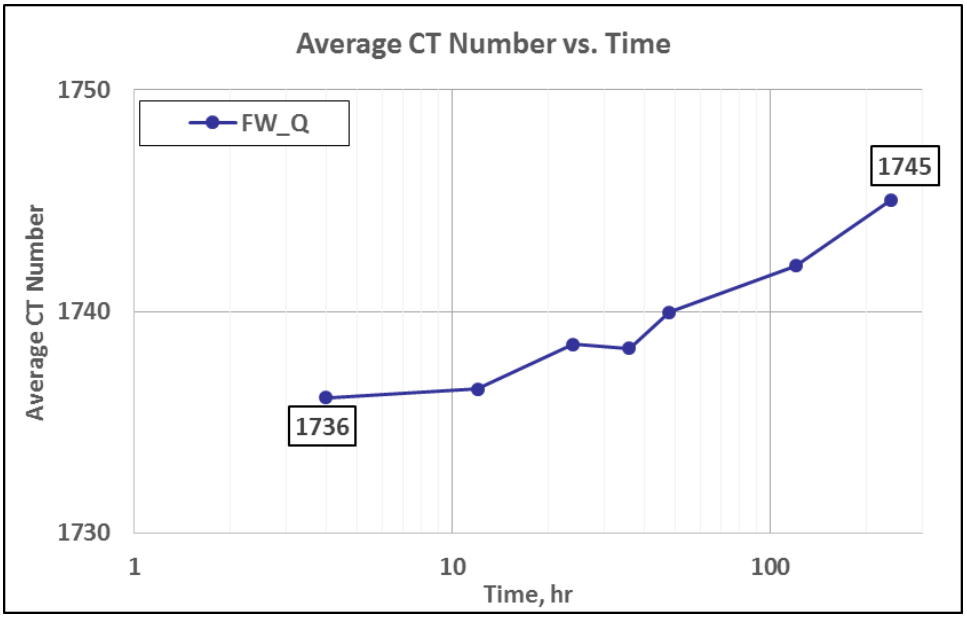

Fig. 108 – Change in Avg. CT Number for FW in WT QR

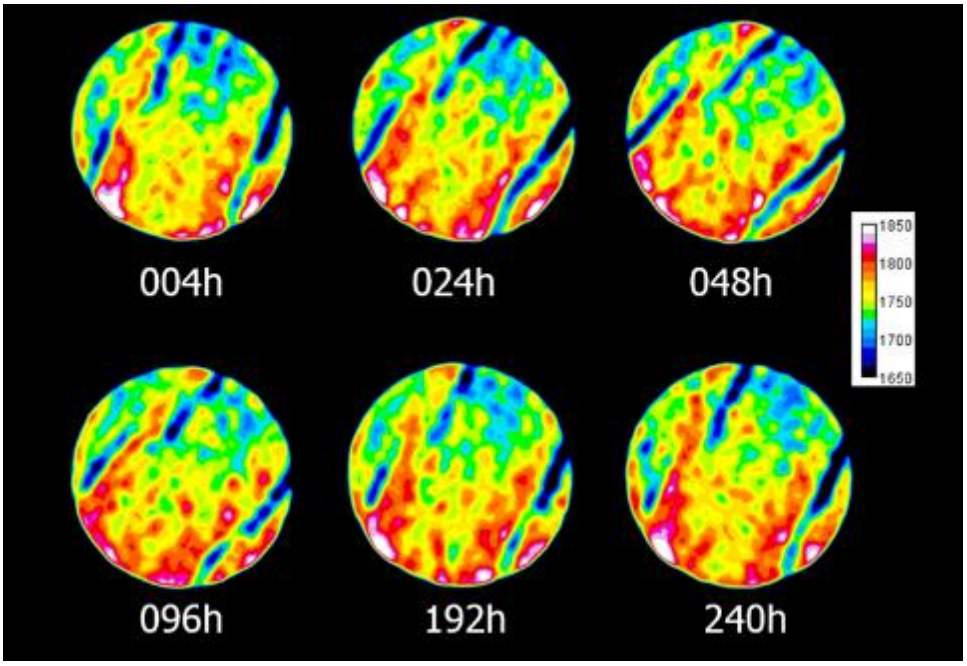

Fig. 109 – Timely Cross-sectional CT Images of a Core for PW in WT QR

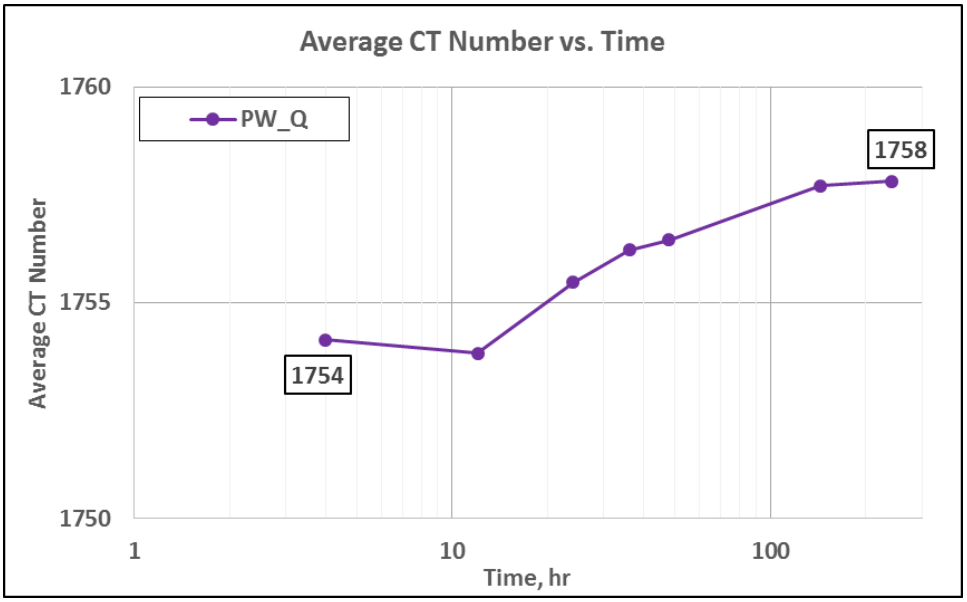

Fig. 110 – Change in Avg. CT Number for PW in WT QR

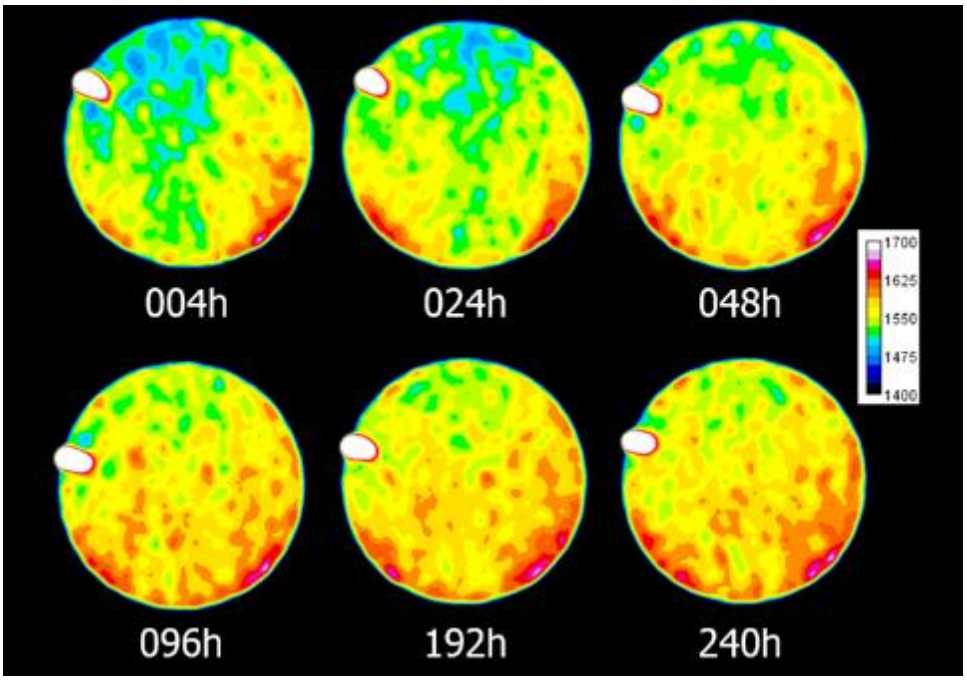

Fig. 111 - Timely Cross-sectional CT Images of a Core for D_NF in WT QR

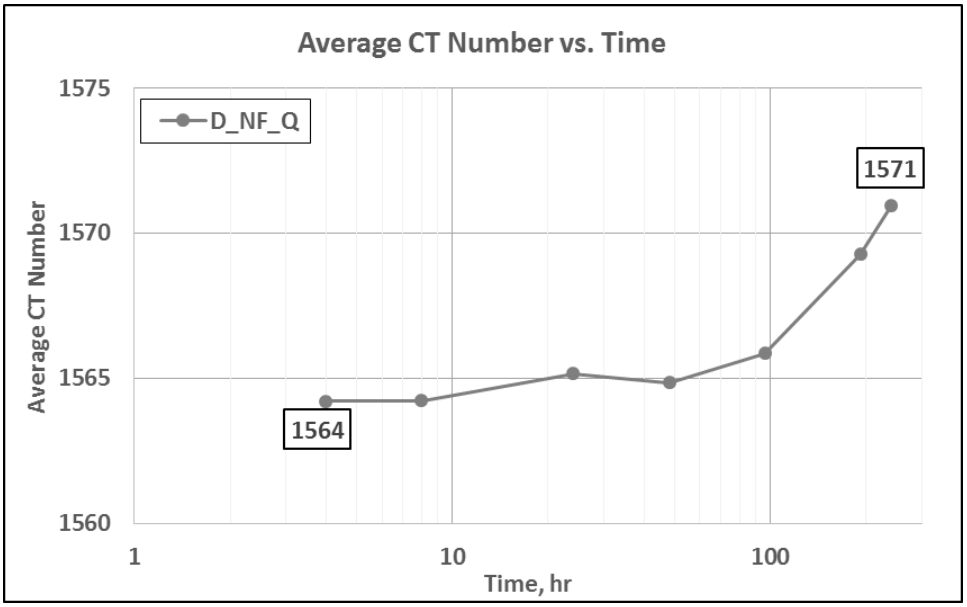

Fig. 112 – Change in Avg. CT Number for D_NF in WT QR

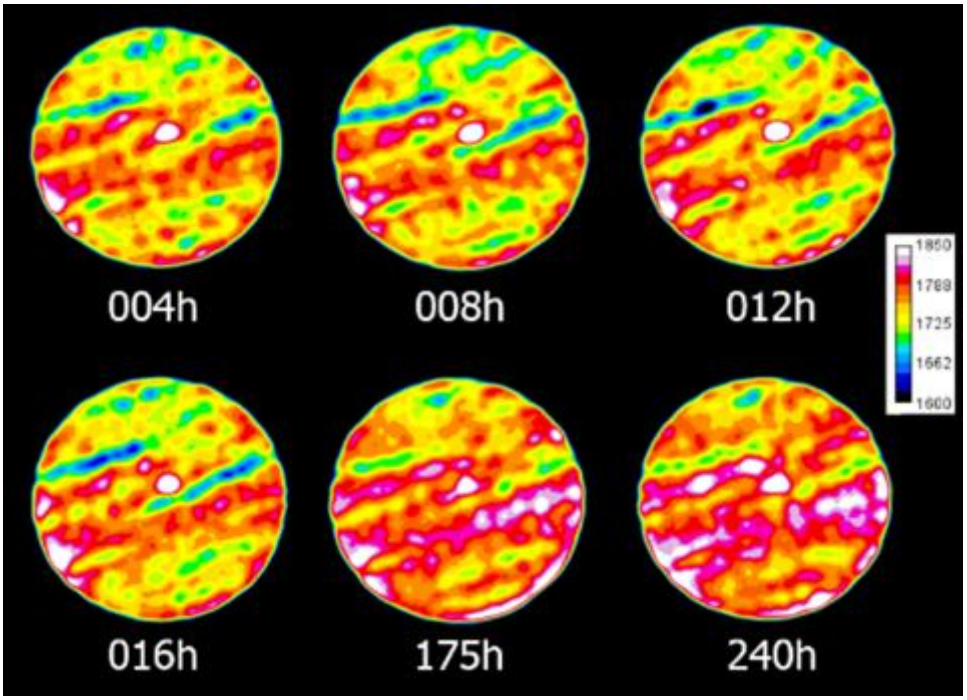

Fig. 113 – Timely Cross-sectional CT Images of a Core for F_NF in WT QR

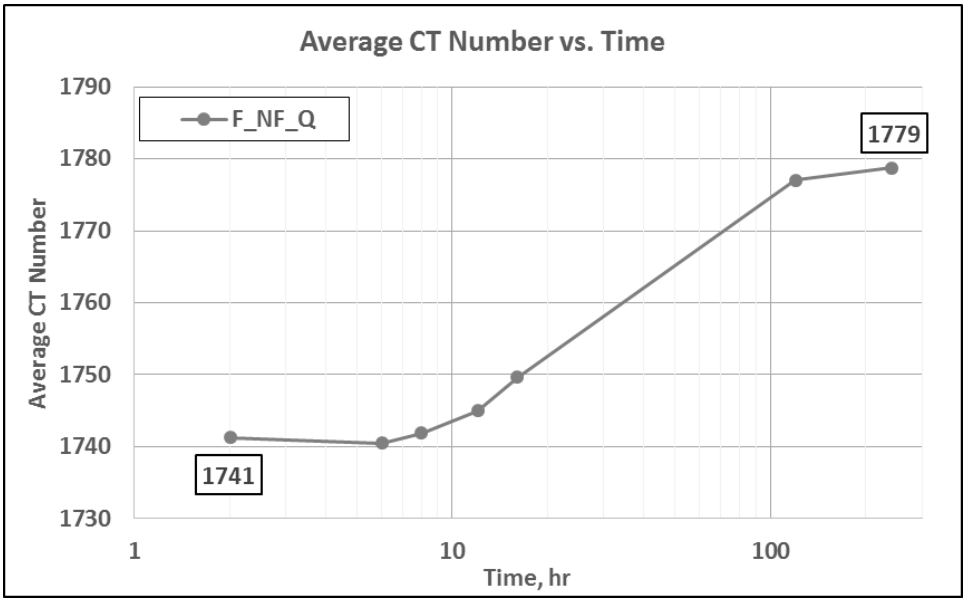

Fig. 114 – Change in Avg. CT Number for F_NF in WT QR

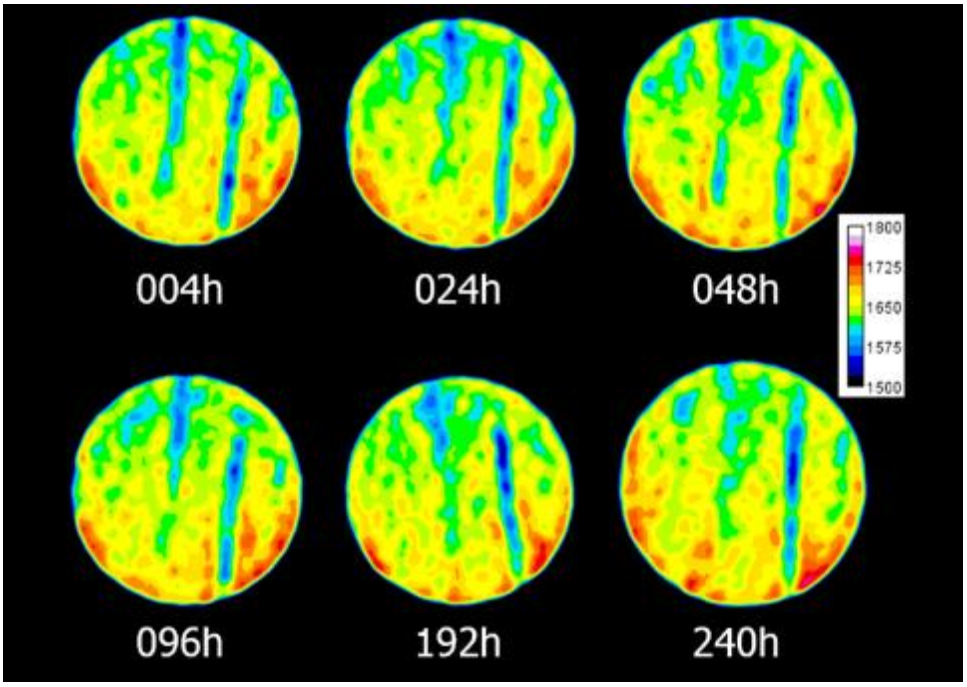

Fig. 115 – Timely Cross-sectional CT Images of a Core for P_NF in WT QR

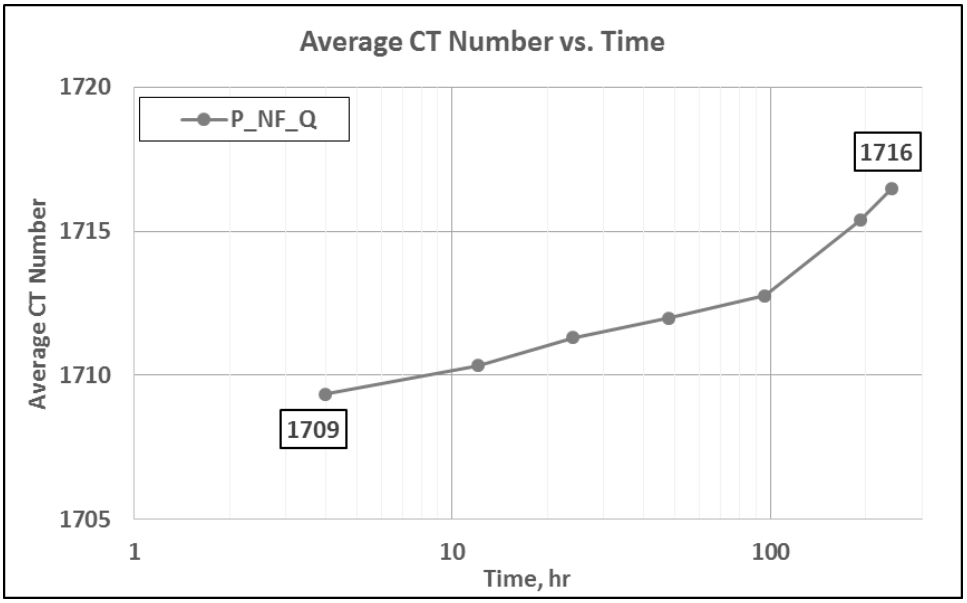

Fig. 116 – Change in Avg. CT Number for P_NF in WT QR

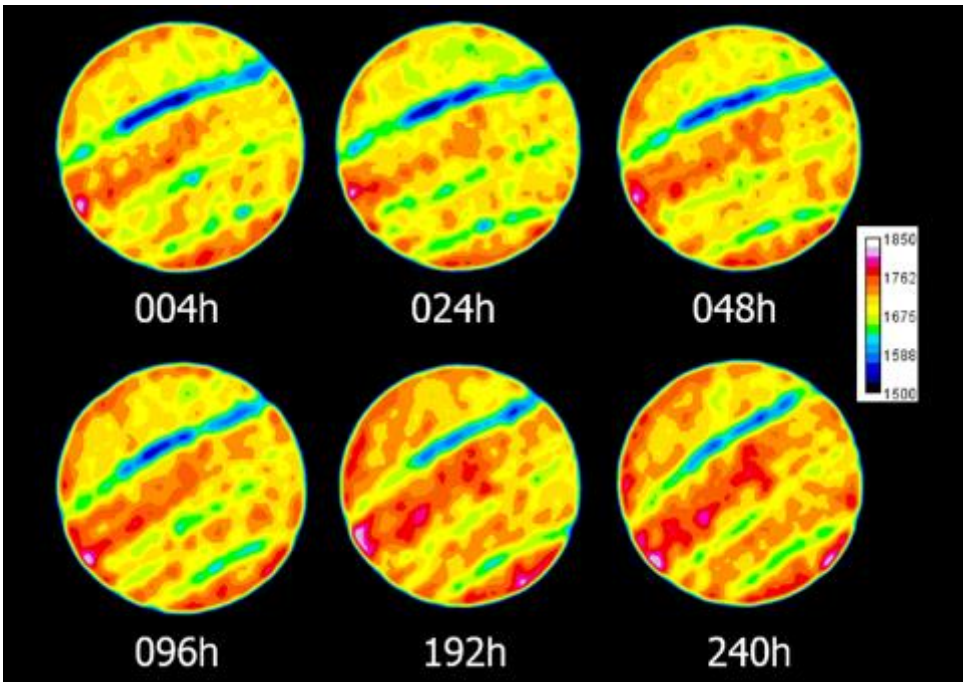

Fig. 117 – Timely Cross-sectional CT Images of a Core for D_S01 in WT QR

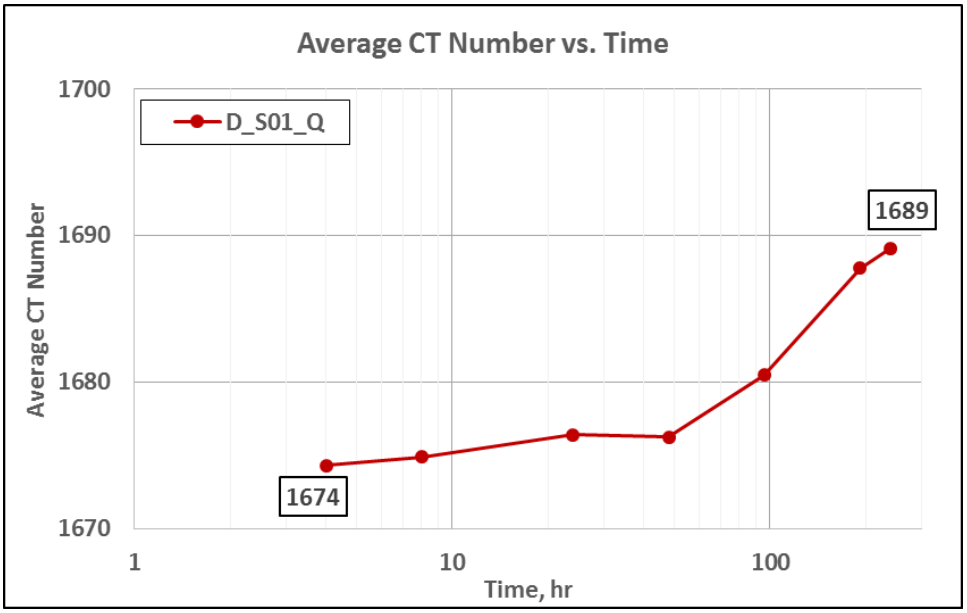

Fig. 118 – Change in Avg. CT Number for D_S01 in WT QR

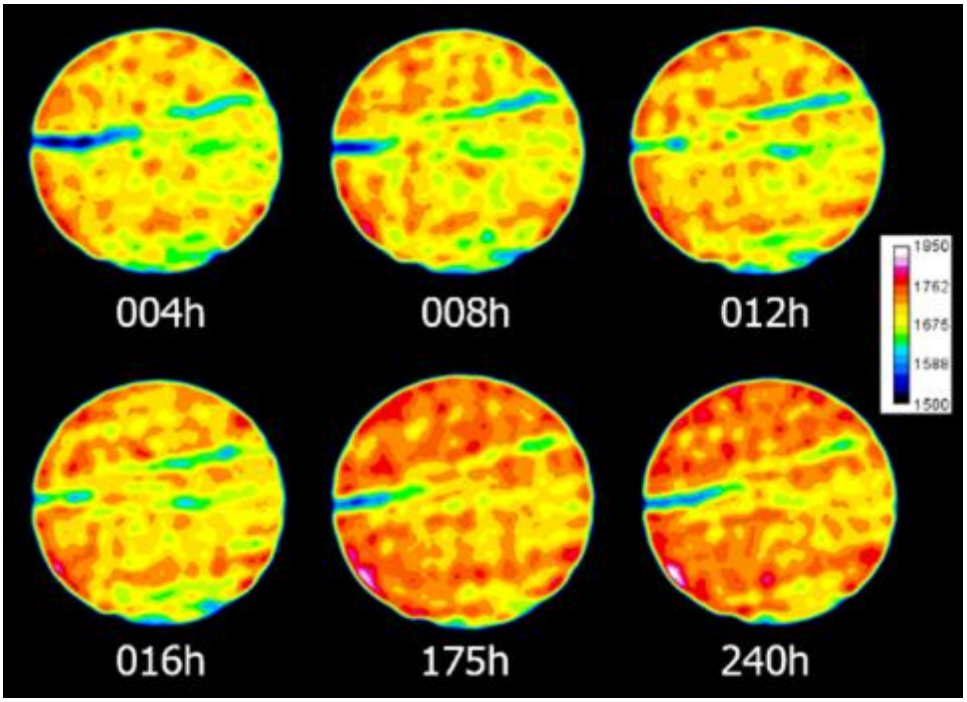

Fig. 119 – Timely Cross-sectional CT Images of a Core for F_S01 in WT QR

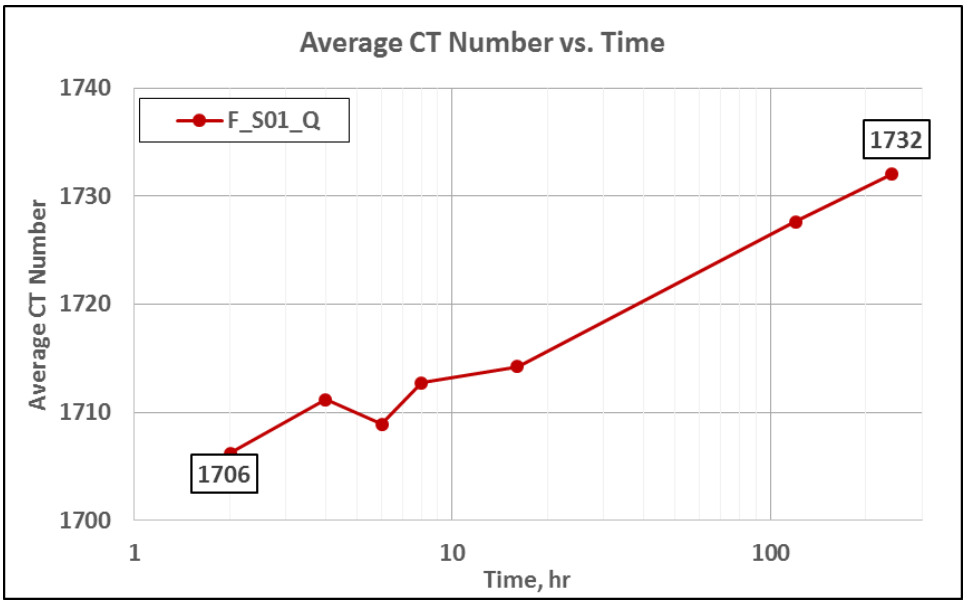

Fig. 120 – Change in Avg. CT Number for F_S01 in WT QR

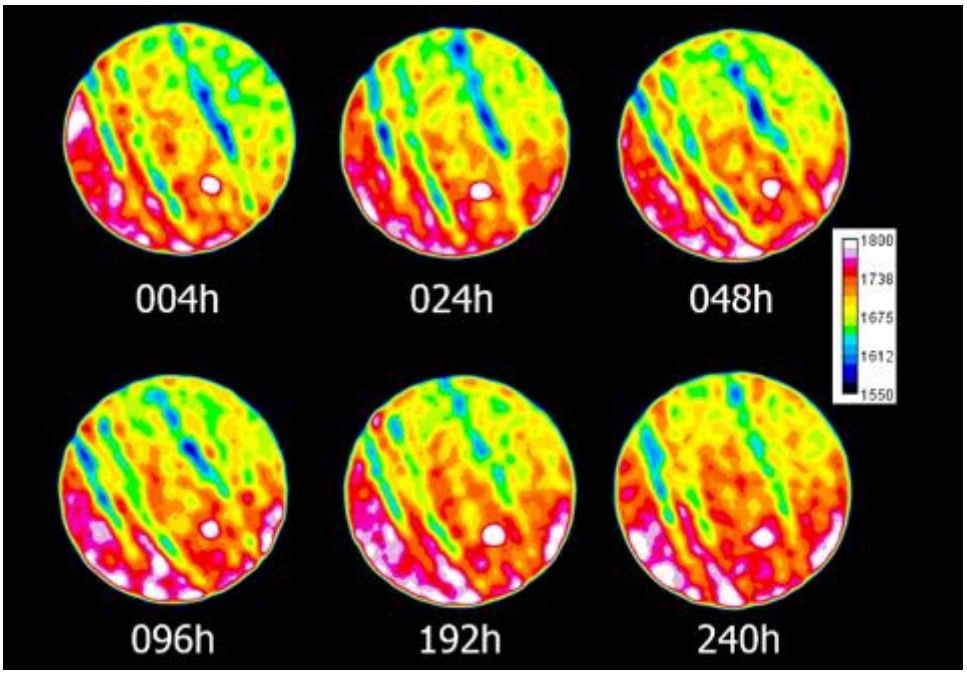

Fig. 121 – Timely Cross-sectional CT Images of a Core for P_S01 in WT QR

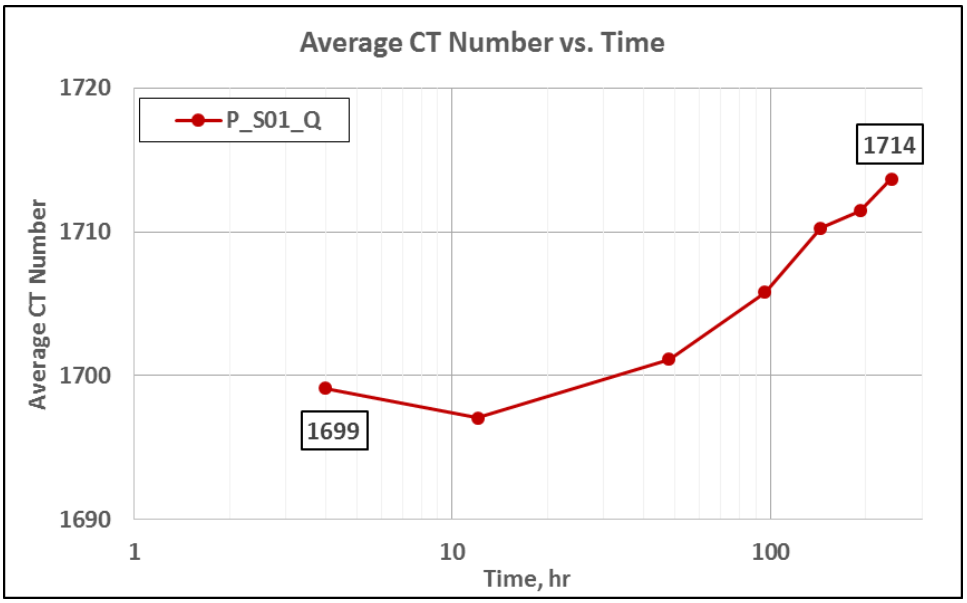

Fig. 122 – Change in Avg. CT Number for P_S01 in WT QR

Table 33 – Results of CT Image, and Weight Analyses for All Fluids in WT QR

Fluid	Initial Ave. CT #	Final Ave. CT #	Penetration Magnitude	Initial Weight, g	Final Weight, g	ΔWeight, g	RF, %
DW_Q	1757	1769	12	82.50	83.50	1.00	11.0%
FW_Q	1736	1745	9	83.44	83.86	0.42	13.1%
PW_Q	1754	1758	4	83.65	83.94	0.29	11.7%
D_NF_Q	1564	1571	7	75.62	75.77	0.16	15.6%
F_NF_Q	1741	1779	38	38.39	38.48	0.09	33.5%
P_NF_Q	1709	1716	7	76.69	76.98	0.29	16.1%
D_S01_Q	1674	1689	15	58.23	58.47	0.24	20.6%
F_S01_Q	1706	1732	26	80.23	80.42	0.20	30.7%
P_S01_Q	1699	1714	15	73.80	74.13	0.33	22.2%

5.4.3 Overall Comparison

Spontaneous imbibition experiments showed that quartz rich cores generally result in higher oil recovery compared to carbonate rich cores, as shown in **Fig. 123**. This phenomenon can be explained by different petrophysical properties of two rock types. In the sample 3D generated CT images in **Fig. 124**, it is clear that the carbonate rich core contains an extreme heterogeneity throughout the whole core, composed of numerous small calcite blocks, and this may cause more compacted and tighter matrix, which affect both porosity and permeability. Meanwhile, sample 3D images of quartz rich core in **Fig. 125** display much less heterogeneous matrix with few bedding planes placed across the whole core, which may allow aqueous phase solutions to penetrate into the core more effectively.

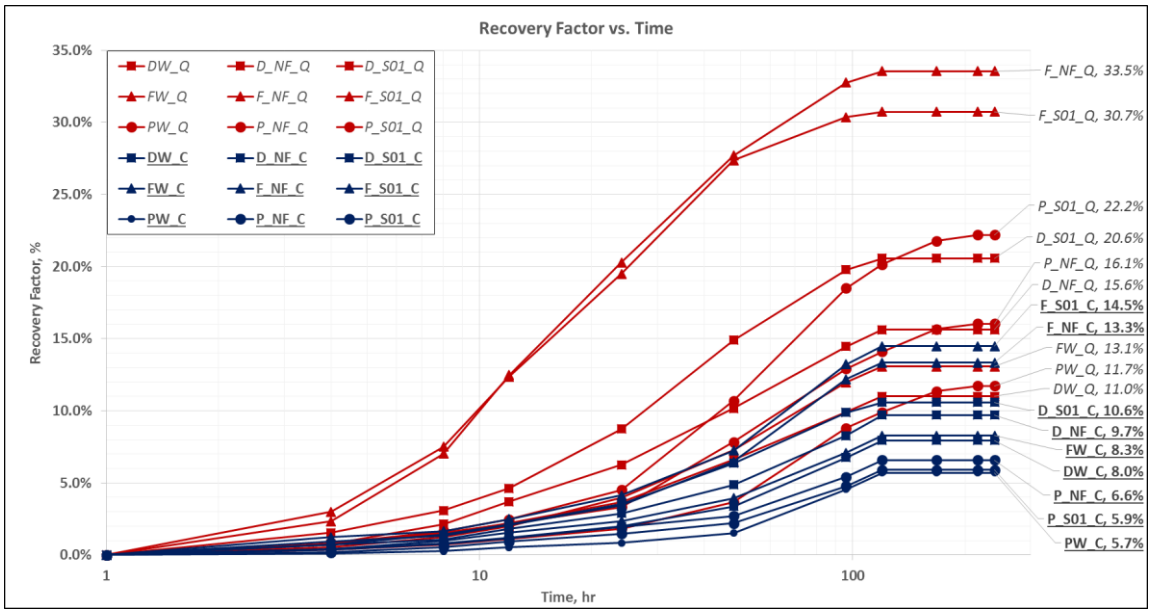

Fig. 123 – Overall Comparison of Spontaneous Imbibition Performance for Each Fluid with Both WT CR (Blue Curves) and WT QR (Red Curves)

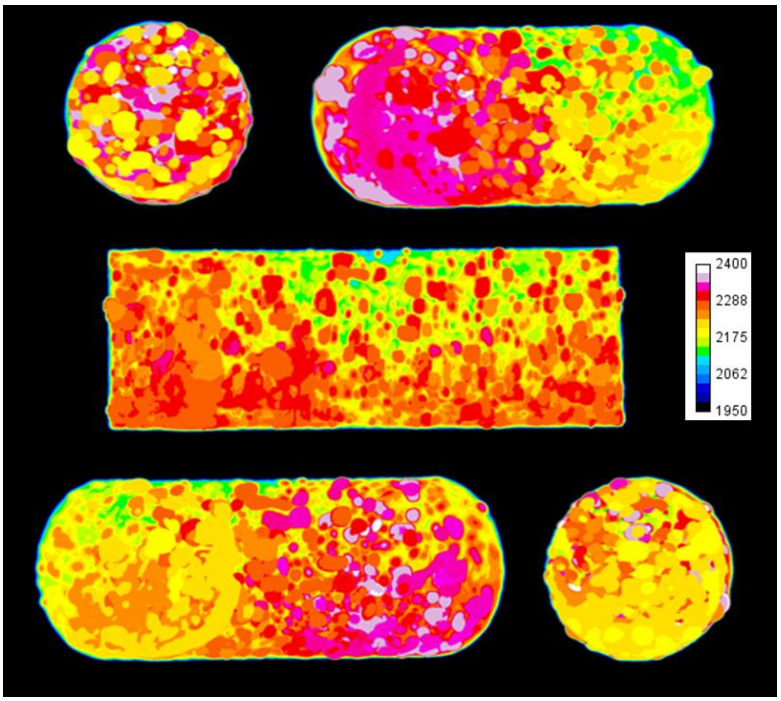

Fig. 124 – Sample 3D CT Images of a WT Carbonate Rich Core

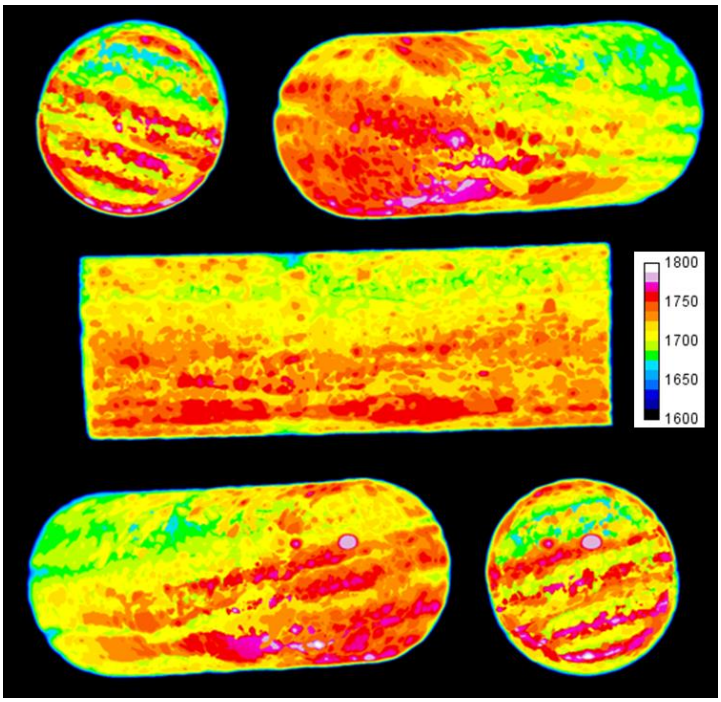

Fig. 125 – Sample 3D CT Images of a WT Quartz Rich Core

As shown in **Table 34**, the maximum recovery factor of 14.5 % was obtained with carbonate rich cores, while quartz rich cores produced up to 33.5 %. A strong relationship between penetration magnitude and oil recovery factor could be noticed, which can be concluded that when more aqueous phase solutions penetrate into the core, more oil is replaced by them from the matrix. This relationship can also be applied to the difference in weight, because when higher density fluids enter the matrix and replace oil, the mass of whole core increases.

Table 34 – Overall Results of Spontaneous Imbibition in WT Formation

Fluid_Rock	Initial Ave. CT #	Final Ave. CT #	Penetration Magnitude	Initial Weight, g	Final Weight, g	ΔWeight, g	RF, %
DW_C	2131	2133	2	80.83	80.96	0.13	8.0 %
FW_C	2268	2272	4	83.26	83.35	0.09	8.3 %
PW_C	2249	2253	4	86.62	86.70	0.08	5.7%
D_NF_C	2193	2198	5	91.16	91.22	0.06	9.7%
F_NF_C	2162	2177	15	84.99	85.15	0.16	13.3 %
P_NF_C	2273	2278	5	86.02	86.14	0.11	6.6%
D_S01_C	2153	2159	6	92.89	92.98	0.09	10.6%
F_S01_C	2132	2145	13	78.41	78.54	0.14	14.5 %
P_S01_C	2262	2266	4	89.71	89.80	0.09	5.9%
DW_Q	1757	1769	12	82.50	83.50	1.00	11.0%
FW_Q	1736	1745	9	83.44	83.86	0.42	13.1%
PW_Q	1754	1758	4	83.65	83.94	0.29	11.7%
D_NF_Q	1564	1571	7	75.62	75.77	0.16	15.6%
F_NF_Q	1741	1779	38	38.39	38.48	0.09	33.5%
P_NF_Q	1709	1716	7	76.69	76.98	0.29	16.1%
D_S01_Q	1674	1689	15	58.23	58.47	0.24	20.6%
F_S01_Q	1706	1732	26	80.23	80.42	0.20	30.7%
P_S01_Q	1699	1714	15	73.80	74.13	0.33	22.2%

It is apparent that the addition of surfactants into aqueous phase solutions improved the oil recovery factor compared to brine without chemical additives. Among all cases, fluids with low salinity of 26,800 ppm enhanced the performance of imbibition the most for both rock types. However, different surfactants were determined to be more favorable for different rock type. **Fig. 126** shows that Surfactant01 was more favorable and achieved the optimum recovery factor when interacted with carbonate rich cores, while **Fig. 127** indicates nano-technology fluid assisted for the highest oil production from quartz rich cores. As concluded in section 5.3 with contact angle, not all surfactant interacts and

performs similarly with all lithology, thus, various types of surfactant must be examined beforehand, and applied for different reservoirs with different petrophysical properties.

Despite the low interfacial tension, fluids with high salinity of 80,400 ppm did not perform as well as low, or no salinity brines. Other than its weaker ability to alter wettability, during the imbibition, another factor was observed which might have caused the less effective performance enhancement. Most of the cores submerged in fluids with high salinity during the imbibition experiments resulted in a thin layer of salt deposits on the surface of cores, as pictured in **Fig. 128**. These scaling tendency of salt components causes blockage of flow path of both aqueous phase solution and crude oil within the formation, leading to a lower recover factor of oil.

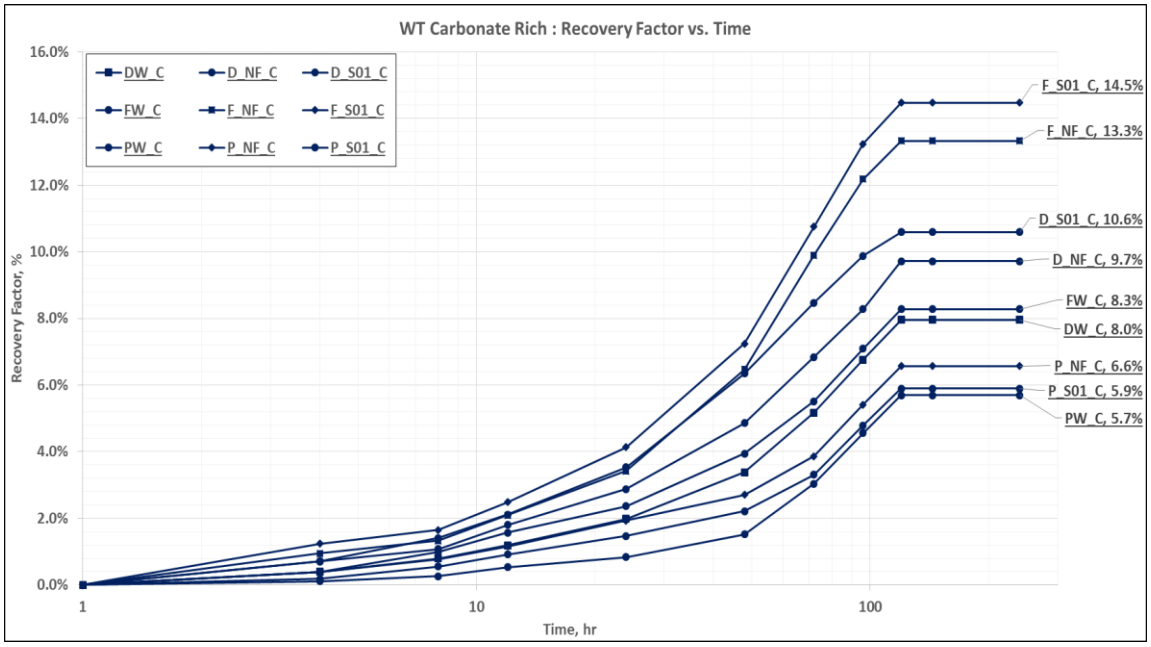

Fig. 126 – Comparison of Imbibition Performance for Each Fluid with WT CR

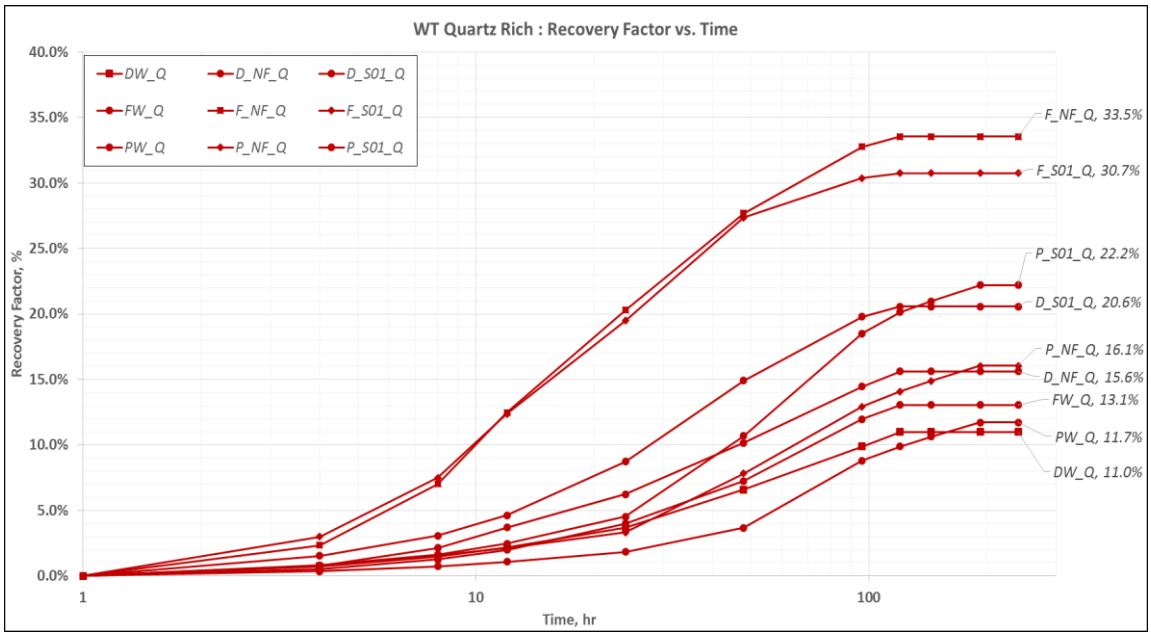

Fig. 127 – Comparison of Imbibition Performance for Each Fluid with WT QR

Fig. 128 – Observation of Scaling when Using Fluids with High Salinity

5.5 Correlations

Using all of experimented parameters and calculated oil recovery factor in the previous sections, correlation analyses were performed to determine the most effective parameter for better oil recovery. 18 sets of zeta potential, interfacial tension, and contact angle were plotted against recovery factor to find the relationship. Additionally, penetration magnitude (PM) obtained from CT image analyses above was also compared with recovery factor. Since zeta potential determines the stability of electrical double layer based on the magnitude, all zeta potential measurements were converted to absolute values. Also, comparison of two rock types was conducted for ZP, CA, and PM to observe the impact of each parameter to each lithology.

Zeta potential did not have a distinct relationship with recovery factor for both rock types, as shown in **Fig. 129** and **Fig. 130**. Presence of salt causes the magnitude of zeta potential to decrease, thinning the electrical double layer surrounding rock particles. However, aqueous phase solutions with low salinity achieved the highest oil recovery factor for both rock types, even with lower magnitude of zeta potential than no salinity fluids. It can be concluded that it is difficult to estimate the ultimate oil recovery and the performance of spontaneous imbibition based on zeta potential, especially when salinity is present within the solutions.

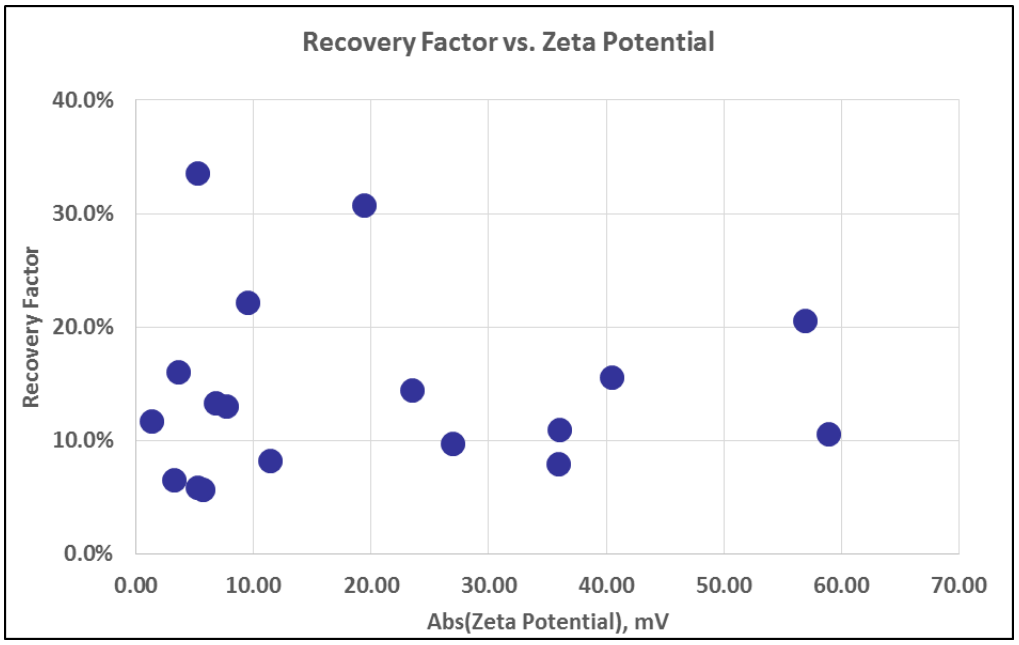

Fig. 129 –Recovery Factor vs. Absolute Value of Zeta Potential for All Cases

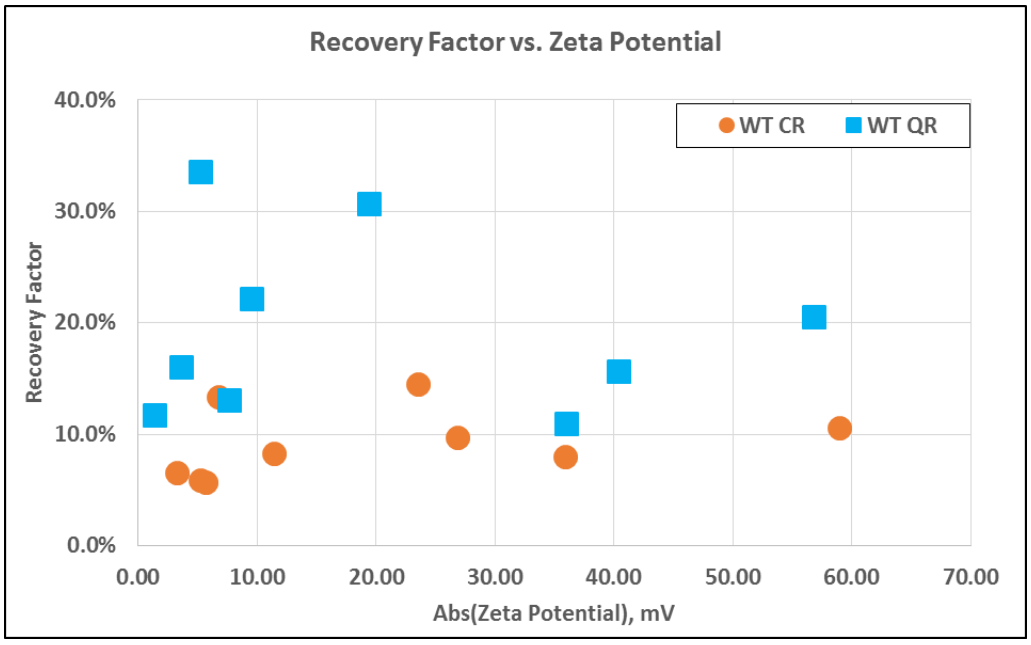

Fig. 130 – Recovery Factor vs. Absolute Value of Zeta Potential for Each Rock Type

IFT, presented in **Fig. 131**, also did not show much relationship with recovery factor, but a slightly better relationship compared to zeta potential. Though it does not show a direct relationship, higher oil recovery occurred the most when IFT was reduced to less than 10 mN/m. This justifies that much more effective gravity and buoyancy assisted imbibition functions as a dominant oil recovery mechanism when IFT between crude oil and aqueous phase solution is lower.

Among all other parameters, contact angle, in **Fig. 132,** showed the strongest relationship with oil recovery factor. When the contact angle was higher than 115 degrees, which is in oil wet range, maximum of 11 % of oil recovery was obtained. However, when the wettability was altered to intermediate range, recovery factor increased up to more than 20 %. Lastly, when rock surface became water wet, the highest recovery factor was achieved. As shown in **Fig. 133**, carbonate rich cores produced less oil than quartz rich. However, the trend and the relationship between surface wettability and recovery factor were very similar for both rock types. Therefore, it can be concluded that the wettability alteration of ULR is the most influential factor for higher oil recovery.

Penetration magnitude, in **Fig. 134**, showed that the larger penetration magnitude occurs when there is higher oil recovery factor, or vice versa. This is an apparent phenomenon that when more aqueous phase solutions with high density enters the core, they are more likely to replace retained oil from the matrix through combination of buoyance and capillary pressure. Since carbonate rich cores resulted in a comparably lower recovery factor, penetration magnitude of carbonate rich was also lower than quartz rich cores, as in **Fig. 135**.

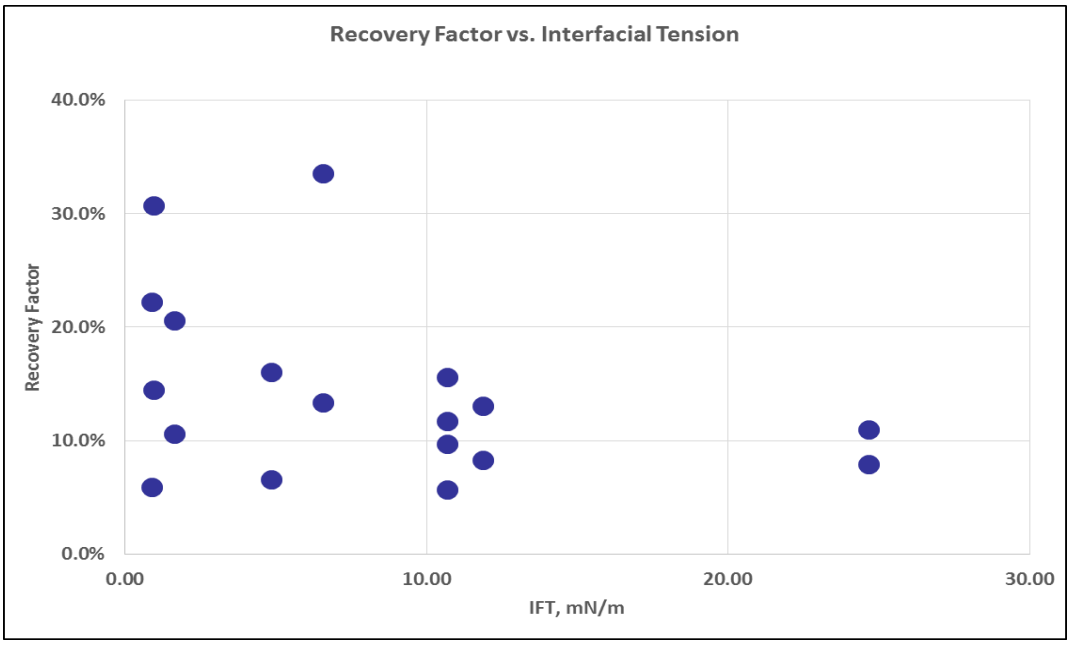

Fig. 131 – Recovery Factor vs. IFT for All Cases

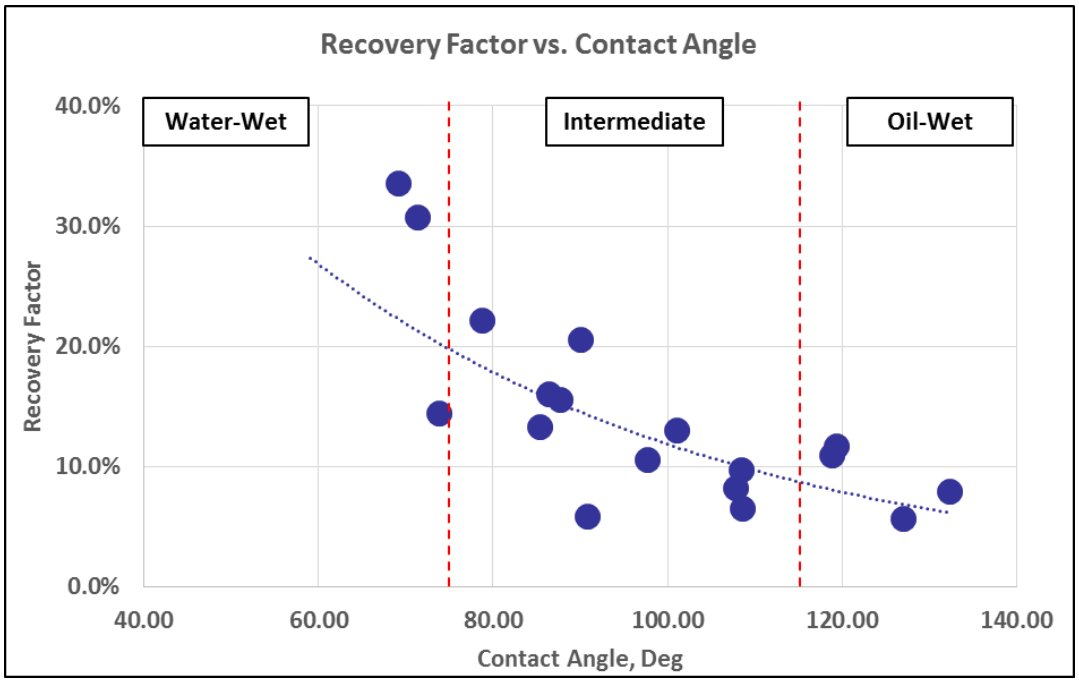

Fig. 132 – Recovery Factor vs. Contact Angle for All Cases

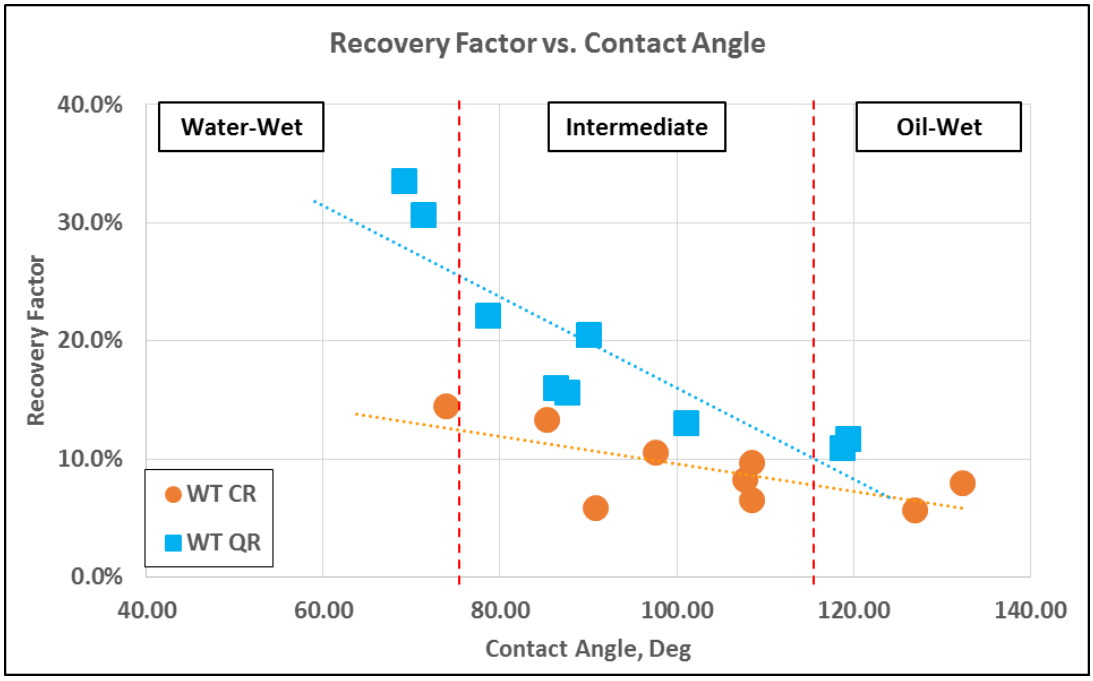

Fig. 133 – Recovery Factor vs. Contact Angle for Each Rock Type

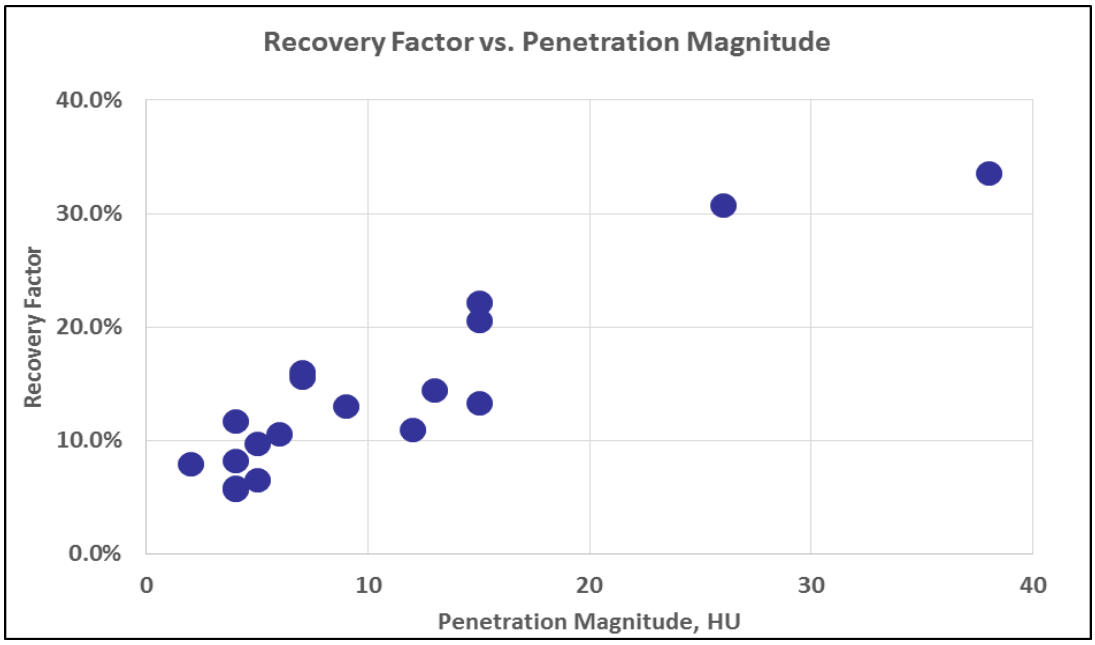

Fig. 134 – Recovery Factor vs. Penetration Magnitude for All Cases

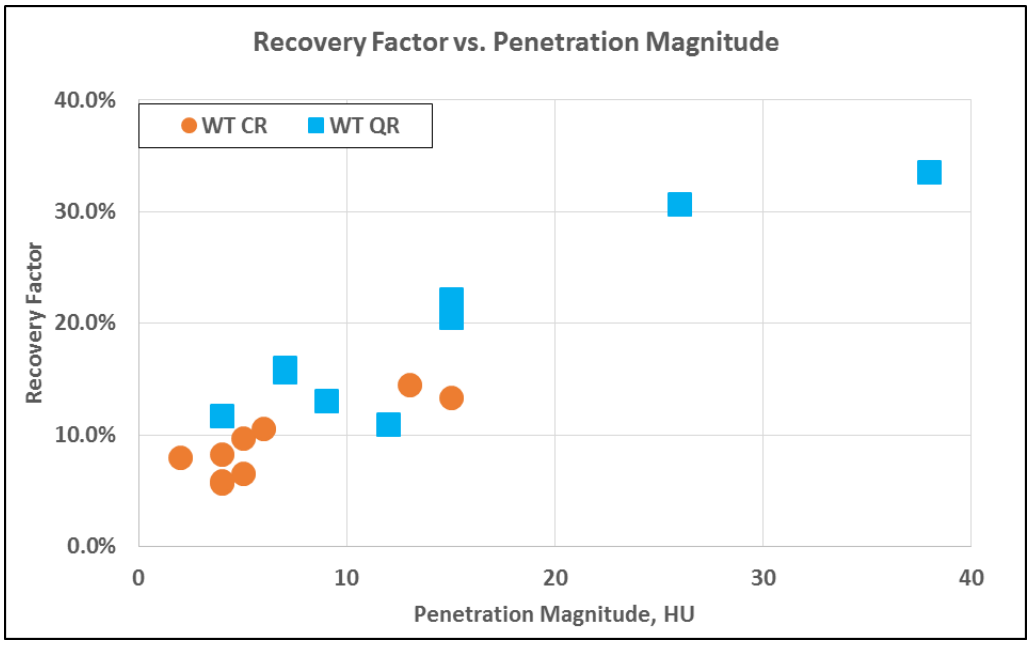

Fig. 135 – Recovery Factor vs. Penetration Magnitude for Each Rock Type

6. CONCLUSION AND SUGGESTED FUTURE WORK

6.1 Conclusion

The purpose of this investigation was to analyze the interactions of surfactant, salt and rocks to achieve the performance enhancements of completion fluids in unconventional liquids-rich reservoirs. Unlike previously conducted researches, this study specifically focuses on the impact of salinity on surfactant-added aqueous phase solutions, and helps to determine the most favorable conditions of the fluids. Also, this investigation potentially provides guidance for utilization of fresh water and large volumes of high salinity produced water, which potentially leads to both economic and environmental benefits, by reducing the water treatment, lowering fresh water demands, and reducing the number of salt water disposal wells. Main conclusions of this study are listed as follows:

- Extreme heterogeneity and ultra-tight matrix were observed in the ULR of West Texas. Two dominant rock types, carbonate rich and quartz rich, are in place within the formation WT.
- The original wettability of WT formation was weakly to strongly oil-wet. Carbonate rich rocks showed more oil-wet surface than quartz-rich rocks.
- The magnitude of zeta potential decreased with increasing salinity, causing a thinning of electrical double layer surrounding rock particles. Salinity weakened the repulsion forces between the rock particles, and led to much stronger hydrophobic rock surface in high salinity level.

- IFT between crude oil and aqueous phase solutions decreased with the addition of salt most effectively until the critical salt concentration (CSC) of 33,000 ppm. Salinity impact was not as effective after, but the reduction of IFT continued marginally.
- Contact angle was highly affected by the salinity level for both rock types, and showed a similar trend for all fluid cases. The highest wettability alteration occurred at lower salinity level of 26,800 ppm. However, as salinity was increased up to 80,400 ppm, surface wettability of both rock types gradually reversed back to its original state of oil-wet behavior.
- 3 fluids, S01, NF and water, and 3 salinity levels, 0, 26800, and 80400 ppm, were selected for spontaneous imbibition experiments to accurately compare the impact of different salinity and surfactants for each rock type.
- Carbonate rich cores produced much less oil than quartz rich cores due to extreme heterogeneity.
- For both rock types, fluids with low salinity achieved the highest oil recovery factor. Fluids with high salinity did not produce much oil from carbonate rich cores compared to fluids with no salinity. However, in quartz rich cores, high salinity fluids produced slightly more oil at slower imbibition rate than no salinity fluids.
- S01 interacted with carbonate rich cores much more favorably than quartz rich cores, while NF was able to produce the most oil from quartz rich cores. Thus,

the examination of interaction between various surfactants and target reservoirs must be conducted prior to the application.

- Zeta potential and interfacial tension did not have strong relationships with oil recovery. However, higher recovery factor occurred with lower IFT.
- Surface wettability determined by the contact angle was the most influential parameter for oil recovery, meaning the more water-wet the surface is, the more oil is likely to be produced. Therefore, the ability of surfactant-salt mixed fluids to alter wettability is the most important factor for higher oil recovery.
- Higher penetration magnitude occurs with higher recovery factor, or vice versa.
- Based on the IFT stability, wettability alteration and the imbibition performances, the most favorable range of salinity for surfactant-added completion fluids was determined to be between 20,000 ppm to 33,000 ppm.

6.2 Suggested Future Work

In order to improve numerous aspects of this investigation, the following work and recommendations are suggested:

- Determining the re-usability of core samples to perform spontaneous imbibition experiments on the same core with different fluids of various surfactant and salinity concentration.

- More accurate estimation of porosity for each core, based on more in-depth CT image calibration with computer software, or mass/volume analyses of each core, to mitigate the variables associated with heterogeneity.
- Investigating the impact of salinity at a different concentration of surfactant to study the impact of surfactant concentration on different salinity fluids.
- Timely chromatographic analysis on produced oil to inspect any compositional changes of oil during imbibition at early time through late time, and to analyze the ability of surfactant-salt mixed fluid accessing smaller pores and heavier hydrocarbon molecules.
- Water analysis on aqueous phase solutions before and after spontaneous imbibition to find any change of fluid properties during the experiment due to naturally occurring components in core samples, e.g. salinity.

REFERENCES

Abdallah, W., Buckley, J.S., Carnegie, A. et al. 2007. Fundamentals of Wettability. *Oilfield Review* **Summer 2007**.

Adibhatla, B. and Mohanty, K.K. 2008. Oil Recovery from Fractured Carbonates by Surfactant-Aided Gravity Drainage: Laboratory Experiments and Mechanistic Simulations. DOI: 10.2118/99773-PA

Alotaibi, M.B., Nasralla, R.A., and Nasr-El-Din, H.A. 2011. Wettability Studies Using Low-Salinity Water in Sandstone Reservoirs. DOI: 10.2118/149942-PA

Alvarez, J.O., Neog, A., Jais, A. et al. 2014. Impact of Surfactants for Wettability Alteration in Stimulation Fluids and the Potential for Surfactant Eor in Unconventional Liquid Reservoirs. Society of Petroleum Engineers. DOI: 10.2118/169001-MS.

Alvarez, J.O., Saputra, I.W.R., and Schechter, D.S. 2017. The Impact of Surfactant Imbibition and Adsorption for Improving Oil Recovery in the Wolfcamp and Eagle Ford Reservoirs. Society of Petroleum Engineers. DOI: 10.2118/187176-MS.

Alvarez, J.O., Saputra, I.W.R., and Schechter, D.S. 2017. Potential of Improving Oil Recovery with Surfactant Additives to Completion Fluids for the Bakken. *Energy & Fuels* **31** (6): 5982-5994. DOI: 10.1021/acs.energyfuels.7b00573

Alvarez, J.O. and Schechter, D.S. 2016a. Altering Wettability in Bakken Shale by Surfactant Additives and Potential of Improving Oil Recovery During Injection of Completion Fluids. Society of Petroleum Engineers. DOI: 10.2118/179688-MS.

Alvarez, J.O. and Schechter, D.S. 2016b. Wettability, Oil and Rock Characterization of the Most Important Unconventional Liquid Reservoirs in the United States and the Impact on Oil Recovery. Unconventional Resources Technology Conference.

Alvarez, J.O. and Schechter, D.S. 2017. Wettability Alteration and Spontaneous Imbibition in Unconventional Liquid Reservoirs by Surfactant Additives. DOI: 10.2118/177057-PA

Alvarez, J.O., Tovar, F.D., and Schechter, D.S. 2017. Improving Oil Recovery in Unconventional Liquid Reservoirs by Soaking-Flowback Production Schedule with Surfactant Additives. Society of Petroleum Engineers. DOI: 10.2118/187483-MS.

Anderson, W.G. 1986a. Wettability Literature Survey- Part 1: Rock/Oil/Brine Interactions and the Effects of Core Handling on Wettability. DOI: 10.2118/13932-PA

Anderson, W.G. 1986b. Wettability Literature Survey- Part 2: Wettability Measurement. DOI: 10.2118/13933-PA

Arthur, J.D., Langhus, B.G., and Patel, C. 2005. *Technical Summary of Oil & Gas Produced Water Treatment Technologies*. ALL Consulting, LLC.

Austad, T. and Milter, J. 1997. Spontaneous Imbibition of Water into Low Permeable Chalk at Different Wettabilities Using Surfactants. Paper presented at the International Symposium on Oilfield Chemistry, Houston, Texas. Society of Petroleum Engineers. DOI: 10.2118/37236-MS.

Babadagli, T. 2003. Analysis of Oil Recovery by Spontaneous Imbibition of Surfactant Solution. Paper presented at the SPE International Improved Oil Recovery

Conference in Asia Pacific, Kuala Lumpur, Malaysia. Society of Petroleum Engineers. DOI: 10.2118/84866-ms.

Bagnall, R.D. and Arundel, P.A. 1978. The Profile Area of Pendant Drops. *The Journal of Physical Chemistry* **82** (8): 898-902. DOI: 10.1021/j100497a011

Blewett, T.A., Weinrauch, A.M., Delompré, P.L.M. et al. 2017. The Effect of Hydraulic Flowback and Produced Water on Gill Morphology, Oxidative Stress and Antioxidant Response in Rainbow Trout (Oncorhynchus Mykiss). *Scientific Reports* **7**: 46582. DOI: 10.1038/srep46582

Boneau, D.F. and Clampitt, R.L. 1977. A Surfactant System for the Oil-Wet Sandstone of the North Burbank Unit. DOI: 10.2118/5820-PA

Burnett, D. 2011. Brine Management: Produced Water and Frac Flowback Brine. DOI: 10.2118/1011-0046-JPT

Chen, H.L., Lucas, L.R., Nogaret, L.A.D. et al. 2000. Laboratory Monitoring of Surfactant Imbibition Using Computerized Tomography. Society of Petroleum Engineers. DOI: 10.2118/59006-MS.

Chen, H.L., Lucas, L.R., Nogaret, L.A.D. et al. 2001. Laboratory Monitoring of Surfactant Imbibition with Computerized Tomography. DOI: 10.2118/69197-PA

Chen, P. and Mohanty, K.K. 2014. Wettability Alteration in High Temperature Carbonate Reservoirs. Society of Petroleum Engineers. DOI: 10.2118/169125-MS.

Chimienti, M.E., Illiano, S.N., and Najurieta, H.L. 1999. Influence of Temperature and Interfacial Tension on Spontaneous Imbibition Process. Paper presented at the

Latin American and Caribbean Petroleum Engineering Conference, Caracas, Venezuela. Society of Petroleum Engineers. DOI: 10.2118/53668-MS.

Cuiec, L.E., Bourbiaus, B., and Kalaydjian, F. 1990. Imbibition in Low-Permeability Porous Media: Understanding and Improvement of Oil Recovery. Paper presented at the 7th Annual Symposium on EOR, Tulsa. Society of Petroleum Engineers.

Donaldson, E.C., Thomas, R.D., and Lorenz, P.B. 1969. Wettability Determination and Its Effect on Recovery Efficiency. DOI: 10.2118/2338-PA

E.I.A. 2017. *Annual Energy Outlook 2017*.

Fakhru'l-Razi, A., Pendashteh, A., Luqman Chuah, A. et al. 2009. *Review of Technologies for Oil and Gas Produced Water Treatment* Original edition. ISBN.

Freyman, M. 2014. *Hydraulic Fracturing & Water Stress: Water Demand by the Numbers*. Ceres.

Gadberry, J.F. and Otterson, R. 2006. Other Types of Surfactants. In *Chemistry and Technology of Surfactants*, ed. Farn, R.J.: Blackwell Publishing Ltd.

Gallegos, T.J., Varela, B.A., Haines, S.S. et al. 2015. Hydraulic Fracturing Water Use Variability in the United States and Potential Environmental Implications. *Water Resources Research* **51** (7): 5839-5845. DOI: 10.1002/2015WR017278

Garg, A., Cartier, C.A., Bishop, K.J.M. et al. 2016. Particle Zeta Potentials Remain Finite in Saturated Salt Solutions. *Langmuir* **32** (45): 11837-11844. DOI: 10.1021/acs.langmuir.6b02824

Ghosh, L., Das, K.P., and Chattoraj, D.K. 1988. Thermodynamics of Adsorption of Inorganic Electrolytes at Air/Water and Oil/Water Interfaces. *Journal of Colloid*

and Interface Science **121** (1): 278-288. DOI: https://doi.org/10.1016/0021-9797(88)90432-8

Guo, B. and Schechter, D.S. 1997. A Simple and Accurate Method for Determining Low Ift from Pendant Drop Measurements. Paper presented at the International Symposium on Oilfield Chemistry, Houston, Texas. Society of Petroleum Engineers. DOI: 10.2118/37216-MS.

Gupta, R. and Mohanty, K.K. 2008. Wettability Alteration of Fractured Carbonate Reservoirs. Paper presented at the SPE Symposium on Improved Oil Recovery, Tulsa, Oklahoma, USA. Society of Petroleum Engineers. DOI: 10.2118/113407-MS.

Handy, L.L., El-Gassier, M., and Ershaghi, I. 1983. A Modified Spinning Drop Method for High-Temperature Applications. DOI: 10.2118/9003-PA

Hepworth, P. 2006. Non-Ionic Surfactants. In *Chemistry and Technology of Surfactants*, ed. Farn, R.J.: Blackwell Publishing Ltd.

Herd, M.D., Lassahn, G.D., Thomas, C.P. et al. 1992. Interfacial Tensions of Microbial Surfactants Determined by Real-Time Video Imaging of Pendant Drops. Paper presented at the SPE/DOE Enhanced Oil Recovery Symposium, Tulsa, Oklahoma. Society of Petroleum Engineers. DOI: 10.2118/24206-MS.

Hibbs, J. 2006. Anionic Surfactants. In *Chemistry and Technology of Surfactants*, ed. Farn, R.J.: Blackwell Publishing Ltd.

Hirasaki, G. and Zhang, D.L. 2004. Surface Chemistry of Oil Recovery from Fractured, Oil-Wet, Carbonate Formations. DOI: 10.2118/88365-PA

Hirasaki, G.J. 1991. Wettability: Fundamentals and Surface Forces. DOI: 10.2118/17367-PA

Hocott, C.R. 1939. Interfacial Tension between Water and Oil under Reservoir Conditions. DOI: 10.2118/939184-G

Hough, E.W. 1966. Correlation of Interfacial Tension of Hydrocarbons. DOI: 10.2118/1565-PA

Huh, C. and Reed, R.L. 1983. A Method for Estimating Interfacial Tensions and Contact Angles from Sessile and Pendant Drop Shapes. *Journal of Colloid and Interface Science* **91** (2): 472-484. DOI: https://doi.org/10.1016/0021-9797(83)90361-2

Instruments, M. 2005. *Tech Note: Zeta Potential - an Introduction in 30 Minutes* Original edition. ISBN.

Jackson, R.B., Vengosh, A., Carey, J.W. et al. 2014. The Environmental Costs and Benefits of Fracking. *Annual Review of Environment and Resources* **39** (1): 327-362. DOI: 10.1146/annurev-environ-031113-144051

Jada, A., Ait Akbour, R., and Douch, J. 2006. Surface Charge and Adsorption from Water onto Quartz Sand of Humic Acid. *Chemosphere* **64** (8): 1287-1295. DOI: https://doi.org/10.1016/j.chemosphere.2005.12.063

Johnson, J.D., Schoppa, D., Garza, J.L. et al. 2010. Enhancing Gas and Oil Production with Zeta Potential Altering System. Paper presented at the SPE International Symposium and Exhibition on Formation Damage Control, Lafayette, Louisiana, USA. Society of Petroleum Engineers. DOI: 10.2118/128048-MS.

Johnston, J.E., Werder, E., and Sebastian, D. 2016. Wastewater Disposal Wells, Fracking, and Environmental Injustice in Southern Texas. *American Journal of Public Health* **106** (3): 550-556. DOI: 10.2105/ajph.2015.303000

Kakadjian, S., Zamora, F., and Venditto, J.J. 2007. Zeta Potential Altering System for Increased Fluid Recovery, Production, and Fines Control. Society of Petroleum Engineers. DOI: 10.2118/106112-MS.

Karsa, D.R. 2006. History and Applications of Surfactants. In *Chemistry and Technology of Surfactants*, ed. Farn, R.J.: Blackwell Publishing Ltd.

Khanamiri, H.H., Torsæter, O., and Stensen, J.Å. 2015. Experimental Study of Low Salinity and Optimal Salinity Surfactant Injection. Society of Petroleum Engineers. DOI: 10.2118/174367-MS.

Kondash, A. and Vengosh, A. 2015. Water Footprint of Hydraulic Fracturing. *Environmental Science & Technology Letters* **2** (10): 276-280. DOI: 10.1021/acs.estlett.5b00211

Li, X., Teklu, T.W., Abass, H. et al. 2016. The Impact of Water Salinity/Surfactant on Spontaneous Imbibition through Capillarity and Osmosis for Unconventional Ior. Paper presented at the Unconventional Resources Technology Conference, San Antonio, Texas, USA. Unconventional Resources Technology Conference.

Mahani, H., Keya, A.L., Berg, S. et al. 2017. Electrokinetics of Carbonate/Brine Interface in Low-Salinity Waterflooding: Effect of Brine Salinity, Composition, Rock Type, and Ph on Z-Potential and a Surface-Complexation Model. DOI: 10.2118/181745-PA

Mantell, M.E. 2011. Produced Water Reuse and Recycling Challenges and Opportunities across Major Shale Plays. In. U.S. Environmental Protection Agency: Chesapeake Energy Corporation.

Mohamed, F., Al Hinai, M., Al Nabhani, H. et al. 2015. Wettability Alteration in Hydraulically Fractured Tight Sand for Flow-Back Improvement. Society of Petroleum Engineers. DOI: 10.2118/177893-MS.

Mohammed, M. and Babadagli, T. 2015. Wettability Alteration: A Comprehensive Review of Materials/Methods and Testing the Selected Ones on Heavy-Oil Containing Oil-Wet Systems. *Advances in Colloid and Interface Science* **220**: 54-77. DOI: https://doi.org/10.1016/j.cis.2015.02.006

Mohanty, K.K. and Chandrasekhar, S. 2013. Wettability Alteration with Brine Composition in High Temperature Carbonate Reservoirs. Paper presented at the SPE Annual Technical Conference and Exhibition, New Orleans, Louisiana, USA. Society of Petroleum Engineers. DOI: 10.2118/166280-MS.

Moniz, E.J., Jacoby, H.D., Meggs, A.J.M. et al. 2011. *The Future of Natural Gas* Original edition. ISBN.

Morrow, N.R. and Mason, G. 2001. Recovery of Oil by Spontaneous Imbibition. *Current Opinion in Colloid & Interface Science* **6**: 321.

Neog, A. and Schechter, D.S. 2016. Investigation of Surfactant Induced Wettability Alteration in Wolfcamp Shale for Hydraulic Fracturing and Eor Applications. Society of Petroleum Engineers. DOI: 10.2118/179600-MS.

Nicot, J.P. and Scanlon, B.R. 2012. Water Use for Shale-Gas Production in Texas, U.S. *Environ. Sci. Technol.* **46** (6): 3580.

Pankaj, P. and Kumar, V. 2010. Well Testing in Tight Gas Reservoir: Today. Society of Petroleum Engineers. DOI: 10.2118/129032-MS.

Pletnev, M.Y. 2001. 1. Chemistry of Surfactants. In *Studies in Interface Science*, ed. Fainerman, V.B., Möbius, D., and Miller, R.: Elsevier. 13.

Rassenfoss, S. 2017. Turning Dirty Produced Water into Fresh Water and Salt to Sell. DOI: 10.2118/1117-0024-JPT

Rosen, M.J. 1984. *Structure/Performance Relationships in Surfactants*. Acs Symposium Series: American Chemical Society. Original edition. ISBN 0-8412-0839-5.

Scanlon, B.R., Reedy, R.C., and Nicot, J.P. 2014. Comparison of Water Use for Hydraulic Fracturing for Unconventional Oil and Gas Versus Conventional Oil. *Environmental Science & Technology* **48** (20): 12386-12393. DOI: 10.1021/es502506v

Schechter, D.S., Denqen, Z., and Orr, F.M., Jr. 1991. Capillary Imbibition and Gravity Segregation in Low Ift Systems. Society of Petroleum Engineers. DOI: 10.2118/22594-MS.

Schechter, D.S., Zhou, D., and Orr, F.M.J. 1994. Low Ift Drainage and Imbibition. *Journal of Petroleum Science and Energy*: 283-300.

Sharma, R., McLin, K., Bjornen, K. et al. 2015. Fit-for-Purpose Treatment of Produced Water for Hydraulic Fracturing – a Permian Basin Experience. International Petroleum Technology Conference. DOI: 10.2523/IPTC-18340-MS.

Shehata, A.M. and Nasr-El-Din, H.A. 2015. Zeta Potential Measurements: Impact of Salinity on Sandstone Minerals. Paper presented at the SPE International Symposium on Oilfield Chemistry, The Woodlands, Texas, USA. Society of Petroleum Engineers. DOI: 10.2118/173763-MS.

SPE. Challenges in Reusing Produced Water. Society of Petroleum Engineers. http://www.spe.org/industry/challenges-in-reusing-produced-water.php.

Spinler, E.A., Zornes, D.R., Tobola, D.P. et al. 2000. Enhancement of Oil Recovery Using a Low Concentration of Surfactant to Improve Spontaneous and Forced Imbibition in Chalk. Paper presented at the SPE/DOE Improved Oil Recovery Symposium, Tulsa, Oklahoma. Society of Petroleum Engineers. DOI: 10.2118/59290-MS.

Standnes, D. and Austad, T. 2000a. *Wettability Alteration in Chalk: 1. Preparation of Core Material and Oil Properties* Original edition. ISBN.

Standnes, D. and Austad, T. 2000b. Wettability Alteration in Chalk: 2. Mechanism for Wettability Alteration from Oil-Wet to Water-Wet Using Surfactants. *Journal of Petroleum Science and Engineering* **28** (3): 123-143. DOI: https://doi.org/10.1016/S0920-4105(00)00084-X

Standnes, D., Nogaret, L.A., Chen, H.L. et al. 2002. An Evaluation of Spontaneous Imbibition of Water into Oil-Wet Carbonate Reservoir Cores Using a Nonionic and a Cationic Surfactant. *Energy & Fuels* **16** (6): 1557-1564. DOI: 10.1021/ef0201127

Sunshine, W.L. 2017. Water Water Byproducts of Shale Gas Drilling and Fracking: A Look at Fracking and Produced Water Fracking Waste. *The Balance*, March 3, 2017.

Trantham, J.C. and Clampitt, R.L. 1977. Determination of Oil Saturation after Waterflooding in an Oil-Wet Reservoir the North Burbank Unit, Tract 97 Project. DOI: 10.2118/5802-PA

Treiber, L.E. and Owens, W.W. 1972. A Laboratory Evaluation of the Wettability of Fifty Oil-Producing Reservoirs. DOI: 10.2118/3526-PA

Valluri, M.K., Alvarez, J.O., and Schechter, D.S. 2016. Study of the Rock/Fluid Interactions of Sodium and Calcium Brines with Ultra-Tight Rock Surfaces and Their Impact on Improving Oil Recovery by Spontaneous Imbibition. Society of Petroleum Engineers. DOI: 10.2118/180274-MS.

Technology, C.o.S.A. 2007. *Research to Improve Water-Use Efficiency and Conservation: Technologies and Practices*, by Veil, J.A., One Hundred Tenth Cong. Washington D.C.

Veil, J.A., Puder, M.G., Elcock, D. et al. 2004. *A White Paper Describing Produced Water from Production of Crude Oil, Natural Gas, and Coal Bed Methane*. U.S. Department of Energy National Energy Technology Laboratory: Argonne National Laboratory.

Vengosh, A., Jackson, R.B., Warner, N. et al. 2014. A Critical Review of the Risks to Water Resources from Unconventional Shale Gas Development and Hydraulic

Fracturing in the United States. *Environmental Science & Technology* **48** (15): 8334-8348. DOI: 10.1021/es405118y

Wang, D., Butler, R., Zhang, J. et al. 2012. Wettability Survey in Bakken Shale with Surfactant-Formulation Imbibition. DOI: 10.2118/153853-PA

Wang, D., Seright, R.S., and Zhang, J. 2012a. Wettability Survey in Bakken Shale Using Surfactant Formulation Imbibition. Society of Petroleum Engineers. DOI: 10.2118/153853-MS.

Wang, D., Seright, R.S., and Zhang, J. 2012b. Wettability Survey in Bakken Shale Using Surfactant Formulation Imbibition. Paper presented at the SPE Improved Oil Recovery Symposium, Tulsa, Oklahoma, USA. Society of Petroleum Engineers. DOI: 10.2118/153853-MS.

Wang, W. and Gupta, A. 1995. Investigation of the Effect of Temperature and Pressure on Wettability Using Modified Pendant Drop Method. Paper presented at the SPE Annual Technical Conference and Exhibition, Dallas, Texas. Society of Petroleum Engineers. DOI: 10.2118/30544-MS.

Wells, P., Rathbarth, S., and Webb, F. The Coming Permian Basin Water Disposal Bottleneck. Digital H2O. https://www.digitalh2o.com/blog/coming-permian-basin-water-disposal-bottleneck.

Whitfield, S. 2017. Permian, Bakken Operators Face Produced Water Challenges. *Journal of Petroleum Technology*. DOI: 10.2118/0617-0048-JPT

Wilson, A. 2015. Permian Basin Fracturing Systems Using Produced Water. DOI: 10.2118/1215-0087-JPT

Wilson, A. 2016. Produced-Water Reinjection - Case Study from Onshore Abu Dhabi. DOI: 10.2118/1216-0072-JPT

Wu, M., Mintz, M., Wang, M. et al. 2009. Water Consumption in the Production of Ethanol and Petroleum Gasoline. *Environ. Manage.* **44** (5): 981.

Zhang, D. 2005. Surfactant-Enhanced Oil Recovery Process for a Fractured, Oil-Wet Carbonate Reservoir. Doctor of Philosophy Dissertation, Rice University.

Zheng, Y. and Rao, D.N. 2010. Surfactant-Induced Spreading and Wettability Effects in Condensate Reservoirs. Society of Petroleum Engineers. DOI: 10.2118/129668-MS.